RL-TR-97-203
Final Technical Report
October 1997

APPLICATION OF THE MODEL REFERENCE APPROACH IN LASER BEAM STEERING SYSTEMS

Advanced Technical Concepts

Victor A. Skormin

Rome Laboratory
Air Force Materiel Command
Rome, New York

This report has been reviewed by the Rome Laboratory Public Affairs Office (PA) and is releasable to the National Technical Information Service (NTIS). At NTIS it will be releasable to the general public, including foreign nations.

RL-TR-97-203 has been reviewed and is approved for publication.

APPROVED:

DONALD J. NICHOLSON
Project Engineer

FOR THE DIRECTOR:

WARREN H. DEBANY, JR., Technical Advisor
Command, Control & Communications Directorate

If your address has changed or if you wish to be removed from the Rome Laboratory mailing list, or if the addressee is no longer employed by your organization, please notify RL/C3BA, 525 Brooks Road, Rome, NY 13441-4505. This will assist us in maintaining a current mailing list.

Do not return copies of this report unless contractual obligations or notices on a specific document require that it be returned.

REPORT DOCUMENTATION PAGE	Form Approved OMB No. 0704-0188

1. AGENCY USE ONLY *(Leave blank)*	2. REPORT DATE	3. REPORT TYPE AND DATES COVERED
	October 1997	Final Jun 96 - May 97

4. TITLE AND SUBTITLE

APPLICATION OF THE MODEL REFERENCE APPROACH IN LASER BEAM STEERING SYSTEMS

5. FUNDING NUMBERS

C - F30602-96-C-0088
PE - 62702F
PR - 4519
TA - 63
WU - P8

6. AUTHOR(S)

Victor A. Skormin

7. PERFORMING ORGANIZATION NAME(S) AND ADDRESS(ES)

Advanced Technical Concepts
352 Ford Hill Road
Berkshire, NY 13736

8. PERFORMING ORGANIZATION REPORT NUMBER

N/A

9. SPONSORING/MONITORING AGENCY NAME(S) AND ADDRESS(ES)

Rome Laboratory/C3BA
525 Brooks Road
Rome, NY 13441-4505

10. SPONSORING/MONITORING AGENCY REPORT NUMBER

RL-TR-97-203

11. SUPPLEMENTARY NOTES

Rome Laboratory Project Engineer: Donald J. Nicholson/C3BA/(315) 330-7437

12a. DISTRIBUTION AVAILABILITY STATEMENT

Approved for public release; distribution unlimited.

12b. DISTRIBUTION CODE

13. ABSTRACT *(Maximum 200 words)*

A model reference control system has been developed to adaptively control the pointing function of a "Pointing, Acquisition and Tracking" system in a satellite-based Laser Communication system. This approach allows the description of the system transfer behavior to be defined in software, and the behavior of the real system to be driven to this software model. The consequence is the isolation of the real, transient and wear affected system from the ideal, modeled system performance, allowing the "forcing function" of the controller to correct for transients (e.g. platform jitter) and for long term effects of wear and operational conditions.

The use of this technique in compensating for bending modes in less expensive optical mirror systems has been experimentally demonstrated.

The consequence of using this improved pointing accuracy and the associated improvement in burst error performance to allow transient control of output carrier power is suggested as a means of enhancing system reliability.

14. SUBJECT TERMS

Communication, Satellite, Optical

15. NUMBER OF PAGES

84

16. PRICE CODE

17. SECURITY CLASSIFICATION OF REPORT	18. SECURITY CLASSIFICATION OF THIS PAGE	19. SECURITY CLASSIFICATION OF ABSTRACT	20. LIMITATION OF ABSTRACT
UNCLASSIFIED	UNCLASSIFIED	UNCLASSIFIED	UL

Table of Contents

INTRODUCTION

Free space laser communications provide the technology which will revolutionize existing information networks and facilitate the creation of the "information super-highway". The information networks of the nearest future are viewed as an extensive system of satellites connected by the means of laser communication and covering the entire planet. Laser communication will be utilized by uploading information onto the nearest satellite, creation of the rational satellite-to-satellite communication channel, and downloading information to the required location. Utilization of laser as a communication medium offers significant benefits over traditional RF systems. They include: higher bandwidth, smaller beam divergence, smaller antenna size, weight, and power. Unfortunately, the smaller beam divergence makes the system susceptible to performance degradation due to mechanical vibrations. The feasibility of the described information network depends on the laser positioning technology capable of offset adverse effects of satellite jitter. This work addresses a small but important part of laser communication technology: further improvement of position control of satellite-borne communication lasers by the application of advanced control.

Adaptive control techniques can significantly improve accuracy and dynamic performance of the existing pointing-acquisition-tracking (PAT) mechanisms used in laser communication systems. Although such systems utilize the most advanced materials and technologies, their performance is adversely affected by the exposure to jitter and natural transients (bending modes) of moving mechanical parts. The main motivation for this research effort is in the fact that application of advanced control procedures, implemented in software, can further improve performance characteristics of a laser beam steering system and assure its high performance over long period of time. The Model Reference (MR) approach has been developed in adaptive control as a technique, capable of "forcing" a control system to follow a particular performance pattern represented by a reference model. It can be said that MR approach utilizes the feedback principle for "controlling the controller" of the original system. As such, MR results in the reduction of system sensitivity to external forcing functions (disturbances) and parameter perturbations of the controlled process. While MR control systems exhibit

high degree of robustness, their control efforts are consistently lower than that of robust control systems with fixed controllers. At the same time, increased amount of calculations, implementing MR control laws, does not constitute a difficulty for modern microprocessors.

Originally, the MR approach was suggested for the modification of the dynamic response of optical mirrors. It allowed to extend performance limits of an optical mirror and improve its dynamics by elimination of bending modes. MR control laws can be applied to reliable but inexpensive microelectronic devices, often just by the modification of software of already existing microprocessor systems. Therefore, the approach facilitates application of relatively simple, reliable, and relatively inexpensive hardware with performance characteristics significantly extended by advanced control schemes.

Effects of satellite jitter on the beam positioning system are quite similar to the effects of bending modes of the optical mirror. The MR approach implies that the response of the existing physical system is "forced" to follow the response of a simulation model implemented in software. The model is subjected to the same commanded input as the beam positioning system, but the model response is not affected by jitter (or any other undesirable effects). While the MR scheme eliminates any discrepancy between the responses of the physical system and the model, it has the potential for jitter rejection.

As with any physical system subjected to long term effects of adverse operational conditions and natural wear, performance of a beam positioning system is expected to deteriorate with time. The required system dynamics, represented by the simulation code of a reference model, is time-invariant. Therefore, the required performance characteristics of a beam positioning system can be assured and maintained via application of the MR approach. It is important that MR technology does not require any additional hardware and numerically is much simpler than the feedforward adaptive jitter compensation.

An investigation of MR applications for reduction of jitter effects and maintaining the required performance characteristics of a beam positioning system over long periods of system operation is conducted. Numerically efficient computational schemes of MR

procedures are defined and tested, both by simulation and experimentally.

The probability of burst errors in an intersatellite lasercom system is dependent, among other factors, on the laser power and laser positioning accuracy. The approach, presented herein, results in increased accuracy of beam positioning. This implies that the required probability of communication errors can be achieved with lower power of the laser beam. Operation of the laser source at a "lower than nominal" power level results in the improved reliability of power electronics. In addition, although solar energy presents an inexhaustible power source, reduced power consumption can be beneficial for extending life time of satellite batteries. Some analyses of the accuracy/power trade-off, leading to the definition of a control law governing the laser power as a function of time-varying beam positioning errors, are obtained. Application of such a law would result in the optimal use of the available power sources, and increased reliability of power electronics.

A further investigation and application of the suggested control law, including analysis of the distribution laws of beam intensity, definition of probability density function required for the analysis of burst error probability, development of a numerical procedure and computer code, is recommended.

The experimental part of the proposed studies is conducted on the PAT testbed of US Air Force Rome Laboratory with the participation of Dr. Timothy E. Busch [21].

1. MATHEMATICAL DESCRIPTION AND COMPUTER SIMULATION OF BEAM STEERING MIRRORS

The use of optical frequencies results in narrow beams and less beam spreading as the beam propagates over the intervening distances between satellites. As a result, a much higher degree of pointing and tracking accuracy are required. Beam steering devices are used to provide fine steering and to stabilize the line of sight of the transmitting beam from platform jitter. The devices fall into the two categories of non-mechanical and mechanical systems. Mechanical devices are mirrors that are attached to a tip/tilt platform and steer the beam through the movment of the mirror. Two types of mirrors are commonly in use. One represents the state of the art in high bandwidth beam steering while the other is a low cost, commercially available device with substantially poorer performance. Both beam steering mechanical systems are subjected to mathematical description and simulation models.

1.1 High bandwidth fine steering mirror

This beam steering system includes a primary surface mirror, two axis flexures, a support structure, eight actuators and four position sensors [1,2]. It is intended for stereeng the beam along the azimuth and elevation axes. Moving mechanical parts of the mirror are balanced so that the mirror assembly would not impart any additional vibrations to the space vehicle.

Mathematical models facilitate the investigation of various control system strategies were established on the basis of a series of laboratory tests. A preliminary mathematical model of the mirror, and quadrant detector including their drive circuitry, was established on the basis of input/ output measurements. This model was then used to formulate and justify by computer simulation some novel control techniques [9,14,15]. However, attempts to implement the controller based on this model revealed that it was unable to accurately predict the systems performance. This led to the development of a much more detailed model. The development of both models is presented below.

A. Simple model of high bandwidth fine steering mirror. During the laboratory tests, voltage signals were applied to the azimuth and elevation inputs of the mirror drive system. The responses of the mirror position were recorded by a PC with the sampling

period of 25×10^{-6} sec connected to the output of the position subsystem. The LAB VIEW software package was utilized for the implementation of data acquisition system.

Mathematical model of the mirror dynamics was defined as follows:

$$\begin{bmatrix} A(s) \\ E(s) \end{bmatrix} = \begin{bmatrix} G_{AA}(s) & G_{AE}(s) \\ G_{EA}(s) & G_{EE}(s) \end{bmatrix} \begin{bmatrix} V_A(s) \\ V_E(s) \end{bmatrix} \qquad (1.1)$$

where

A(s) and E(s) are the azimuth and elevation mirror positions, represented by the electrical signals of the position sensors,

$V_A(s)$ and $V_E(s)$ are voltage signals applied to the mirror drive system,

$G_{AA}(s)$ and $G_{EE}(s)$ are transfer functions describing the main dynamic channels of the mirror,

$G_{EA}(s)$ and $G_{AE}(s)$ are transfer functions, representing the cross-effects between the main dynamic channels of the mirror (so-called cross-coupling terms), and

argument s is the Laplace variable.

The following tasks were performed:

1) a 5 Hz square wave voltage signal with a magnitude of 0.05 V was applied to the azimuth input of the mirror drive. Responses $A(s)=G_{AA}(s)V_A(s)$ and $E(s)=G_{EA}(s)V_A(s)$ to this signal were recorded. The choice of the 5 Hz frequency of the input signal provided sufficient time for these responses to reach steady state. The responses contain complete information for the estimation of transfer functions $G_{AA}(s)$ and $G_{EA}(s)$.

2) a 5 Hz square wave voltage signal with a magnitude of 0.05 V was applied to the elevation input of the mirror drive. Responses $E(s)=G_{EE}(s)V_E(s)$ and $A(s)=G_{AE}(s)V_E(s)$ to this signal were recorded. The responses contain complete information for the estimation of transfer functions $G_{EE}(s)$ and $G_{AE}(s)$.

3) experiments 1) and 2) were repeated with a step magnitude of 0.025 V to detect possible nonlinearities in the mirrors characteristics. This is done to insure that

we are operating in a linear portion of the mirrors response.

4) experiments 1), 2), and 3) were conducted several times to assure the repeatability of the results.

The following figures represent the recorded responses of the mirror system.

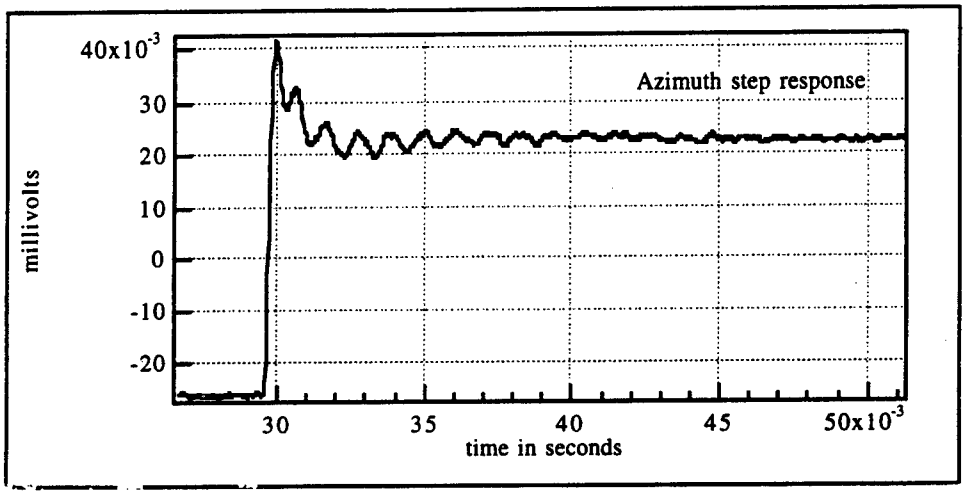

Figure 1-1. Step response of the azimuth channel to the azimuth input.

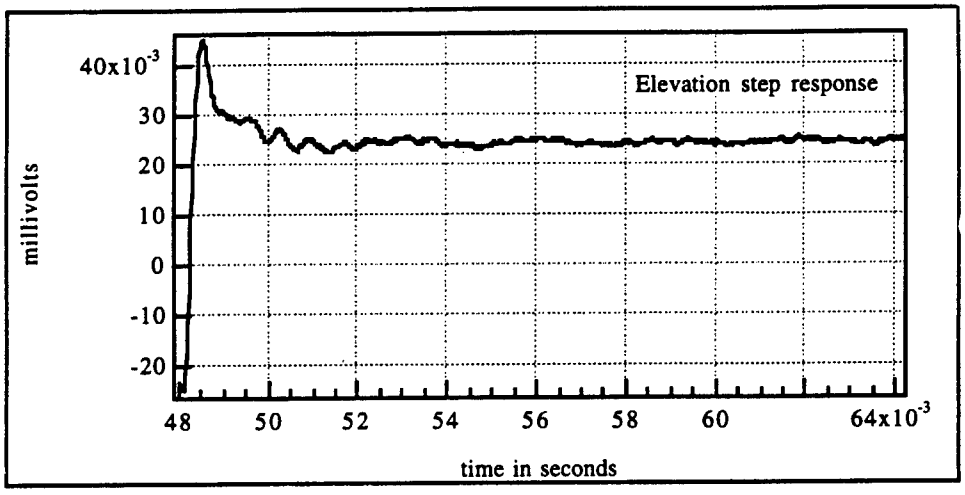

Figure 1-2. Step response of the elevation channel to the elevation input.

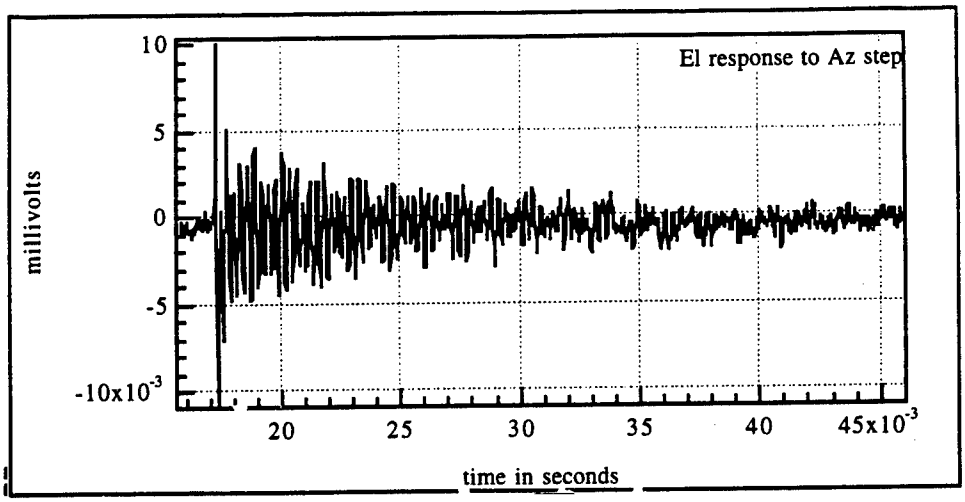

Figure 1-3. Step response of the elevation channel to the azimuth input.

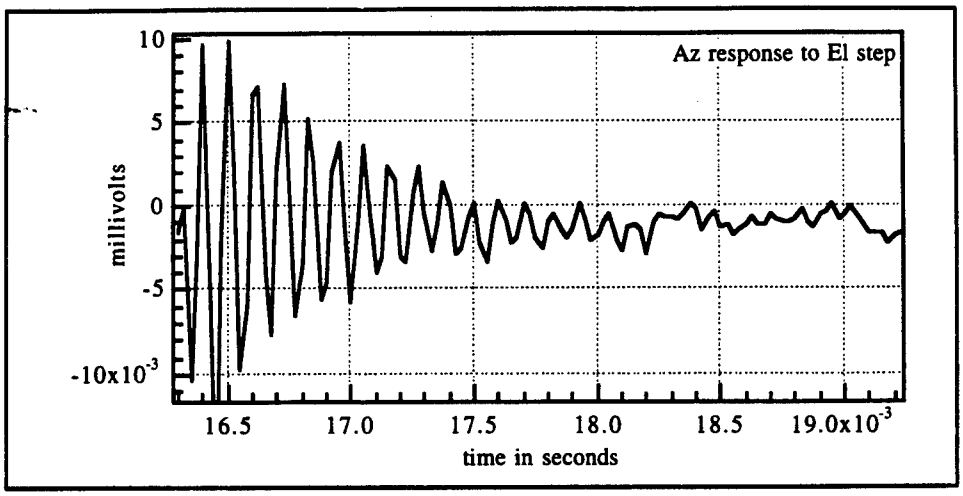

Figure 1-4. Step response of the azimuth channel to the elevation input.

Analysis of the obtained responses indicates that

• dynamics of Az-to-Az and El-to-El channels is comprised of "main" dynamics and vibration (bending modes). The main dynamics are typical for a "one zero - two complex poles system". The bending modes have a dominant frequency of approximately 1 KHz and settle within .015 seconds

• in addition, the elevation response exhibits a 100 Hz mode with a very low magnitude

• the response of the El-to-Az and Az-to-El channels exhibits a 1 KHz vibration with a settling time of approximately .02 sec

• magnitudes of responses to .025 V signals are approximately 50% lower than magnitudes of responses to .05 V signals which indicates that within this range of magnitudes the system is linear.

The following are the transfer functions describing appropriate dynamic channels of the mirror system were established by analyzing of the above responses of the mirror systems,

$$G_{AA}(s)=\frac{1026(s+1006)}{s^2+8000s+1.1e7}+\frac{18s(1+.000927s)}{s^2+550s+3.e7(1+000027s)}$$

$$G_{EE}(s)=\frac{1039(s+1100)}{s^2+8000s+1.1e6}+\frac{20s}{s^2+460s+3.e7}+\frac{8s}{s^2+375s+8.e5}$$

$$G_{AE}(s)=\frac{100s}{s^2+260s+3.e7}$$

$$G_{EA}(s)=\frac{120s}{s^2+8000s+1.1e6} \qquad (1.2)$$

These transfer functions represent the "main" dynamics of the Az-to-Az and El-to-El channels, and the "undesirable" dynamic components, known as the bending modes. Implemented in the Matlab™ software, transfer functions (1.2) were used to simulate Az and El responses of the mirror position. Parameters of (1.2) were manually tuned to achieve close resemblance of the recorded responses. Simulated step responses are given in Figure 1-5 through Figure 1-8 below.

The obtained results indicate that 5 KHz mirror with the existing control system has the following flaws:

• "unwanted" high frequency oscillatory transient component (bending modes),

• cross coupling between the Az and El channels in the frequency range of the

bending mode,

- nonlinear frequency response within the operational frequency range,
- its bandwidth is definitely below the required 5 Khz.

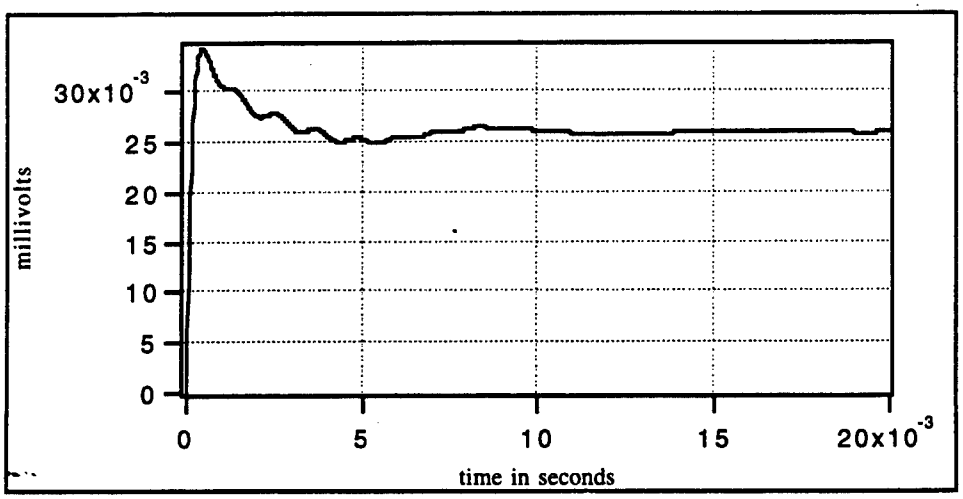

Figure 1-5. Simulated step response of the elevation output to the elevation input.

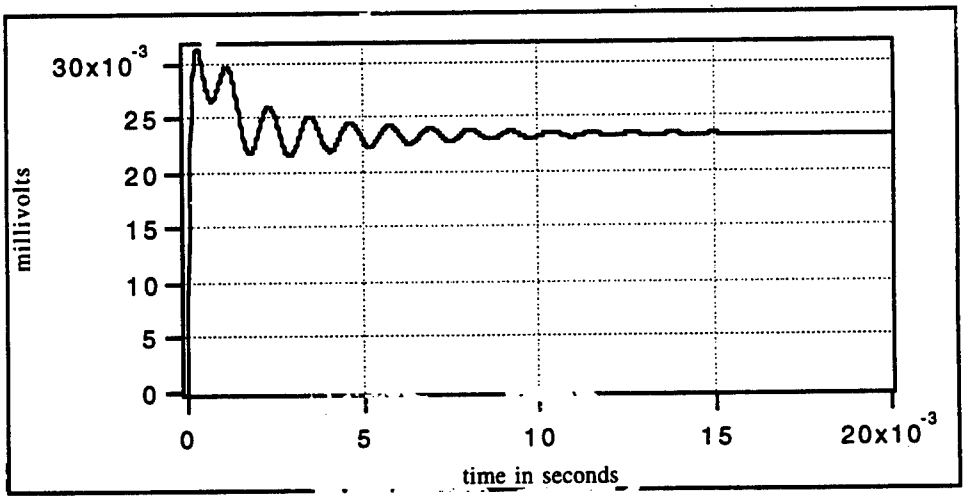

Figure 1-6. Simulated step response of the azimuth output to the azimuth input.

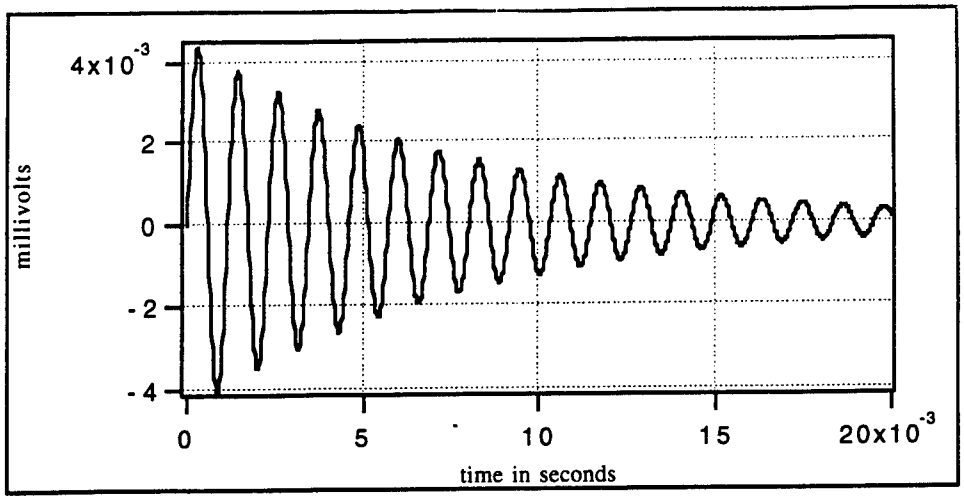

Figure 1-7. Simulated step response of the elevation output to the azimuth input.

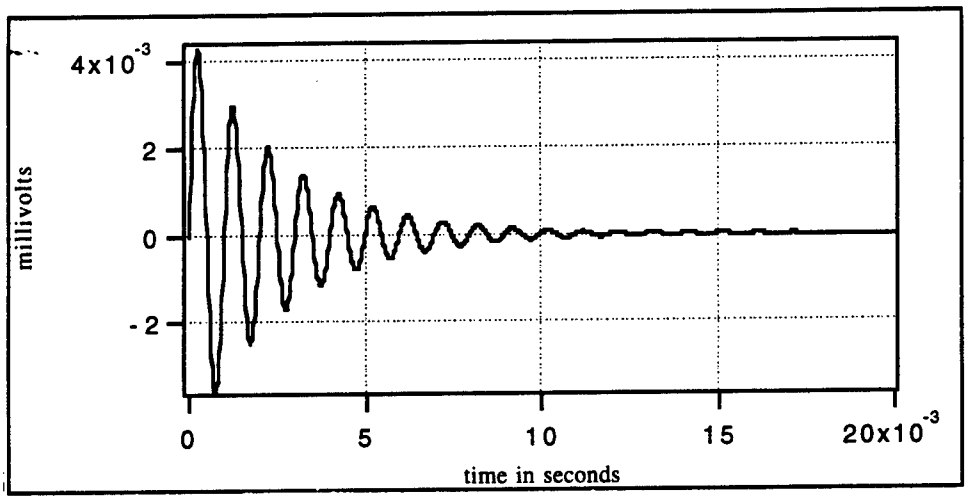

Figure 1-8. Simulated step response of the azimuth output to the elevation input.

B. Detailed model of a high bandwidth fine steering mirror. The simple model of the high bandwidth fine steering mirror was not able to accurately predict the systems response to the addition of the model reference controller. This led to the development of a model with higher fidelity [21]. Although the use of the position sensor allowed for easier measurement of the system, the optical quadrant detector was designated as the

position sensor. This was justified by the fact that in practice the quad cell is the sensor actually used to close the position control loop.

The model was developed based on a series of measurements of the output of the quad cell in response to a step applied directly to the mirror drive amplifier. These were an open loop measurements of the actuator drive amplifier, mirror, and quad cell only. The control electronics were then modeled based on the component values. The following proceedures were followed:

1) The tracking laser from remote terminal #2 was energized.

2) The beam was centered on the quadrant tracking detector using the coarse steering mirrors on the primary station and by bias voltages applied to the fast steering mirror drive circuitry

3) a 0.25 Hz square wave voltage signal with the magnitude of 900 μV was applied to the drive of the M1/3 actuators. Recall that the actuators are located in the corners of the mirrors while the position is measured relative to the upper-lower center of the mirror (elevation) and the left-right center of the mirror (azimuth). This corresponds to a 45° coordinate rotation. Responses $A(s)=G_{M1/3A}(s)V_{M1/3}(s)$ and $E(s)=G_{M1/3E}(s)V_{M1/3}(s)$ to this signal were recorded. The choice of 0.25 Hz frequency of the input signal provided sufficient time for these responses to reach steady-state. These responses contained complete information for the estimation of transfer functions $G_{M1/3A}(s)$ and $G_{M1/3E}(s)$.

4) a 0.25 Hz square wave voltage signal with the magnitude of 900 μV was applied to the drive of the M2/4 actuators. Responses $El(s)=G_{M2/4E}(s)V_{M2/4}(s)$ and $Az(s)=G_{M2/4A}(s)V_{M2/4}(s)$ to this signal were recorded. These responses contained complete information for the estimation of transfer functions $G_{M2/4E}(s)$ and $G_{M2/4A}(s)$.

5) experiments 3) and 4) were repeated with the magnitude of 1.3 mV in order to detect possible nonlinearities in mirror characteristics.

6) experiments 3), 4), and 5) were conducted several times to assure the repeatability of the results.

The recorded step responses are given below. Figure 1-9 shows the response of

the azimuth position to the 900 μV step signal applied to the M1/3 driver. Figure 1-10 shows the response of the elevation position to the 900 μV step signal applied to the M2/4 input. Similar results were obtained for the magnitude of the input signal of 1.3 mV.

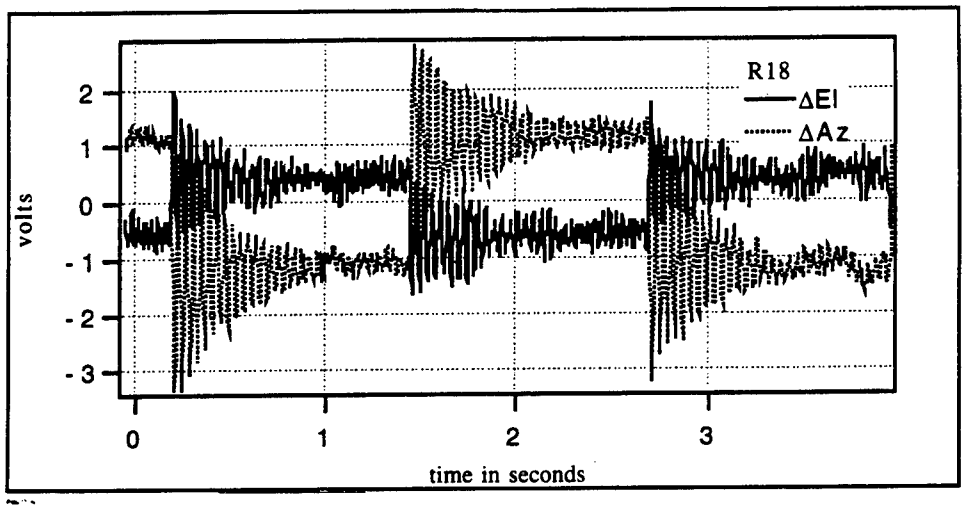

Figure 1-9. Measured azimuth response to voltage applied to actuators M1/3.

The elevation response to the M1/3 input exhibits a settling time of about 0.95 second with an oscillation frequency of 24 Hz with step response that is negative with respect to the input.

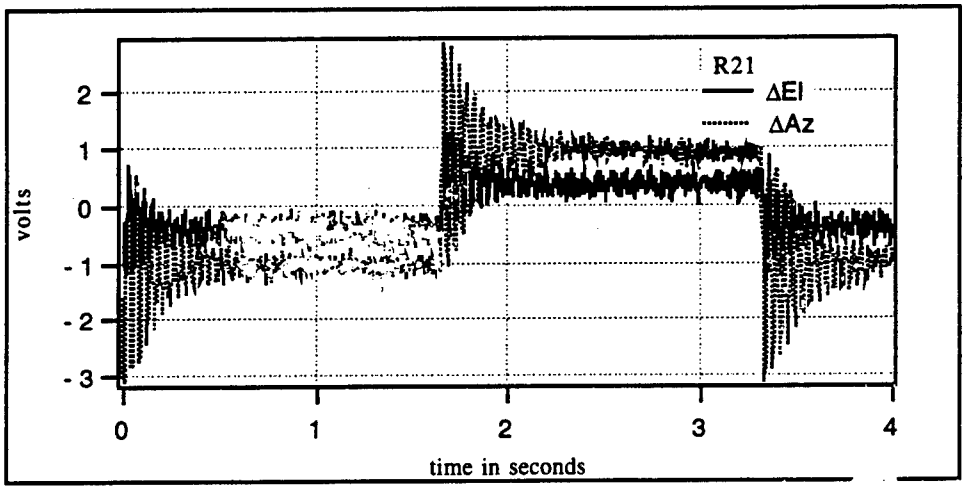

Figure 1-10. Measured elevation response to voltage applied to actuators M2/4.

The azimuth response exhibits a 0.6 second settling time and an oscillation frequency of 25 Hz. The elevation response to the M2/4 input exhibits a settling time of about 0.25 second and a oscillation frequency of 25 Hz.

Analysis of the results once again reveals a response that is consistent with a one zero and two complex pole system. The same proceedure of hand tuning the transfer functions with the MatLab software was used. The resultant transfer functions are:

$$G_{M2/4A}(s)=\frac{754(s+7200)}{s^2+3.3s+24651}$$

$$G_{M@/4E}(s)=\frac{-900(s+3200)}{s^2+5s+24655}$$

$$G_{M1/3A}(s)=\frac{-800(s+6907)}{s^2+4s+24653}$$

$$G_{M1/3E}(s)=\frac{-900(s+3248)}{s^2+8s+24665} \qquad (1.3)$$

Implemented in software, (1.3) were used to obtain the following simulated system responses.

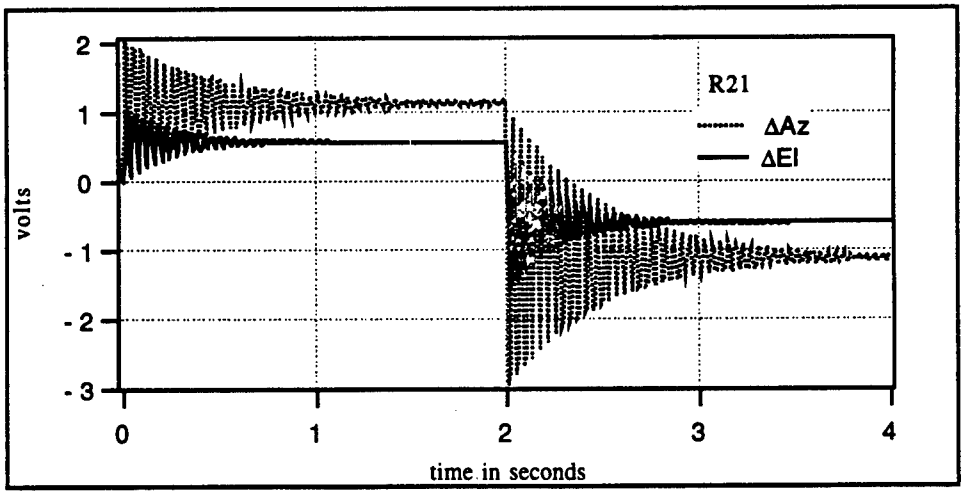

Figure 1-11. Simulated response to excitation of the M2/4 actuators.

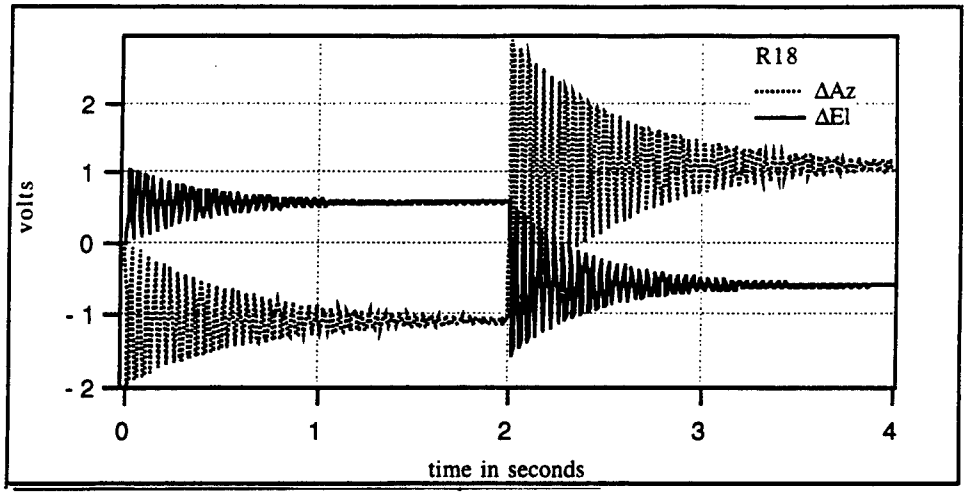

Figure 1-12. Simulated response to excitation applied to the M1/3 actuators.

Once the mirror quad cell model was complete, the control system model was established based on the designed component values and inherent nonlinearities. The resulting overall model is shown as a MATLAB Simulink block diagram in Figure 1-13. The designations for the transfer functions listed in Figure 1-13 relate them to the operational amplifiers shown on the schematics. Operational amplifiers are prefixed with a U for example U10 and I added the sufix letter to designate the appropriate channel (azimuth or elevation). The saturation blocks were added to model the real saturation experienced by the op amps. Saturation occurs a little below the op amp supply voltage of ±15V.

The system was subjected to a ±200 mv square wave with a frequency of 10 Hz. A comparison of the input to output exhibited a 90 μs delay. The delay is implemented in simulink through the use of the Padé approximation.

The ±200 mv square wave was introduced in the system at the mirror controller via the tracking offset port. The input of this signal is applied to U18. The output of the quad cell is measured at the tracking position connector which is connected to the output of U19. Both connectors are BNC type and located on the front pannel of the mirror controller.

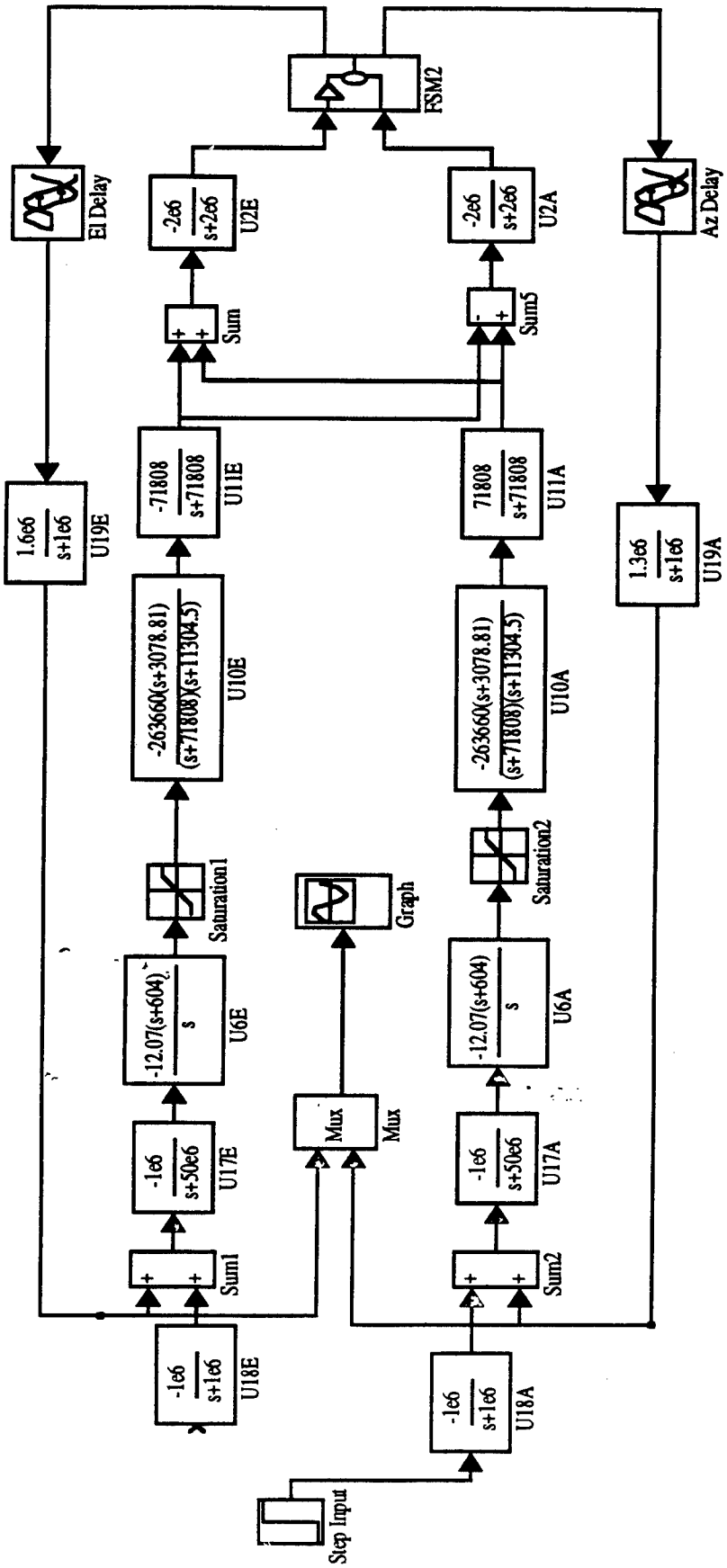

Figure 1-13. Simulink representation of detailed model.

Figure 1-14 and Figure 1-15 show the systems measured response to a square wave applied to the elevation and azimuth input. The data was collected using a Phillips digital oscilloscope and the trace includes a 500 μs delay. Both channels exhibit a 25% overshoot in the principal channel and some cross channel coupling. Notice that this coupling is smaller than presented for the case where the DIT position sensors were used to close the position control loop.

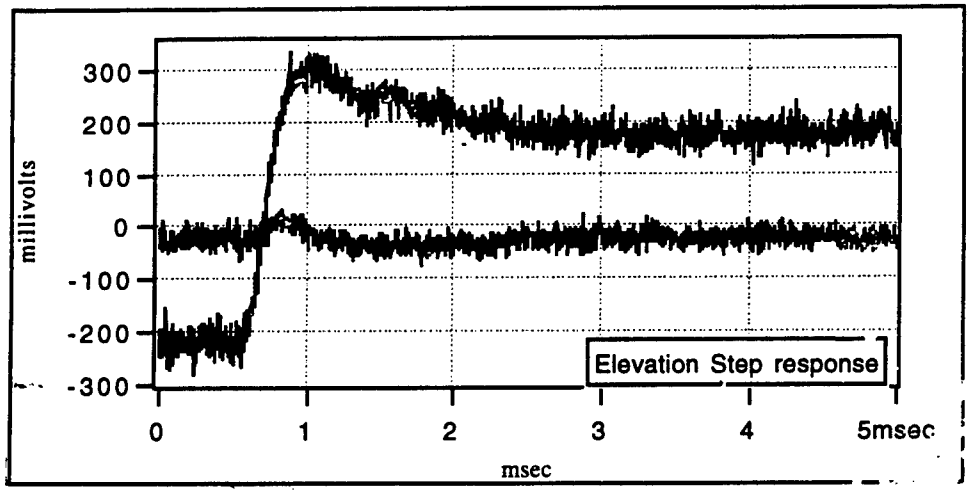

Figure 1-14. Measured response to a step applied to the elevation channel.

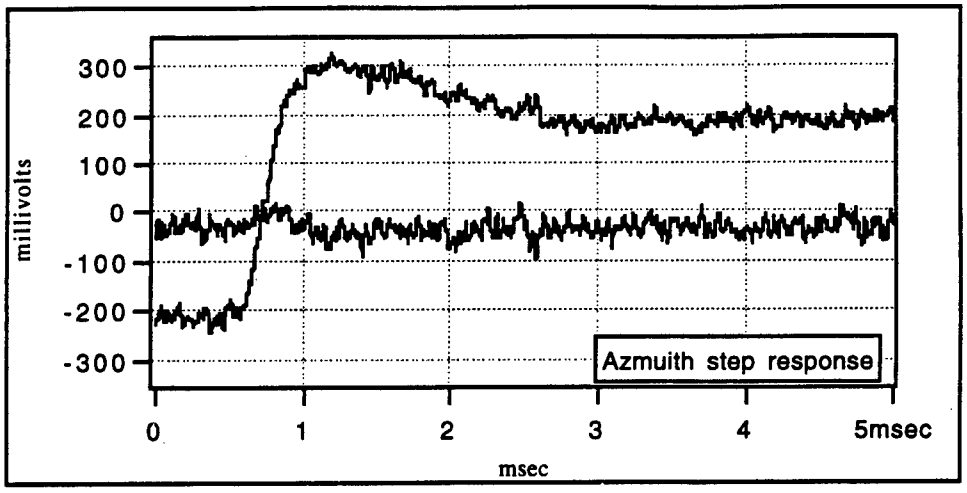

Figure 1-15. Measured response to a step applied to the azimuth channel.

Figure 1-16 and Figure 1-17 show the simulated response to a step input for both the elevation and azimuth channel.

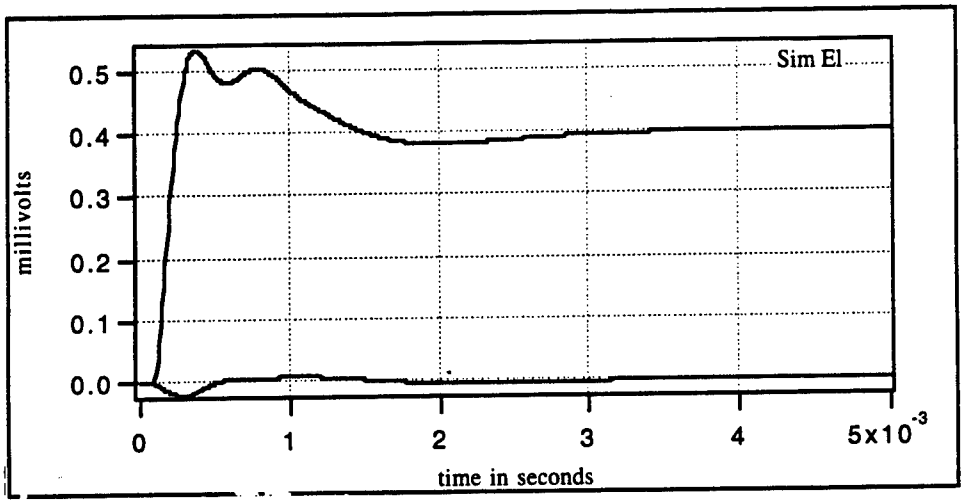

Figure 1-16. Simulated response to a step applied to the elevation channel.

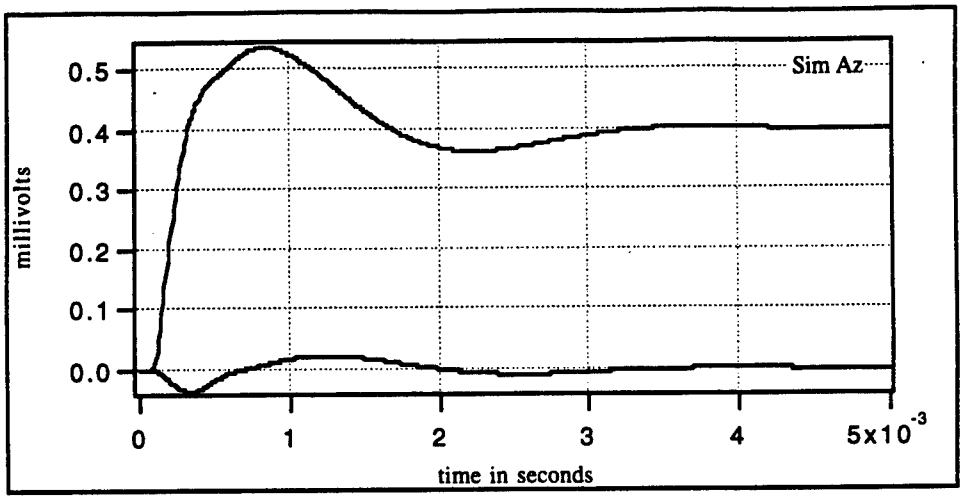

Figure 1-17. Simulated response to a step applied to the azimuith channel.

1.2 Piezo-electric mirror

Piezo-electric mirror intended for fine steering of the laser beam was a Physik Instrumente S-330 Low voltage, 3 axis, tilting mirror. The mathematical model of this mirror, including its control circuitry, is based on the series of transient responses

recorded during laboratory testing. A square wave is applied to each of the input channels and the output of the quadrant detector is recorded. A mathematical model of the system is described as follows:

$$\begin{bmatrix} A(s) \\ E(s) \end{bmatrix} = \begin{bmatrix} G_{A1}(s) & G_{A2}(s) & G_{A3}(s) \\ G_{E1}(s) & G_{E2}(s) & G_{E3}(s) \end{bmatrix} \begin{bmatrix} V_1(s) \\ V_2(s) \\ V_3(s) \end{bmatrix} \qquad (1.4)$$

Once again the following tasks were performed:

1) a 1 Hz square wave voltage signal with a magnitude of 0.02 V was applied to the channel 1 input of the mirror drive. Responses $A(s)=G_{A1}(s)V_1(s)$ and $E(s)=G_{E1}(s)V_1(s)$ to this signal were recorded. The choice of the 5 Hz frequency of the input signal provided sufficient time for these responses to reach steady state. The responses contain complete information for the estimation of transfer functions $G_{A1}(s)$ and $G_{E1}(s)$.

2) a 1 Hz square wave voltage signal with a magnitude of 0.02 V was applied to the channel 2 input of the mirror drive. Responses $A(s)=G_{A2}(s)V_2(s)$ and $E(s)=G_{E2}(s)V_2(s)$ to this signal were recorded. The responses contain complete information for the estimation of transfer functions $G_{A2}(s)$ and $G_{E2}(s)$.

3) a 1 Hz square wave voltage signal with a magnitude of 0.02 V was applied to the channel 3 input of the mirror drive. Responses $A(s)=G_{A3}(s)V_3(s)$ and $E(s)=G_{E3}(s)V_3(s)$ to this signal were recorded. The responses contain complete information for the estimation of transfer functions $G_{A3}(s)$ and $G_{E3}(s)$.

4) experiments 1) , 2) and 3) were repeated with a step magnitude of 0.04 V to detect possible nonlinearities in the mirrors characteristics. This is done to insure that we are operating in a linear portion of the mirrors response.

5) experiments 1), 2), and 3) were conducted several times to assure the repeatability of the results.

Figures 1-18, 1-19, 1-20 below represent the measured step responses of channels 1, 2, and 3 respectivly. These measurements reveal a fairly significant degree of cross

coupling, or exchange of bending moodes as evidenced by the beat present in the channel 2 and 3 response. These responses are consistent with a 3 zero, 4 pole response.

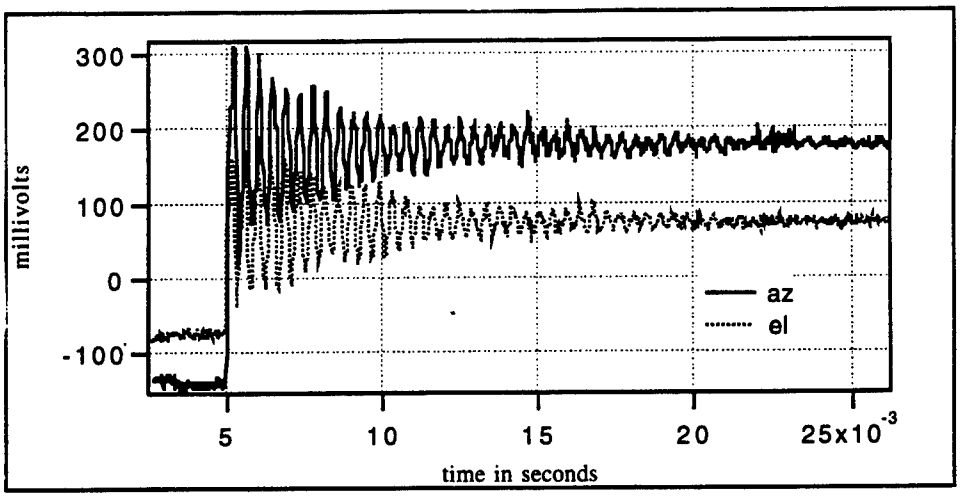

Figure 1-18. Step response for channel 1.

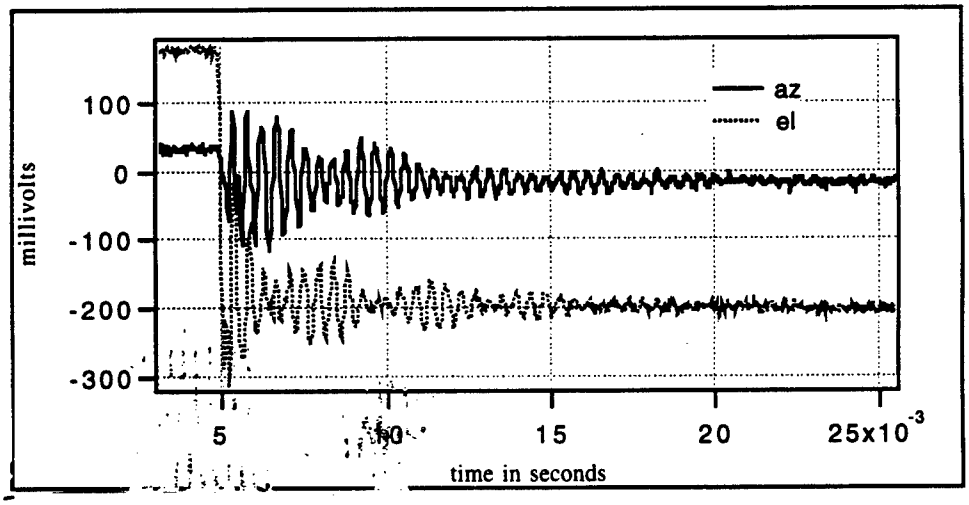

Figure 1-19. Step response for channel 2

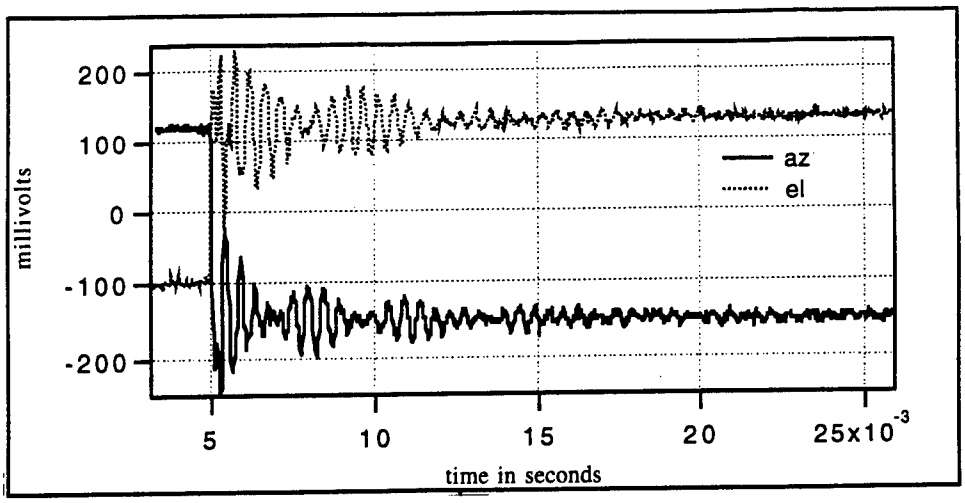

Figure 1-20. Step response channel 3.

A simulation model was developed on the basis of measurements and then hand tuned until it resembled the above responses. Figures 1-21, 1-22, and 1-23 depict the simulated responses of channels 1,2 and 3 of the model. Figure 1-24 represents resultant model in the form of a simulation setup.

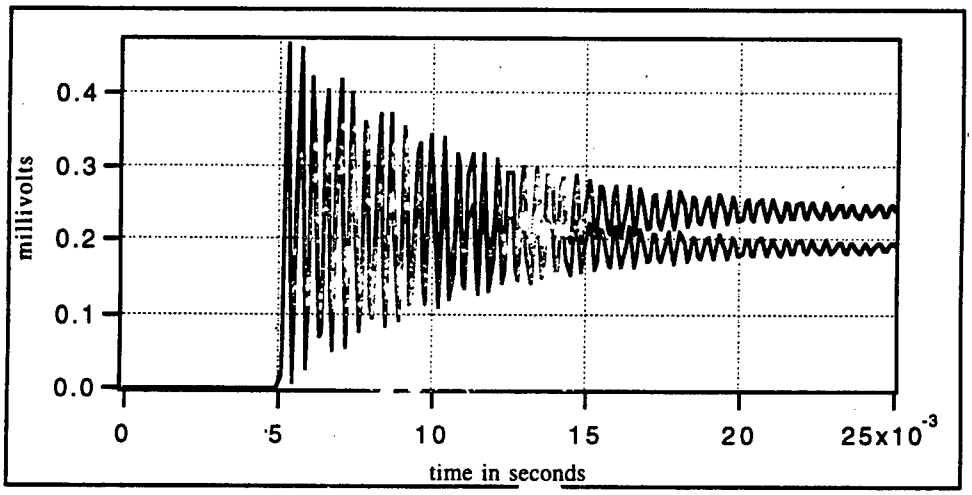

Figure 1-21. Simulated channel 1 step response.

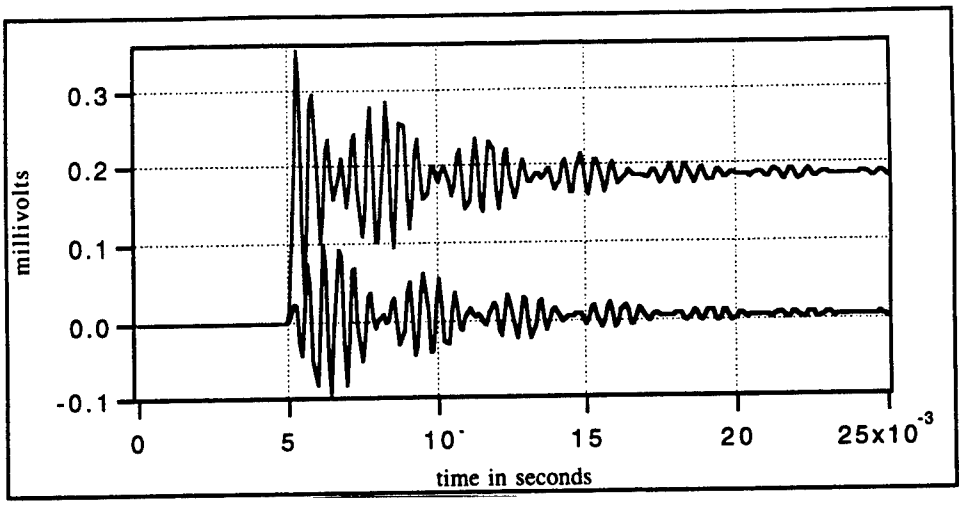

Figure 1-22. Simulated channel 2 step response.

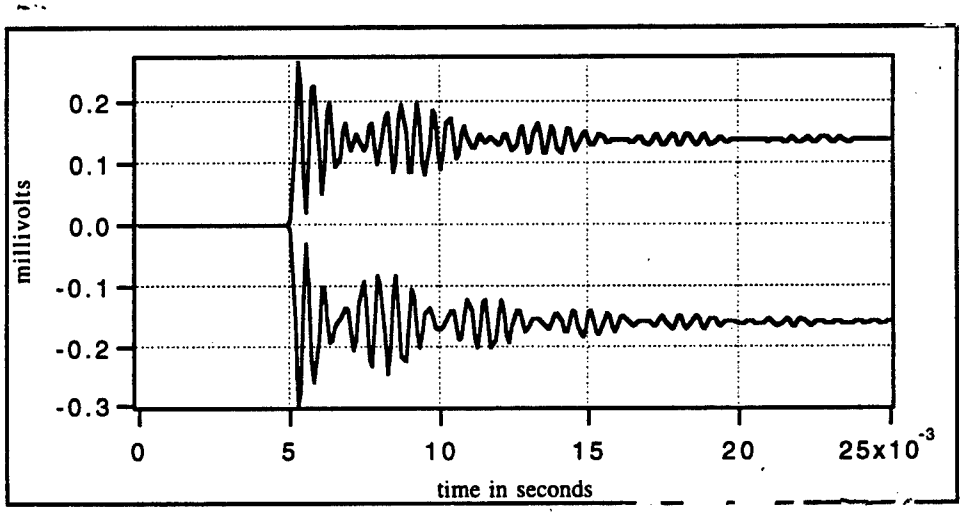

Figure 1-23. Simulated channel 3 step response.

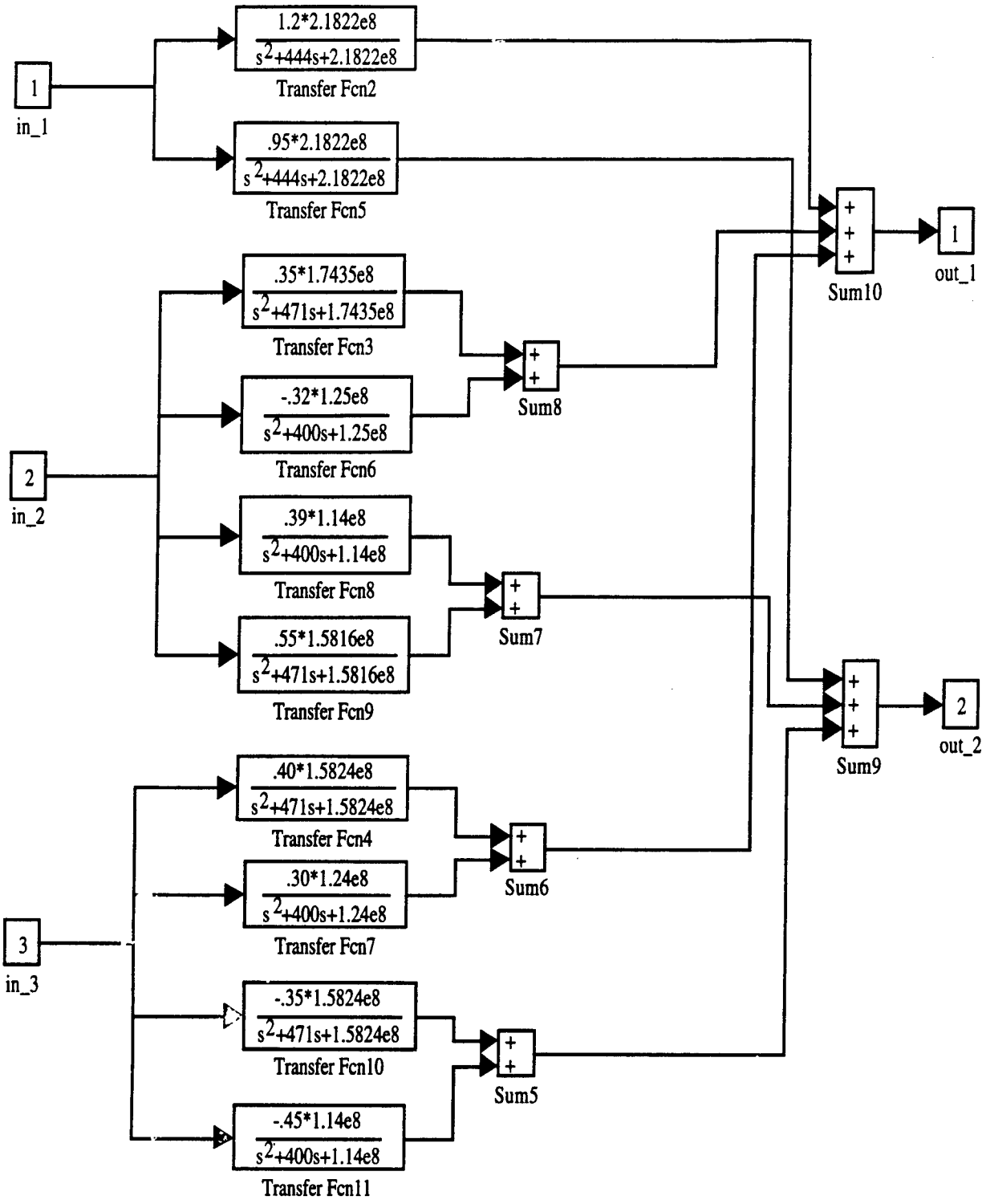

Figure 1-24. Simulink model of piezo mirror.

2. MODEL REFERENCE CONTROL OF BEAM STEERING MIRRORS

A mechanical beam steering element is the critical component of the entire PAT system, responsible for its major operational limitations. Much work has been devoted to the development of high performance/bandwidth steering mirrors and other non-mechanical beam steering devices. Currently, these devices are available only as developmental models and consequently are very expensive. Commonly, a high bandwidth feedback control is used to stabilize mechanical beam steerers.

Applications of advanced control techniques, such as model reference (MR) control, applied to commercially available mirrors provides a means of achieving the required performance at a reasonable cost. MR approach implies that the response of the existing physical system is "forced" to follow the response of a model implemented in analog circuitry or in software. The model is subjected to the same commanded input as the laser beam positioning system, but the model response is "perfect" and not affected by satellite jitter or any other undesirable effects. MR approach was suggested for extending performance limits of an optical mirror and improving its dynamics [12,13,16]. While the MR scheme eliminates any discrepancy between the responses of the physical system and the model, it has the potential for jitter rejection. As with any physical system subjected to long term effects of adverse operational conditions and natural wear, performance of a beam positioning system is expected to deteriorate with time. The required system dynamics, represented by the simulation code of a reference model, is time-invariant. Therefore, the required performance characteristics of a beam positioning system can be assured and maintained via application of MR approach. It is important that MR technology does not require any additional hardware and numerically is much simpler than the feedforward adaptive jitter compensation.

MR approach is suggested for further improvement of the existing pointing-acquisition-tracking (PAT) systems intended for laser communication: reduction of adverse effect of satellite jitter, and increase of system robustness. It can be implemented via a number of schemes. Inherent limitations, advantages and disadvantages of the particular schemes, and various aspects of practical implementation

of this approach are investigated below.

A typical beam steerer includes a high performance optical mirror, drives, position sensors, and feedback control circuitry. The mirror has two control channels, elevation and azimuth. The beam position, defined by a quadrant detector, is controlled by the application of the appropriate control efforts in compliance with the reference signals. While it is desired that dynamic channels be controlled independently, the cross-coupling effects, which can be viewed as the "exchange of bending modes" could be always observed. Analyses of closed-loop dynamics of particular channels indicate nonlinearity and quite limited bandwidth of the appropriate frequency responses. In addition, satellite jitter constitutes a permanent source of beam positioning errors.

Application of MR control schemes has the potential for alleviation of the above listed problems. Conceptually, it implies that a reference model representing the desired closed-loop system performance be established in the form of an analog circuit or a computer code. In a MR scheme, an additional control signal defined by a specially designed controller, "forces" the beam steerer to follow the response of the reference model. Understandably, a reference model not only has perfect dynamic characteristics, but cannot be affected by satellite jitter and hardware deterioration. Therefore, in addition to improved dynamics, this approach results in jitter rejection and increased system robustness. Limitations of the MR approach are related to the limited magnitude of control effort which can be applied to a beam steerer, and the complexity of its implementation.

Conventional MR schemes, capable of decoupling, extended system bandwidth, reduction of jitter effects, and high system robustness, require state-variable implementation and are overly complex (numerically intensive) for many applications. In many instances, when some of the above listed effects are not required, particular simplifications of a "general" MR control can be suggested.

Described below, is a model-following, rather than MR, control scheme utilizes so-called System Error Equation Method. This method results in performance modification and jitter rejection, but not in robust performance. Such an approach can

be recommended when system dynamics is fairly well defined and assumed to be time-invariant. The system utilizes readily available input-output signals.

The second system, described herein, utilizes an adaptive predictor and is intended for digital implementation. It exhibits all features of a MR scheme, but does not require a state observer.

2.1 System Error Equation Method of Model-Following

Consider closed-loop dynamics of a mechanical beam steerer described in the form,

$$Y(s)=G(s)U_P(s) \tag{2.1}$$

the reference model is defined as follows,

$$Y_M(s)=M(s)U(s) \tag{2.2}$$

the output error is defined as,

$$E(s)=Y_M(s)-Y(s) \tag{2.3}$$

and the controller implementing the MR concept is,

$$U_P(s)=U(s)+W(s)E(s) \tag{2.4}$$

where

$G(s)=[g_{ij}(s),\ i,j=1,2]$ and $M(s)=[m_{ij}(s),\ i,j=1,2]$ are appropriate transfer matrices; it is expected that G(s) is non-diagonal, and M(s) is a diagonal matrix,

$Y=[y_1\ y_2]'$, and $Y_M=[y_{M1}\ y_{M2}]'$ are elevation and azimuth position components of the existing beam steerer and the reference model,

$U_P=[u_{P1}\ u_{P2}]'$, and $U=[u_1\ u_2]'$ are control signals applied to the existing beam steerer and to the reference model (also known as the commanded input), and

$W(s)=[w_{ij}(s),\ i,j=1,2]$ is the MR controller.

Rewrite equation (2.1) as follows,

$$Y(s)=G(s)U(s)+G(s)W(s)E(s)=G(s)U(s)+G(s)W(s)[Y_M(s)-Y_P(s)]=$$

$$G(s)U(s)+G(s)W(s)Y_M(s)-G(s)W(s)Y_P(s),$$

then

$$Y(s)+G(s)W(s)Y_P(s)=G(s)U(s)+G(s)W(s)Y_M(s), \text{ or}$$

$$[I+G(s)W(s)]Y(s)=[G(s)+G(s)W(s)M(s)]U(s)$$

Finally,

$$Y(s)=[I+G(s)W(s)]^{-1}G(s)[I+W(s)M(s)]U(s) \quad (2.5)$$

Redefine the output error as

$$E(s)=\{M(s) - [I+G(s)W(s)]^{-1}G(s)[I+W(s)M(s)]\}U(s) \quad (2.6)$$

Define an arbitrary transfer matrix

$$Q(s)=[q_{ij}(s), i,j=1,2] \quad (2.7)$$

representing the desired dynamics of the "commanded input - error" channels. The implication of the word "desired" are,

- transfer matrix Q(s) must be stable,
- settling time not to exceed 1/2 of the settling time of the reference model, and
- sufficiently small steady-state values of the error response, which can be assured by $\|Q(0)\| < 1$

Note, that there is no need to achieve the error decoupling. Then the following equation should be established,

$$M(s) - [I+G(s)W(s)]^{-1}G(s)[I+W(s)M(s)]=Q(s) \quad (2.8)$$

which results in the definition of the controller W(s),

$$W(s)=G(s)^{-1}M(s)Q(s)^{-1} - G(s)^{-1} - Q(s)^{-1} \quad (2.9)$$

It should be noted that the major advantage of this approach is a very high flexibility in the particular choice of error equation matrix Q(s). Indeed, upon exploration of equation (9) allows for the choice of such Q(s) which would result in the sufficiently simple definition of the controller W(s). The disadvantage of this approach is quite typical of any linear model-following design: it implies that matrix G(s) is accurately known and time-invariant. However, according to our preliminary results, the developed model-following scheme can be successfully extended to a MR scheme utilizing input-output signals.

The following numerical example is based on a simplified mathematical

description of a beam steerer. Particular elements of the matrix G(s) are,

$g_{11}(s)=2.6186E8/(s^2+444s+2.1822E8)$

$g_{12}(s)=2.0731E8/(s^2+444s+2.1822E8)$

$g_{21}(s)=1.E8[1.005s^2+428.39s+1.3735E8]/[(s^2+471s+1.5824E8)(s^2+400s+1.24E8)]$

$g_{22}(s)=-1.E8[1.067s^2+463.16s+1.4985E8]/[(s^2+471s+1.5824E8)(s^2+400s+1.24E8)]$ (2.10)

The reference model transfer matrix is defined as,

$$m_{11}(s)=m_{22}(s)=3000/(s+3000)$$

$$m_{12}(s)=m_{21}(s)=0$$

The following is the definition of the "error transfer matrix" Q(s),

$$q_{11}(s)=q_{22}(s)=.001*s/(s+6000)$$

$$q_{12}(s)=q_{21}(s)=0$$

leading to the definition of controller W(s),

$$w_{11}(s)=-1.E11w_0(s)[2.6s^4+1.925E4s^3+1.87E8s^2+1.23E12+1.49E15]$$

$$w_{12}(s)=37.1w_0(s)[(s^2+426s+1.37E8)(s^2+444s+2.18E8)(s^2+400s+1.14E8)]$$

$$w_{21}(s)=76.5w_0(s)[(s^2+471s+1.58E8)(s^2+400s+1.14E8)(s^2+400s+1.24E8)]$$

$$w_{22}(s)=-1.E11w_0(s)[3.24s^4+3.29E4s^3+2.72E8s^2+1.86E12+5.09E15]$$

where

$$w_0(s)=[s(s+3000)(s^4+831s^3+2.56E8s^2+1.059E11s+1.62E16]^{-1}$$

Computer simulation results, see pages 30, 31, indicate that the obtained controller, even after reasonable simplification, is capable of "enforcing" the required system dynamics on the beam steerer and reduced the effect of satellite jitter on the beam positioning accuracy.

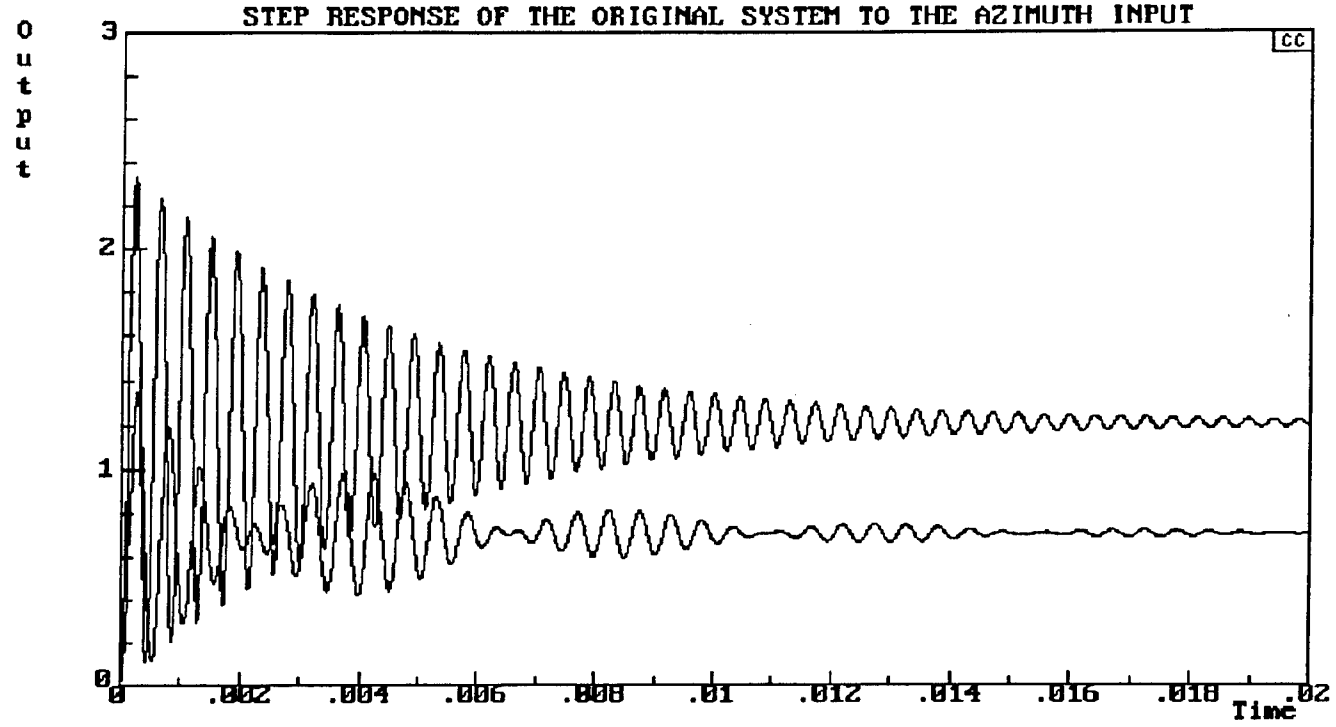
STEP RESPONSE OF THE ORIGINAL SYSTEM TO THE AZIMUTH INPUT
CC
Output
3
2
1
0
0
.002
.004
.006
.008
.01
.012
.014
.016
.018
.02
Time

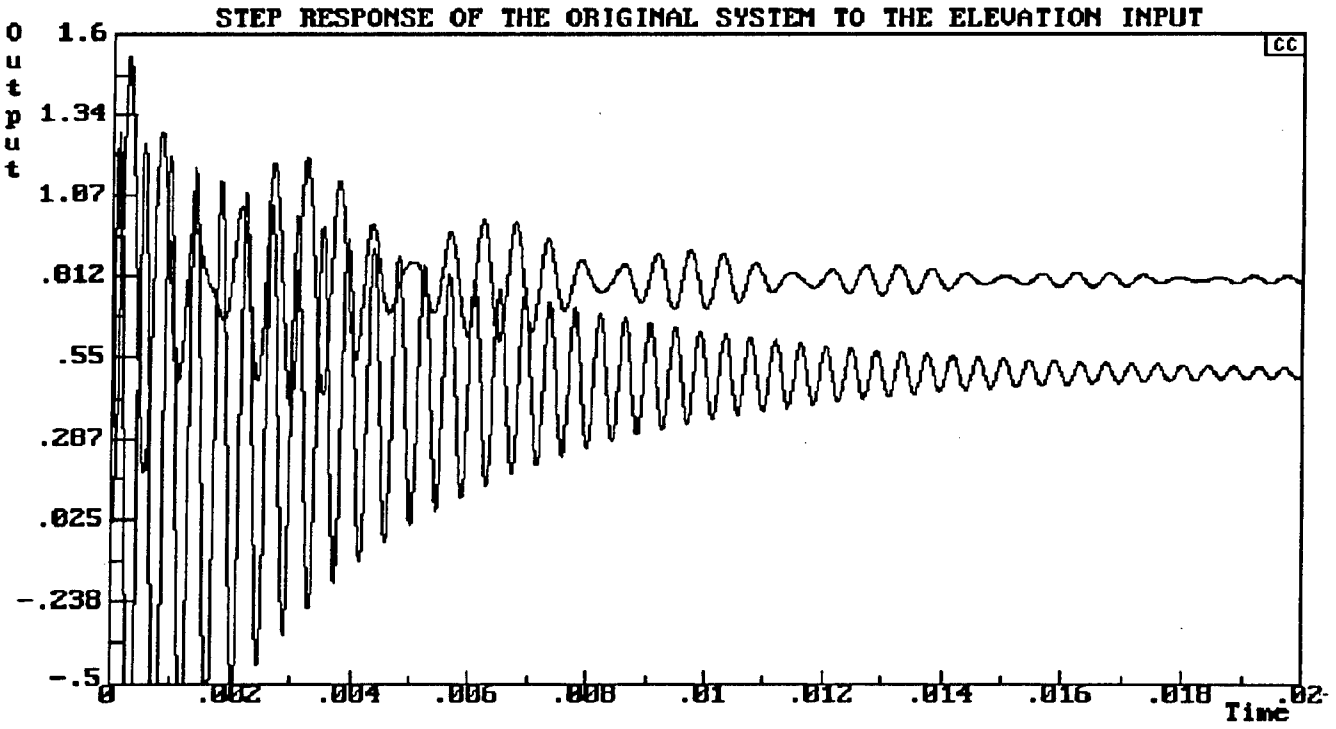
STEP RESPONSE OF THE ORIGINAL SYSTEM TO THE ELEVATION INPUT
CC
Output
1.6
1.34
1.07
.812
.55
.287
.025
-.238
-.5
0
.002
.004
.006
.008
.01
.012
.014
.016
.018
.02
Time

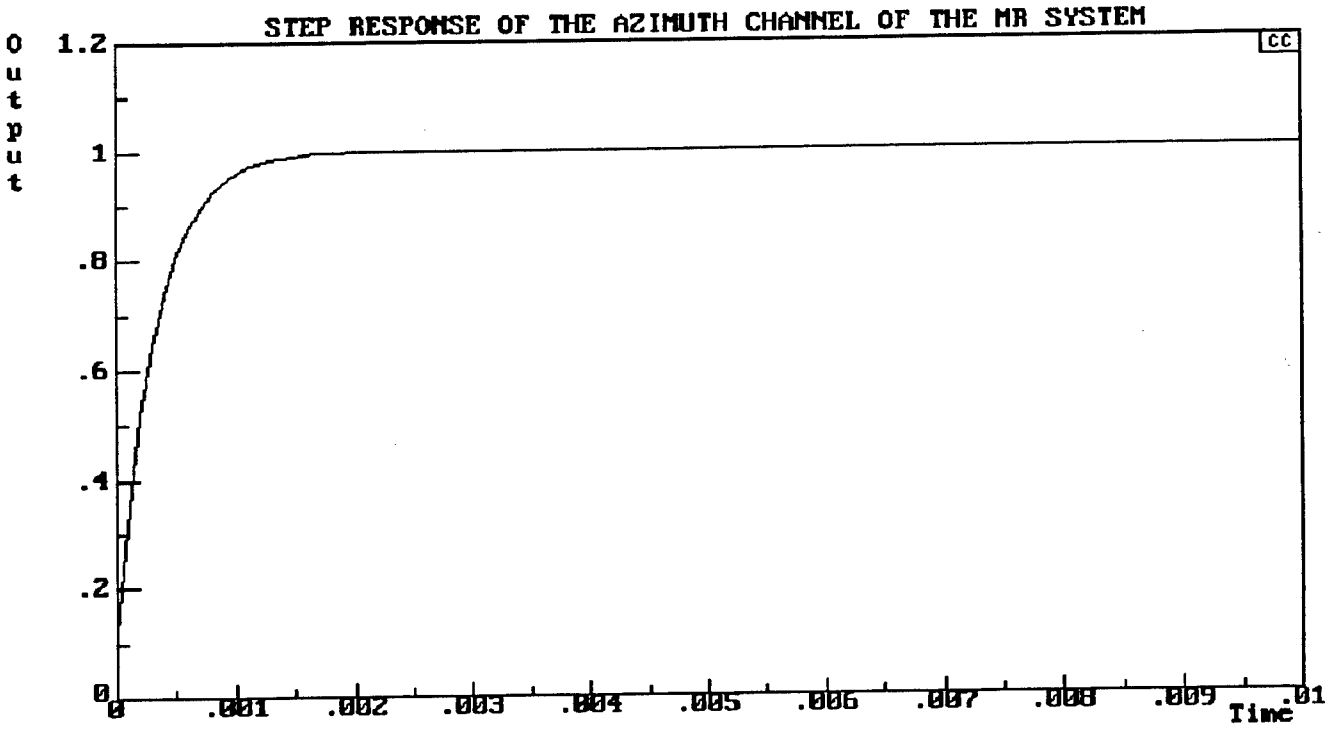
STEP RESPONSE OF THE AZIMUTH CHANNEL OF THE MR SYSTEM
CC
Output
1.2
1
.8
.6
.4
.2
0
0
.001
.002
.003
.004
.005
.006
.007
.008
.009
.01
Time

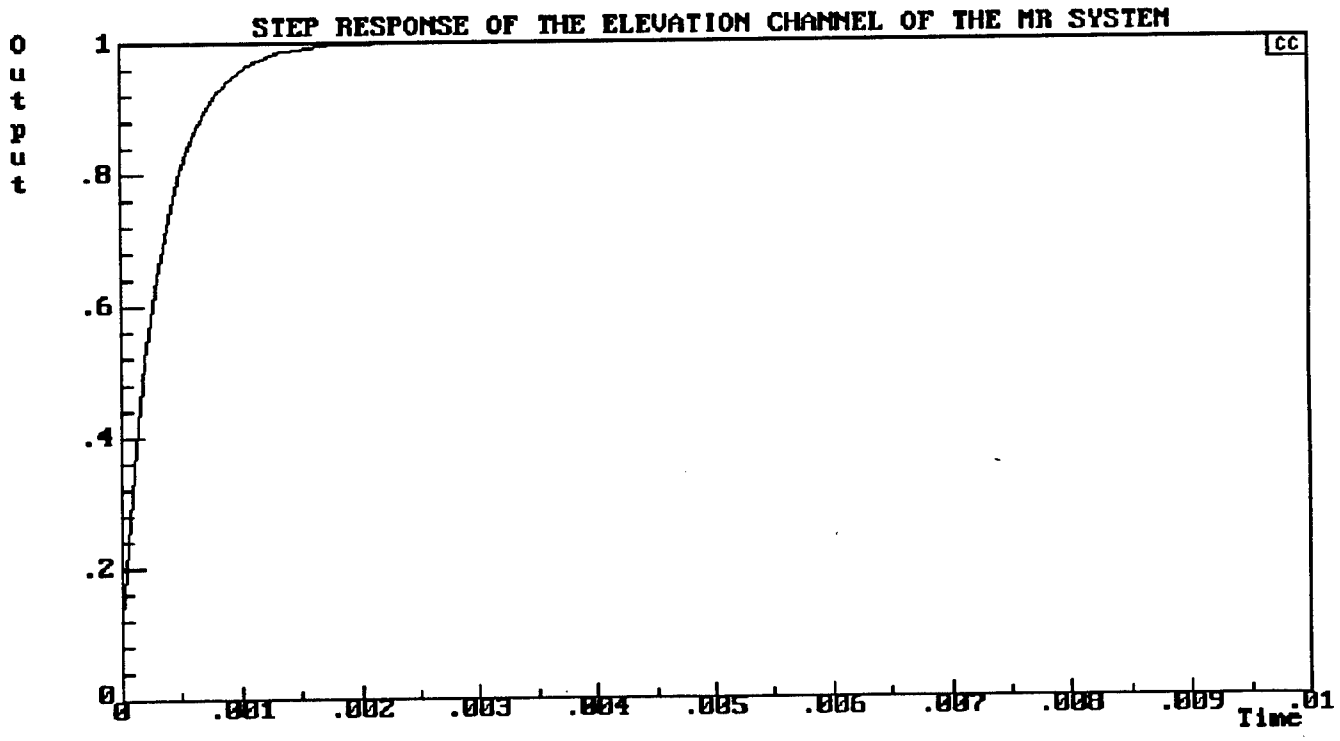
STEP RESPONSE OF THE ELEVATION CHANNEL OF THE MR SYSTEM
CC
Output
1
.8
.6
.4
.2
0
0
.001
.002
.003
.004
.005
.006
.007
.008
.009
.01
Time

2.2 System Error Equation Method. State-Variable Formulation

Consider a controlled plant and a reference model and defined by state equations:

$$X'=A_PX+B_PU_P \qquad (2.11)$$

$$Z'=A_MZ+B_MU \qquad (2.12)$$

where

$X=[x_1, x_2,...,x_n]^T$ and $Z=[z_1, z_2,...,z_n]^T$ are transposed state vectors of the controlled plant and the model,

U and U_P are vectors of reference signals (commanded input) and control effort applied to the plant and the model through matrices B_P and B_M,

A_P and A_M are fundamental matrices of the controlled plant and the reference model, and

^{T} is transpose symbol.

Define the state generalized error as:

$$E=Z-X \qquad (2.13)$$

The control law is defined as follows:

$$U_P=-K_PX+K_UU+WE \qquad (2.14)$$

where

K_P represents the existing state-variable feedback controller,

K_U is the matrix gain in the reference channel, and

W is the matrix representing the model reference controller, responsible for the elimination of the discrepancy between the state vectors of the plant and the model.

Redefine the plant with its state-variable feedback:

$$X'=A_PX-B_PK_PX+B_PK_UU+B_PWE \qquad (2.15)$$

Obtain and transform the expression of the error derivative:

$E'=Z'-X'$, or

$E'=A_MZ+B_MU-A_PX+B_PK_PX-B_PK_UU-B_PWE$, or

$E'=A_MZ+B_MU-A_P(Z-E)+B_PK_P(Z-E)-B_PK_UU-B_PWE$, or

$$E' = A_M Z + B_M U - A_P Z + A_P E + B_P K_P Z - B_P K_P E - B_P K_U U - B_P W E, \text{ or}$$

$$E' = A_P E - B_P K_P E - B_P W E + A_M Z - A_P Z + B_P K_P Z + B_M U - B_P K_U U, \text{ or}$$

$$E' = (A_P - B_P K_P - B_P W)E + (A_M - A_P + B_P K_P)Z + (B_M - B_P K_U)U \qquad (2.16)$$

Note that matrix-vector equation (2.16) describes dynamics of the state generalized error driven by two "external" signals, commanded input U, and state vector of the reference model, Z. One should realize that both signals, U(t) and Z(t), are "well behaving" signals, and therefore, the desired convergence rate of error E is dependent upon matrix $Q = A_P - B_P K_P - B_P W$.

Introduce matrix a $n \times n$ matrix Q such that,

- its eigenvalues assure the necessary error convergence rate,
- $\|Q^{-1}(A_M - A_P + B_P K_P)\| < 1$ and $\|Q^{-1}(B_M - B_P K_U)\| < 1$

to assure small steady-state error values of the "natural motion" terms of the error.

Then, the following expression for the model reference controller can be obtained:

$$W = B_P^{-1}(A_P - Q) - K_P \qquad (2.17)$$

It can be seen that the existence of a solution requires that matrix B_P be non-singular.

Numerical example.

Assume the following definition of the controlled plant and the reference model:

$$A_P = \begin{bmatrix} 0 & 1 & 0 & 0 & 0 & 0 \\ 0 & 0 & 1 & 0 & 0 & 0 \\ -2 & 0 & 3 & 0 & 0 & 0 \\ 0 & 0 & 0 & 0 & 1 & 0 \\ 0 & 0 & 0 & 0 & 0 & 1 \\ 0 & 0 & 0 & 1 & 2 & 2 \end{bmatrix} \quad B_P = \begin{bmatrix} 0 & 0 \\ 0 & 0 \\ 1 & .8 \\ 0 & 0 \\ 0 & 0 \\ -.8 & 1 \end{bmatrix}$$

$$A_M = \begin{bmatrix} 0 & 1 & 0 & 0 & 0 & 0 \\ 0 & 0 & 1 & 0 & 0 & 0 \\ -2800 & -710 & -56 & 0 & 0 & 0 \\ 0 & 0 & 0 & 0 & 1 & 0 \\ 0 & 0 & 0 & 0 & 0 & 1 \\ 0 & 0 & 0 & -2800 & -710 & -56 \end{bmatrix} \quad B_M = \begin{bmatrix} 0 & 0 \\ 0 & 0 \\ 1 & 0 \\ 0 & 0 \\ 0 & 0 \\ 0 & 1 \end{bmatrix}$$

One can realize that the controlled plant is coupled, and the reference model is uncoupled and reflects the following design specifications: overshoot of 0% and settling time of .5 sec. The following state-variable controller was introduced in the system:

$$K_p = \begin{bmatrix} 248 & 105 & 21 & 0 & 0 & 0 \\ 0 & 0 & 0 & 251 & 107 & 20 \end{bmatrix}$$

which indicates that the designers of the original system were interested in the overshoot of 0% and settling time of 1 sec for each dynamic channel. The matrix gain in the reference channel of this system was defined as

$$K_U = \begin{bmatrix} 250 & 0 \\ 0 & 250 \end{bmatrix}$$

Simulated step responses of the designed system are shown on page 35. They indicate that the designed system exhibits cross-coupling between channels. However, in the situation when parameters of the plant are not accurately known, it could be expected that system performance will be much more different from the original design specifications.

Introduction of the MR controller is expected to significantly modify system performance and reduce the cross-coupling effects. Following the equation error approach, first introduce matrix Q:

$$Q = \begin{bmatrix} 0 & 1 & 0 & 0 & 0 & 0 \\ 0 & 0 & 1 & 0 & 0 & 0 \\ -16100 & -1210 & -60 & 0 & 0 & 0 \\ 0 & 0 & 0 & 0 & 1 & 0 \\ 0 & 0 & 0 & 0 & 0 & 1 \\ 0 & 0 & 0 & -16100 & -1210 & -60 \end{bmatrix}$$

which reflects the requirement that state generalized error converge within .4 sec

Now the MR controller represented by matrix W can be defined according to

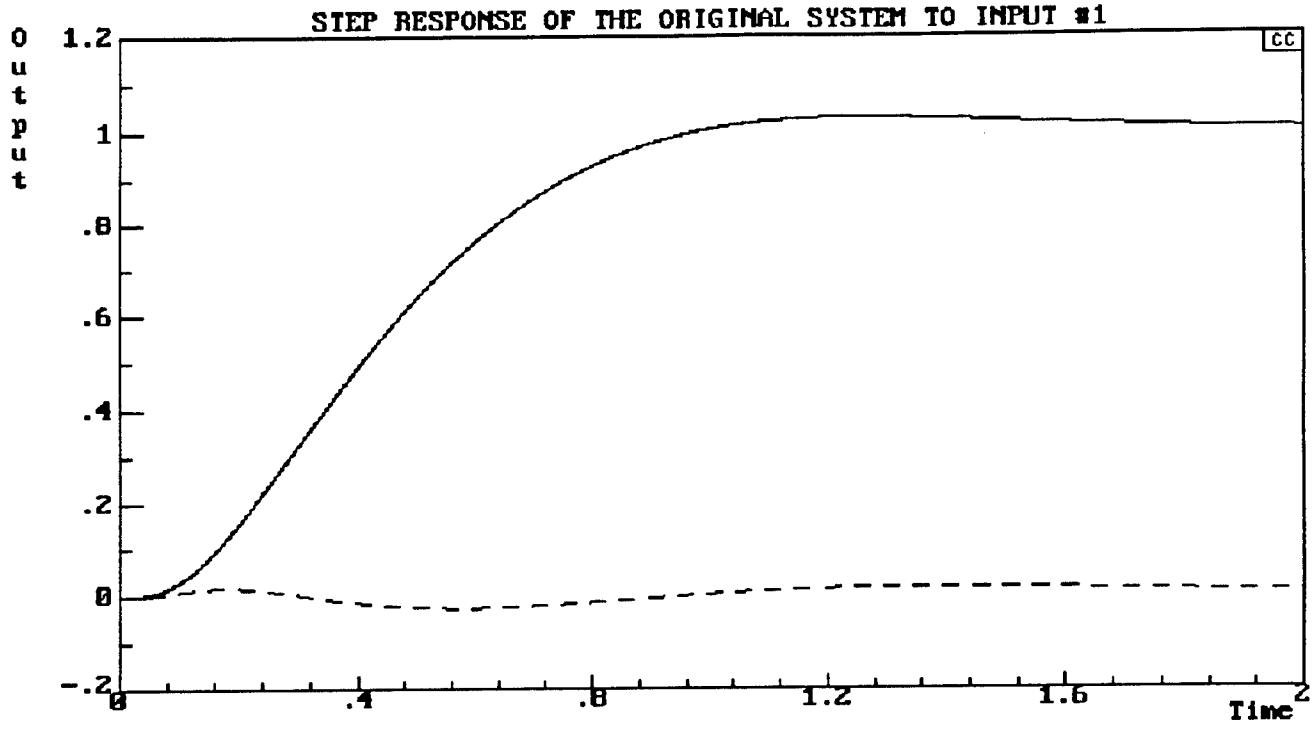
STEP RESPONSE OF THE ORIGINAL SYSTEM TO INPUT #1
Output
1.2
1
.8
.6
.4
.2
0
-.2
0
.4
.8
1.2
1.6
2
Time
CC

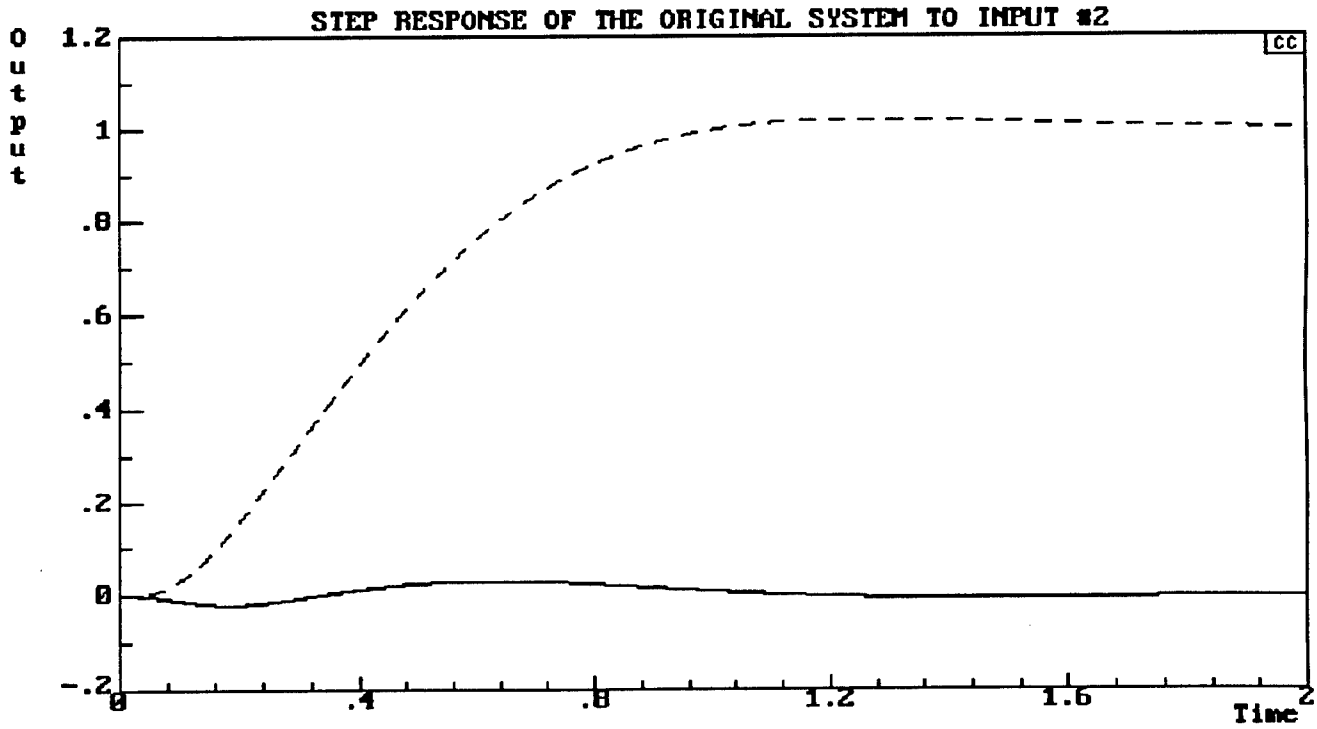
STEP RESPONSE OF THE ORIGINAL SYSTEM TO INPUT #2
Output
1.2
1
.8
.6
.4
.2
0
-.2
0
.4
.8
1.2
1.6
2
Time
CC

equation (2.17). First, realize that matrix B_P is not a square one and its inverse in (2.17) must be replaced by a left pseudo-inverse $H=(B_P^TB_P)^{-1}B_P^T$. Note that

$$HB_P=(B_P^TB_P)^{-1}B_P^TB_P=(B_P^TB_P)^{-1}(B_P^TB_P)=I$$

providing that the inverse $(B_P^TB_P)^{-1}$ exists. In our situation,

$$H=\begin{bmatrix} .0 & .0 & .609756 & .0 & .0 & .487805 \\ .0 & .0 & -.487805 & .0 & .0 & .609756 \end{bmatrix}$$

and, finally matrix W is defined as:

$$W=\begin{bmatrix} 9.5678e3 & 632.805 & 17.4146 & 7.8541e3 & 591.219 & 30.2439 \\ -7.8527e3 & -590.244 & -30.7317 & 9.5667e3 & 632.024 & 17.8049 \end{bmatrix}$$

Simulated step responses of the designed MR system are shown on page 37. They indicate that the designed system exhibits modified performance and cross-coupling transients decay within the time designated for the error convergence.

2.3 Decoupling MR Control with an Adaptive Predictor

Consider a beam steerer described by a transfer matrix G(s). Assume that elements of the same row of matrix G(s) are brought to a common denominator. Convert matrix G(s) to its discrete-time equivalent, G(z), assuming that the steerer is driven through a zero-order-hold. Then

the following difference equations could be used for the description of the beam steerer,

$$y_1(i)=-\Sigma a_{1j}y_1(i-j) + \Sigma b_{1j}u_{P1}(i-j) + \Sigma c_{1j}u_{P2}(i-j)$$

$$y_2(i)=-\Sigma a_{2j}y_1(i-j) + \Sigma b_{2j}u_{P1}(i-j) + \Sigma c_{2j}u_{P2}(i-j), \qquad (2.18)$$

where i is the discrete-time index. One can see that summation in (11) is performed with respect to time index j=1,2,3,... , and coefficients a_{1j}, b_{1j}, c_{1j}, a_{2j}, b_{2j}, and c_{2j}, are the parameters of the z-domain transfer functions $g_{11}(z)$, $g_{12}(z)$, $g_{21}(z)$, and $g_{22}(z)$, and as such are dependent on the time discretization step.

Note that since y_k , k=1,2 are azimuth and elevation positions of the laser beam

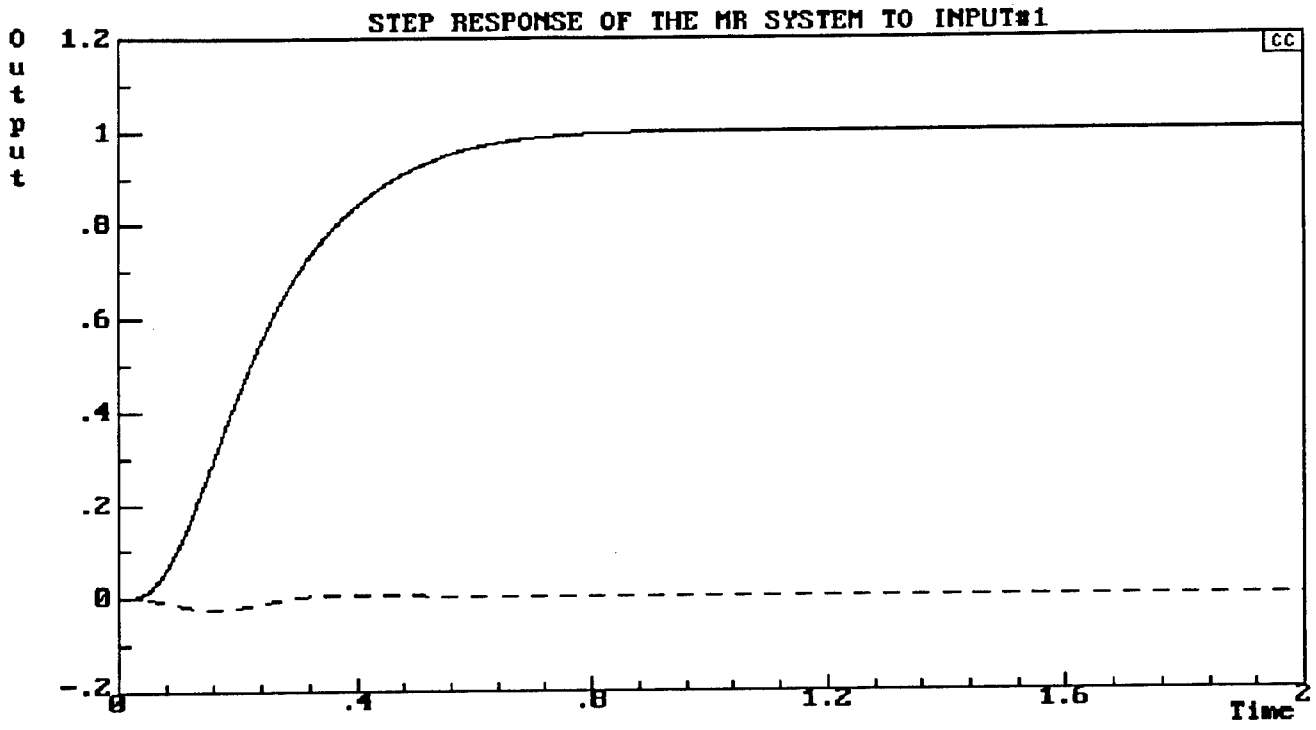
STEP RESPONSE OF THE MR SYSTEM TO INPUT#1
Output
1.2
1
.8
.6
.4
.2
0
-.2
0
.4
.8
1.2
1.6
2
Time
CC

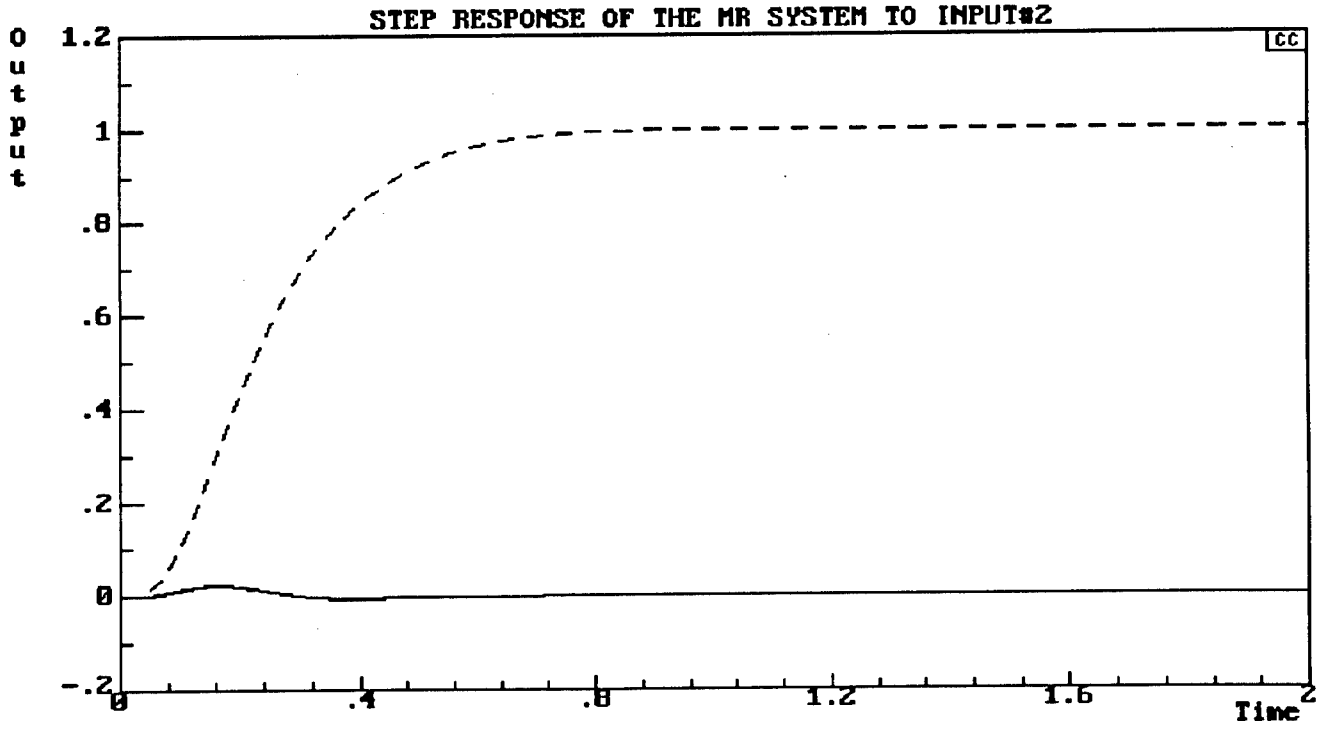
STEP RESPONSE OF THE MR SYSTEM TO INPUT#2
Output
1.2
1
.8
.6
.4
.2
0
-.2
0
.4
.8
1.2
1.6
2
Time
CC

accurately defined by the quadrant detector, and u_{Pk} , k=1,2, are known control signals, parameters a_{1j}, b_{1j}, c_{1j}, a_{2j}, b_{2j}, and c_{2j}, can be continuously updated by the application of a finite-memory recursive least squares procedure [20]. Although the success of the parameter updating can be assured by good initial values of these parameters and low measurement noise, it is known that when required, the procedure can be enhanced by orthogonalization of variables $y_1(i-j)$, $y_2(i-j)$, $u_{P1}(i-j)$, and $u_{P2}(i-j)$ and consequent modification of the obtained estimates. Implementation of the parameter updating procedure is instrumental in situations when parameters of the controlled process are poorly known and/or time-dependent due to hardware deterioration and environmental effects.

Availability of accurately estimated parameters of the equations (2.18) facilitates the use of these equations for the prediction of azimuth and elevation positions. Then continuous parameter updating provides the assurance of the prediction accuracy. Indeed, if (2.18) holds then the following "one step ahead" prediction can be achieved as

$$y_1(i+1)=-\Sigma a_{1j}y_1(i-j+1) + \Sigma b_{1j}u_{P1}(i-j+1) + \Sigma c_{1j}u_{P2}(i-j+1)$$

$$y_2(i+1)=-\Sigma a_{2j}y_1(i-j+1) + \Sigma b_{2j}u_{P1}(i-j+1) + \Sigma c_{2j}u_{P2}(i-j+1) \qquad (2.19)$$

Introduce a reference model in the form of two fixed-parameter difference equations, reflecting the desired closed-loop dynamics of the beam steerer,

$$y_{M1}(i+1)=-\Sigma m_{1j}y_{M1}(i-j) + \Sigma n_{1j}u_1(i-j)$$

$$y_{M2}(i+1)=-\Sigma m_{2j}y_{M1}(i-j) + \Sigma n_{2j}u_1(i-j) \qquad (2.20)$$

One can see that equations (2.20) represent a decoupled system. Computation of the predicted azimuth and elevation, $y_1(i+1)$ and $y_2(i+1)$, and their reference values $y_{M1}(i+1)$, $y_{M2}(i+1)$ facilitates computation of the expected position errors,

$$e_1(i+1)=y_{M1}(i+1)-y_1(i+1) \qquad (2.21)$$

$$e_2(i+1)=y_{M2}(i+1)-y_2(i+1)$$

Define increments of control signals, $\Delta u_{p1}(i)$ and $\Delta u_{p2}(i)$ to assure that position errors have zero values,

$$b_{11}\Delta u_{P1}(i) + c_{11}\Delta u_{P2}(i) = -e_1(i+1)$$

$$b_{21}\Delta u_{P1}(i) + c_{21}\Delta u_{P2}(i) = -e_2(i+1) \qquad (2.22)$$

Then control signals $u_{P1}(i+1)$ and $u_{P2}(i+1)$ can be defined as follows,

$$u_{P1}(i+1)=u_{P1}(i+1)+\Delta u_{P1}(i)$$
$$u_{P2}(i+1)=u_{P2}(i+1)+\Delta u_{P2}(i) \qquad (2.23)$$

The proposed MR control procedure performing parameter updating, solution of equations (2.22), and definition of the control signals as per (2.23) at each step of the discrete-time procedure, i=1,2,3,..., has been implemented in software and tested by simulation. It is important that the proposed decoupling MR technique can be extended from two to any practical number of input-output channels.

The following are difference equations representing the beam steerer, originally defined by transfer functions, at sampling frequency 32.5 KHz,

$$y_1(i)=1.7857y_1(i-1)-.9865y_1(i-2)+.1207[u_{P1}(i-1)+.9954u_{P1}(i-2)]+$$
$$.0956[u_{P2}(i-1)+.9954u_{P2}(i-2)]$$
$$y_2(i)=3.7122y_2(i-1)-5.41815y_2(i-2)+3.6628y_2(i-3)-.9736y_2(i-4)+$$
$$.0466[u_{P1}(i-1)-.8649u_{P1}(i-2)-.8649u_{P1}(i-3)+.9825u_{P1}(i-4)] -$$
$$.0495[u_{P2}(i-1)-.8612u_{P2}(i-2)-.8616u_{P2}(i-3)+.9823u_{P2}(i-4)]] \qquad (2.24)$$

The reference model is represented by expressions

$$y_{M1}(i)=.912y_{M1}(i-1) + .08799u_1(i-1)$$
$$y_{M2}(i)=.912y_{M2}(i-1) + .08799u_2(i-1) \qquad (2.25)$$

Computer simulation results indicate that recursive least squares procedure allows for fast and reliable convergence of the parameter updating process, both in the estimation and tracking modes. The control procedure, especially upon convergence of the parameter updating process, allows for successful model following. Utilization of the continuous parameter updating provides a high degree of robustness of the resultant control system.

Graphs of page 40 indicate that a high degree of decoupling and model-following has been achieved by the application of the above approach. A practical question, however, arises: how crucial the accuracy of prediction is for the performance of the MR

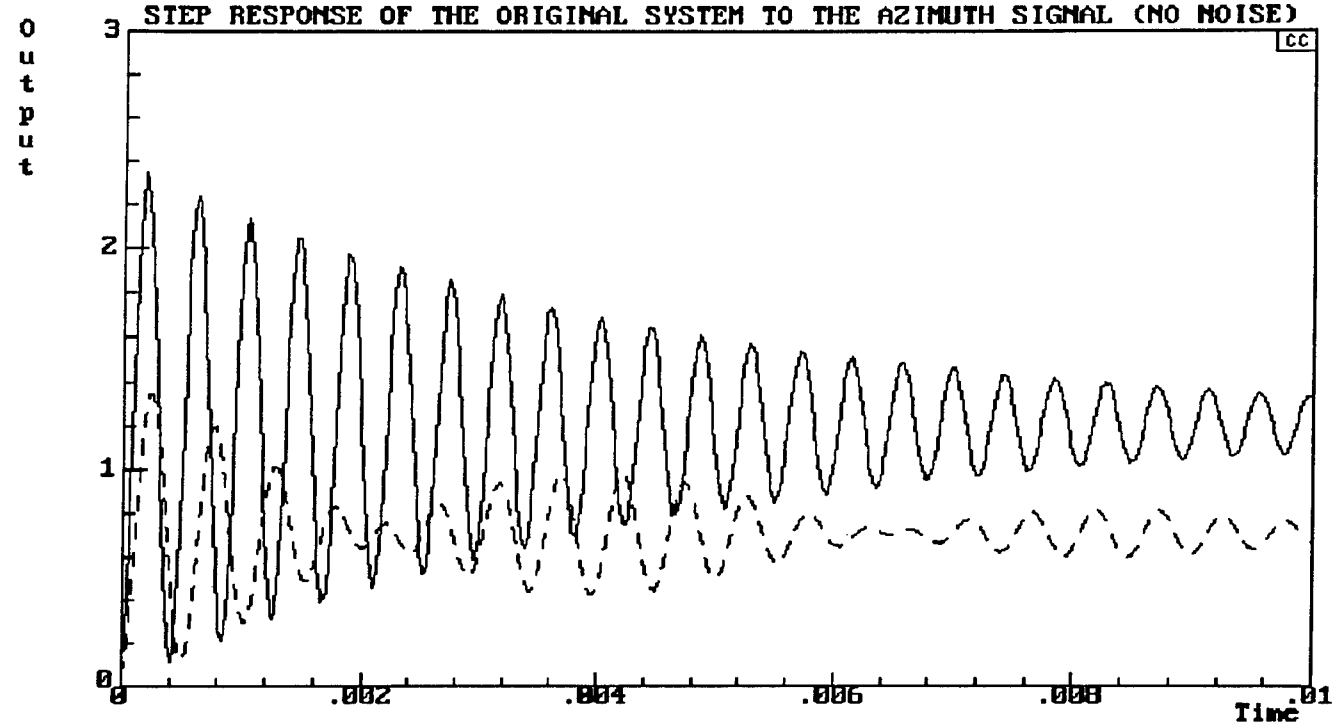
STEP RESPONSE OF THE ORIGINAL SYSTEM TO THE AZIMUTH SIGNAL (NO NOISE)
Output
3
2
1
0
0
.002
.004
.006
.008
.01
Time
CC

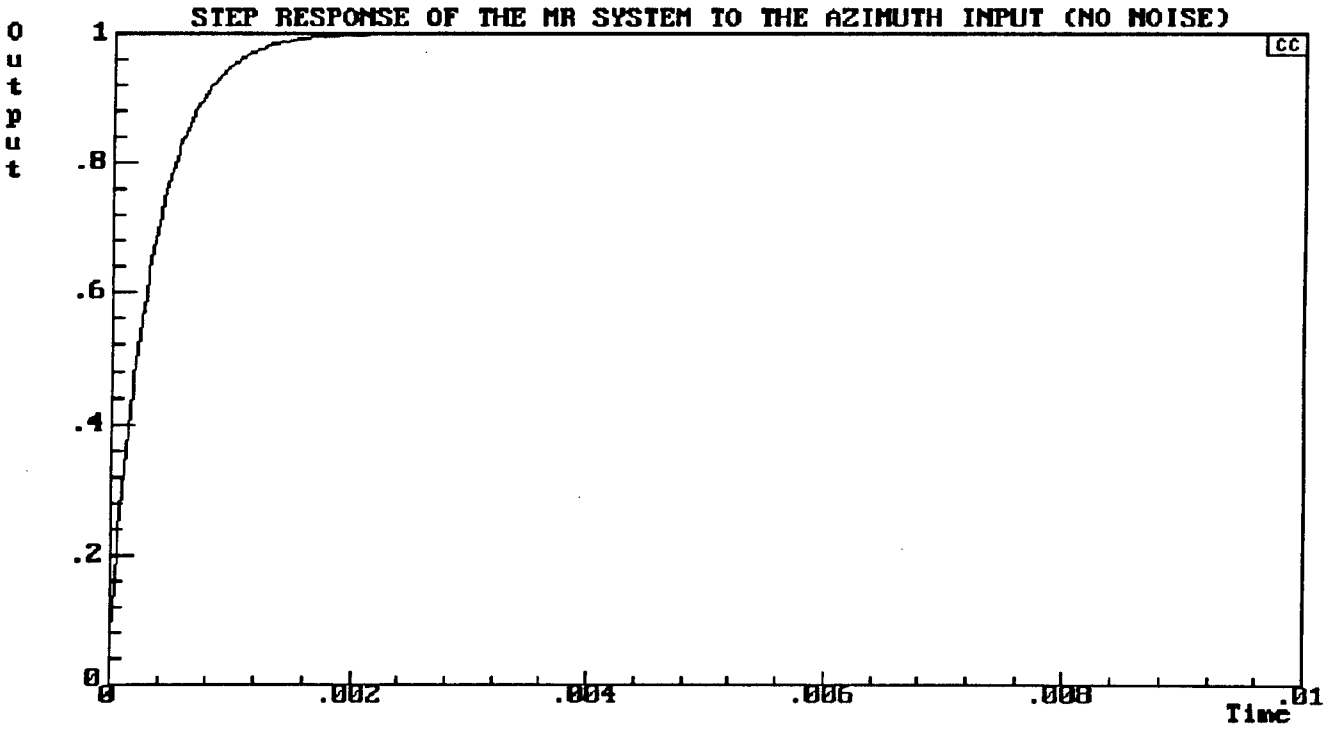
STEP RESPONSE OF THE MR SYSTEM TO THE AZIMUTH INPUT (NO NOISE)
Output
1
.8
.6
.4
.2
0
0
.002
.004
.006
.008
.01
Time
CC

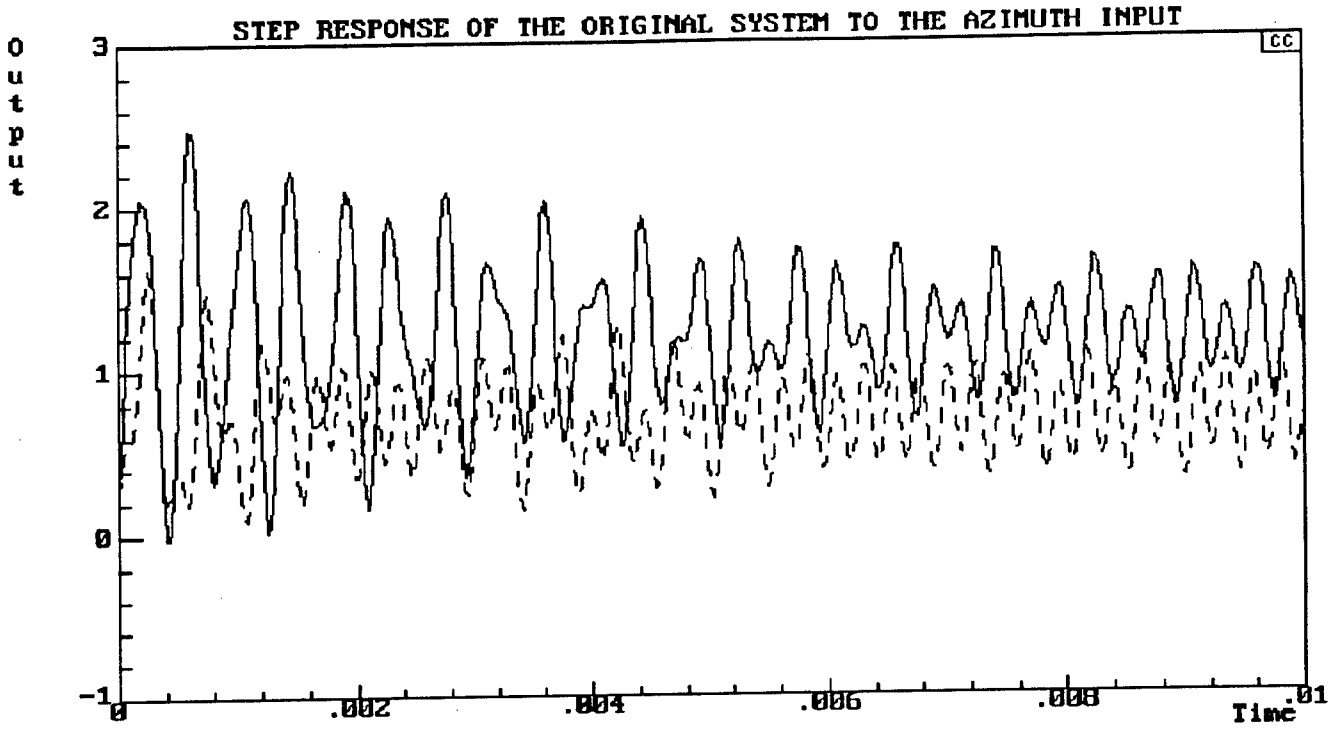
STEP RESPONSE OF THE ORIGINAL SYSTEM TO THE AZIMUTH INPUT
Output
3
2
1
0
-1
0
.002
.004
.006
.008
.01
Time
CC

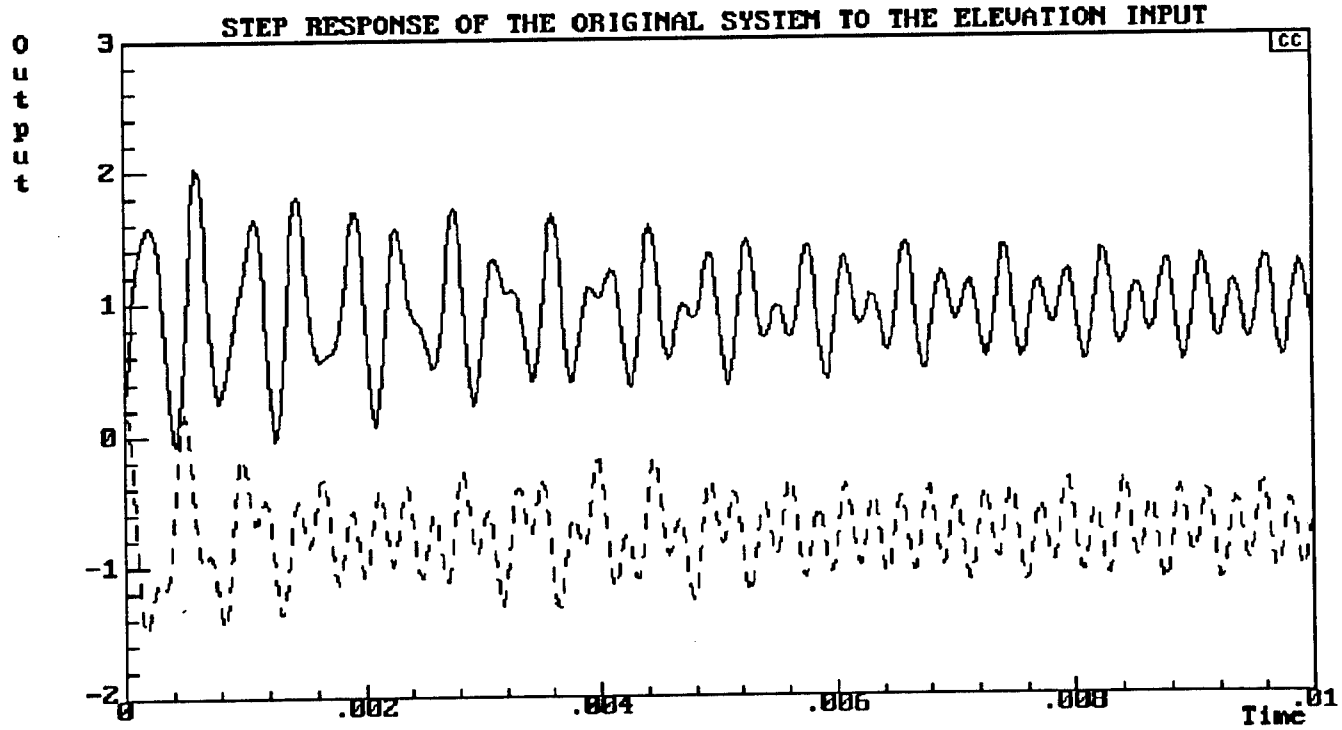
STEP RESPONSE OF THE ORIGINAL SYSTEM TO THE ELEVATION INPUT
Output
3
2
1
0
-1
-2
0
.002
.004
.006
.008
.01
Time
CC

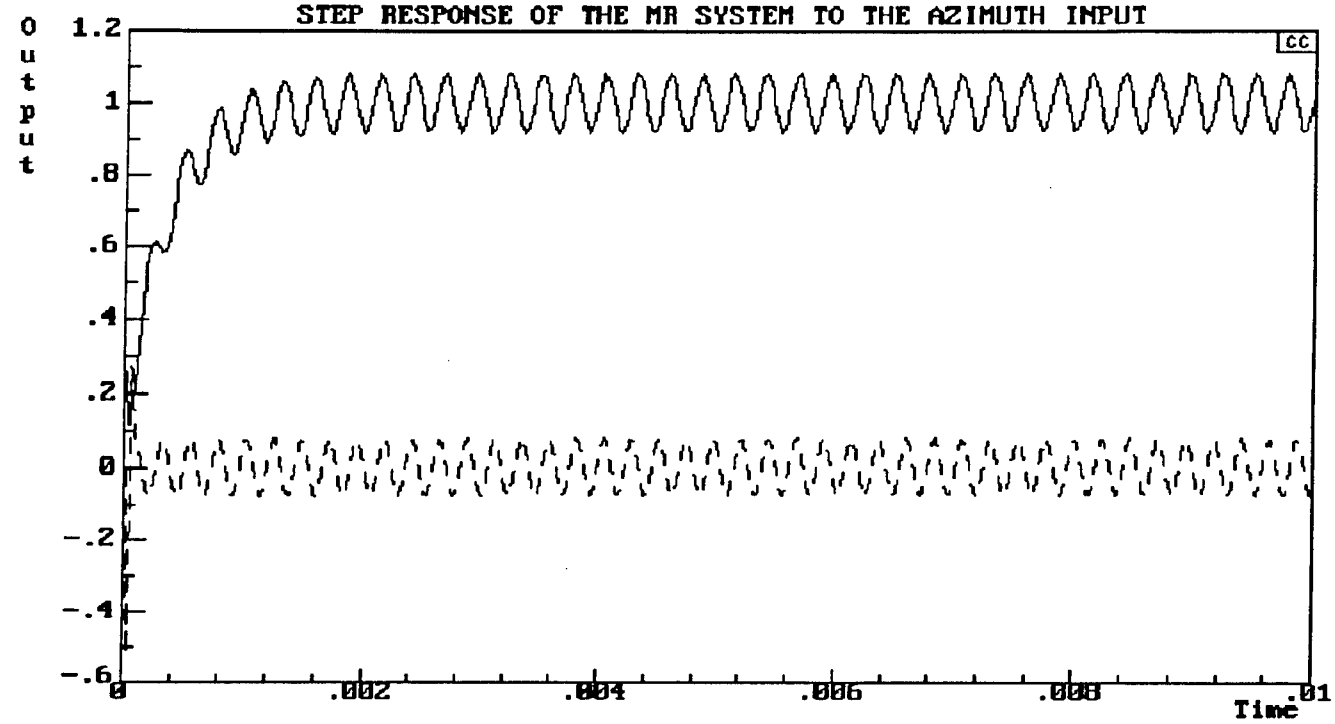
STEP RESPONSE OF THE MR SYSTEM TO THE AZIMUTH INPUT
Output
1.2
1
.8
.6
.4
.2
0
-.2
-.4
-.6
0
.002
.004
.006
.008
.01
Time
CC

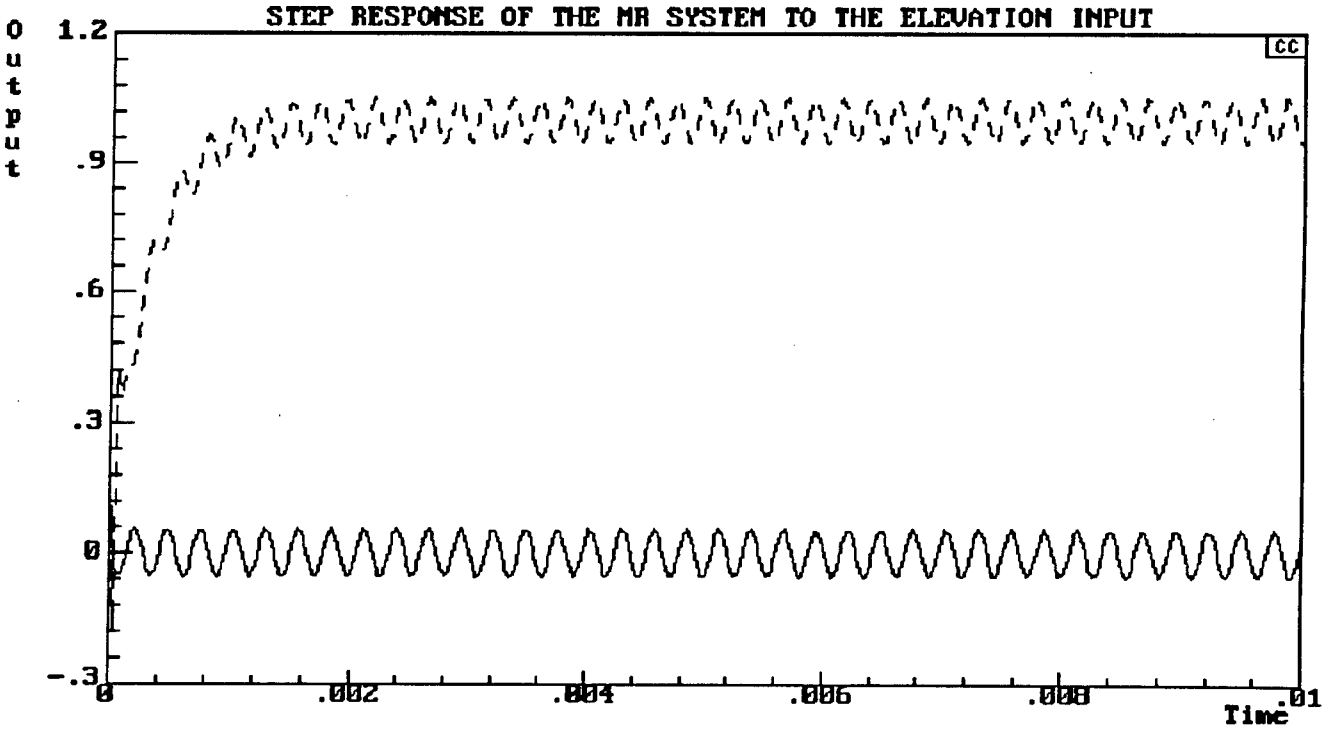
STEP RESPONSE OF THE MR SYSTEM TO THE ELEVATION INPUT
Output
1.2
.9
.6
.3
0
-.3
0
.002
.004
.006
.008
.01
Time
CC

system? The answer to this question is provided by the graphs of pp. 41 and 42. During the simulation experiment, the "true" output of the process has been contaminated by noise which is not accounted for by the predictor. In spite that the level of noise is approximately 30% of the signal magnitude, the proposed procedure allows for successful decoupling and model following.

Parameter tracking. While the necessary accuracy of model-following is assured by the existing feedback mechanisms, the proposed control law is dependent only on the ability to provide accurate on-line estimation/tracking of the parameters a, b, c of equation (2.19). This task can be carried out by the following procedure implementing the Recursive Least Squares Method (RLSM) with exponential forgetting [Astrom, K.J. and Wittenmark, B., "Adaptive Control," Addison-Wesley Publishing Company]. In order to describe RLSM application to our problem, define first equation of (2.19) in more detail:

$$y_1(i+1)=-\sum_{j=1}^{N} a_{1j}y_1(i-j+1) + \sum_{j=1}^{M} b_{1j}u_{P1}(i-j+1) + \sum_{j=1}^{K} c_{1j}u_{P2}(i-j+1) \qquad (2.26)$$

where

N, M, and K are defined by the order of denominator and numerators of the appropriate z-domain transfer functions.

Define the following vectors,

$$X(i)=[y_1(i-j+1),j=1,...,N,\ u_{P1}(i-j+1),j=1,...,M,\ u_{P2}(i-j+1),j=1,...,K\ ]^T \qquad (2.27)$$

$$A=[a_{1j},\ j=1,...,N,\ b_{1j},\ j=1,...,M,\ c_{1j},\ j=1,...,K]^T \qquad (2.28)$$

then the RLSM equations can be defined as follows.

$$K(i+1)=P(i)X(i+1)[\lambda+X(i+1)^TP(i)X(i+1)]^{-1} \qquad (2.29)$$

$$\alpha(i+1)=\alpha(i)+K(i+1)[y(i+1)-\alpha(i)^TX(i+1)] \qquad (2.30)$$

$$P(i+1)=[I-K(i)X(i+1)^T]P(i)/\lambda \qquad (2.31)$$

where

$i=1,2,3,...$ discrete time index,

$\alpha(i)$, $i=1,2,3,...$ is a series of estimates of vector A, generated by the RLSM

procedure,

vector X(i+1) represents recorded values of the appropriate variables as per (2.27),

vector α(i) represents the most recent vector of parameter estimates,

P(i) and K(i+1) are L×L matrices, L=N+M+K (note that square brackets of (2.29) contain a scaler and this expression does not imply matrix inversion),

$y(i+1)=y_1(i+1)$ is the most recent value of this variable recorded,

λ is the forgetting parameter, $0<\lambda<1$.

Successful implementation of a RLSM procedure is dependent upon the choice of its initial parameters A(0) and P(0), measurement accuracy, and the value of the forgetting factor λ..

The choice of A(0) should be consistent with the available parameter values of the appropriate z-domain transfer functions of the system.

It is recommended that P(0) be defined as a diagonal matrix, and the value of .1 should be assigned to all diagonal elements. This choice may be reconsidered depending on the results of the trial runs of the RLSM procedure: noticeable oscillations of the parameter estimates, converging or diverging, indicate that the values of the diagonal terms of matrix P(0) should be reduced. Slow convergence of the parameter estimates indicates that the values of the diagonal terms of matrix P(0) should be increased.

The choice of parameter λ controls the balance between the ability of the RLSM procedure to operate under measurement noise and the ability to track time-varying parameters A. Parameter λ defines the "memory size" of the RLSM procedure, i.e. determines the number of most recent measurements which are primarily responsible for the values of estimates A. The memory of the RLSM procedure is defined as $1/(1-\lambda)$. One can see that, while $0<\lambda<1$, an increase of the parameter λ results in the reduction of memory size and, therefore, improves tracking capability of the procedure. A decrease of the parameter λ results in the increase of memory size and, therefore, improves the ability of the procedure to "average out" measurement noise. At the same time, tracking capability of the procedure decreases.

A FORTRAN text of an RLSM procedure developed for this project can be seen below.

```
      SUBROUTINE RLSM(N,TH,Y,FAI,P,FF)
      DIMENSION TH(10),G(10),FAI(10),P(10,10)
      DIMENSION C(10,10),D(10,10),H(10,10)
      DO 6 I=1,N
6     H(1,I)=FAI(I)
      CALL MULT(H,P,1,N,N,C)
      CALL MULT(C,FAI,1,N,1,D)
      E=1.0/(D(1,1)+FF)
      DO 1 I=1,N
1     Y=Y-FAI(I)*TH(I)
      CALL MULT(P,FAI,N,N,1,C)
      DO 2 I=1,N
2     G(I)=C(I,1)*E
      DO 3 I=1,N
3     TH(I)=TH(I)+G(I)*Y
      DO 4 I=1,N
      DO 4 J=1,N
      D(I,J)=-G(I)*FAI(J)
      IF (I.EQ.J) D(I,J)=D(I,J)+1.0
4     CONTINUE
      CALL MULT(D,P,N,N,N,C)
      DO 5 I=1,N
      DO 5 J=1,N
5     P(I,J)=C(I,J)/FF
      RETURN
      END
C
      SUBROUTINE MULT(A,B,M,K,N,C)
C  A(MxK)    B(KxN)     C(MxN)
      DIMENSION A(10,10),B(10,10),C(10,10)
      DO 1 I=1,M
      DO 2 J=1,N
      C(I,J)=0.0
      DO 3 KK=1,K
3     C(I,J)=C(I,J)+A(I,KK)*B(KK,J)
2     CONTINUE
1     CONTINUE
      RETURN
      END
```

Graphs given on page 46 illustrate the ability of the procedure to estimate and to track system parameters. To dramatize the situation, initial parameter values are chosen to be zeros.

Graphs of page 47 illustrate the ability of the RLSM estimates to follow time-varying "true" parameters of the system.

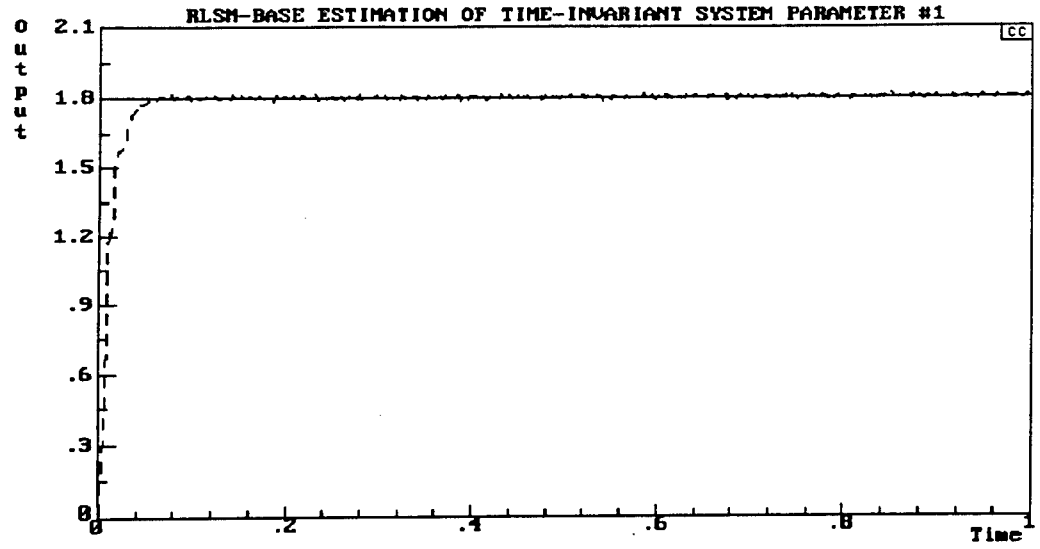
RLSM-BASE ESTIMATION OF TIME-INVARIANT SYSTEM PARAMETER #1
output
2.1
1.8
1.5
1.2
.9
.6
.3
0
.2
.4
.6
.8
1
Time
CC

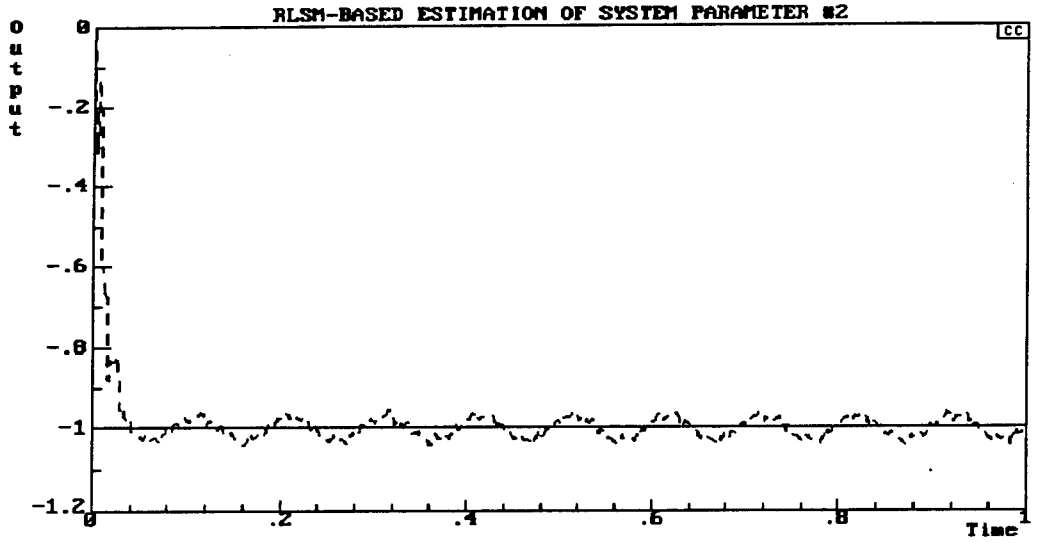
RLSM-BASED ESTIMATION OF SYSTEM PARAMETER #2
output
0
-.2
-.4
-.6
-.8
-1
-1.2
.2
.4
.6
.8
1
Time
CC

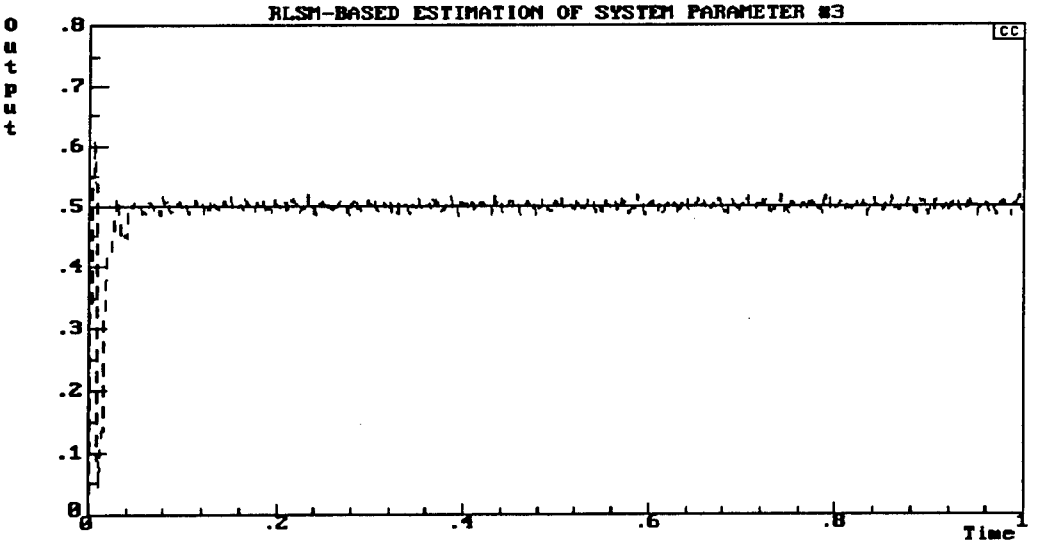
RLSM-BASED ESTIMATION OF SYSTEM PARAMETER #3
output
.8
.7
.6
.5
.4
.3
.2
.1
0
.2
.4
.6
.8
1
Time
CC

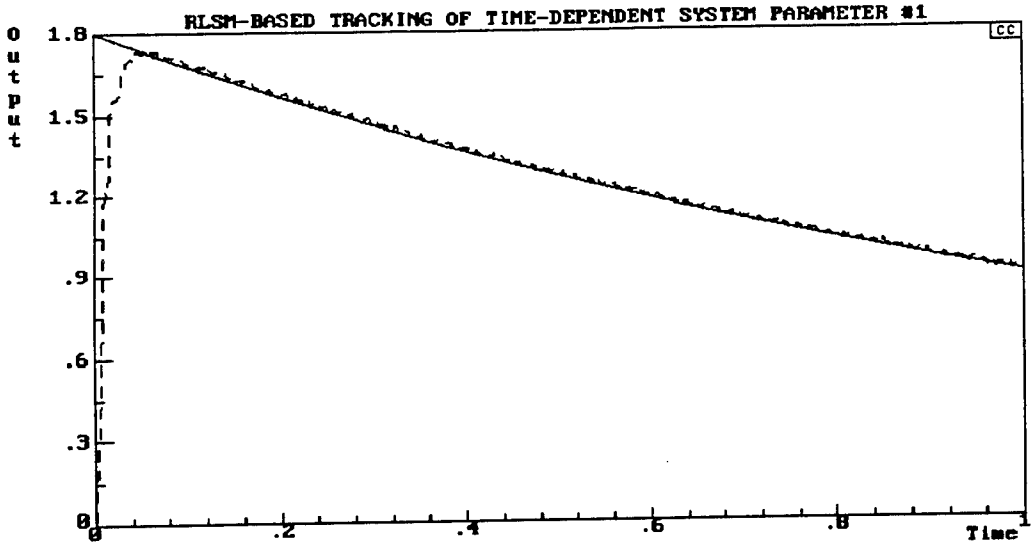
RLSM-BASED TRACKING OF TIME-DEPENDENT SYSTEM PARAMETER #1
Output
1.8
1.5
1.2
.9
.6
.3
0
.2
.4
.6
.8
1
Time
CC

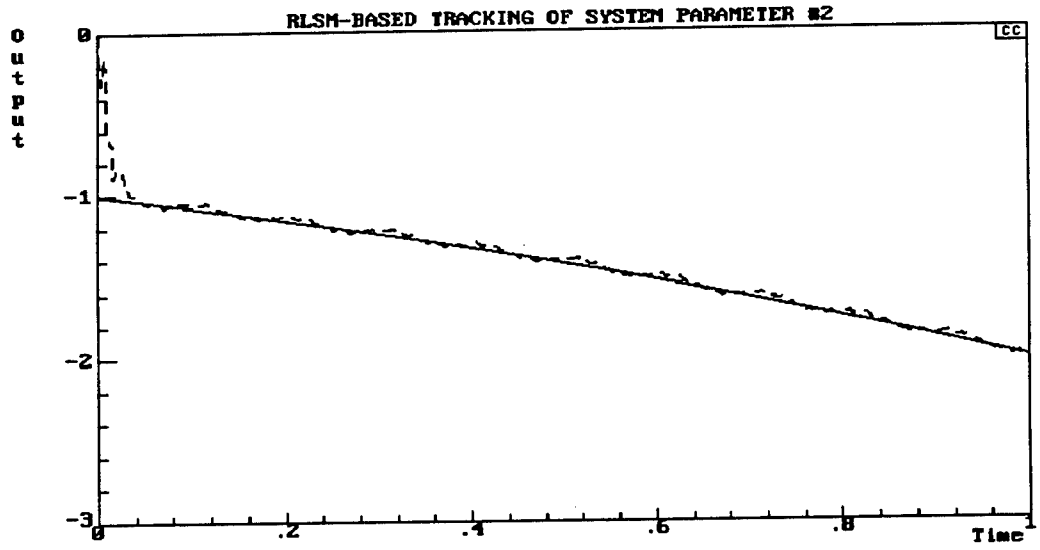
RLSM-BASED TRACKING OF SYSTEM PARAMETER #2
Output
0
-1
-2
-3
.2
.4
.6
.8
1
Time
CC

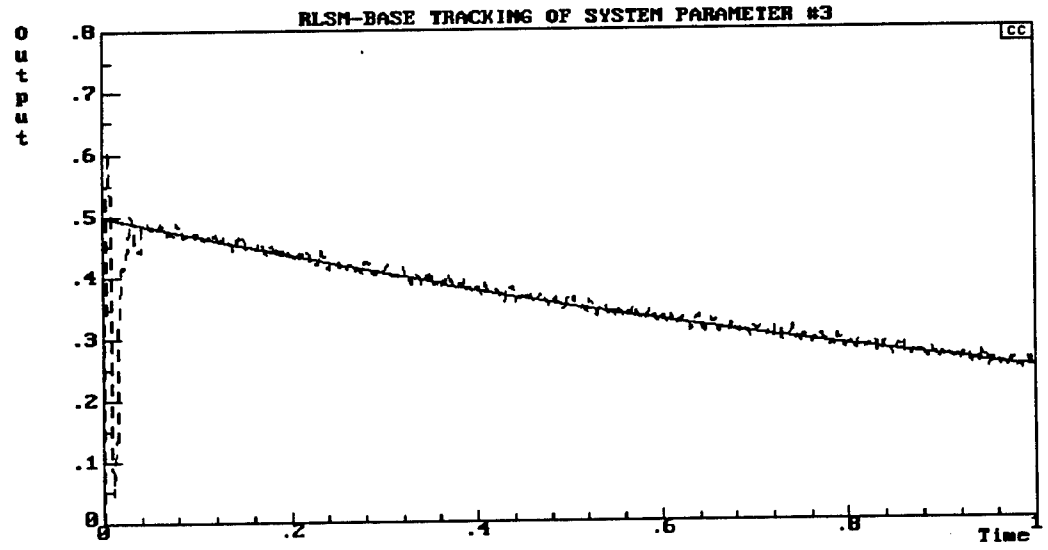
RLSM-BASE TRACKING OF SYSTEM PARAMETER #3
Output
.8
.7
.6
.5
.4
.3
.2
.1
0
.2
.4
.6
.8
1
Time
CC

Accuracy analysis of the MR system. The purpose of this section is to assess the risk of the application of the proposed above procedure associated with the fact that RLSM estimates of system parameters may or may not become effectively close to their "true" values. In order to perform this analysis, rewrite equations (2.19) as follows

$$y_1(i+1)=-\sum_{j=1}^{N} a_{1j}y_1(i-j+1) + \sum_{j=2}^{M} b_{1j}u_{P1}(i-j+1) + \sum_{j=2}^{K} c_{1j}u_{P2}(i-j+1) + b_{11}u_{P1}(i) + c_{11}u_{P2}(i)$$

$$y_2(i+1)=-\sum_{j=1}^{N} a_{2j}y_2(i-j+1) + \sum_{j=2}^{M} b_{2j}u_{P1}(i-j+1) + \sum_{j=2}^{K} c_{2j}u_{P2}(i-j+1) + b_{22}u_{P1}(i) + c_{22}u_{P2}(i) \quad (2.32)$$

Introduce the following vectors,

$V(i)=[y_1(i-j+1),\ y_2(i-j+1),\ j=1,...,N,\ u_{P1}(i-j+1),\ j=2,...,M,\ u_{P2}(i-j+1),\ j=2,...,K]^T$

$U(i)=[u_{P1}(i)\ u_{P2}(i)]^T$,

$Y(i+1)=[y_1(i+1)\ y_2(i+1)]^T$, and

$Y_M(i+1)=[y_{M1}(i+1)\ y_{M2}(i+1)]^T$

and matrices of appropriate dimensions, R and Q, such that equations (2.32) could be rewritten in the matrix-vector form

$$Y(i+1)=RV(i)+QU(i) \quad (2.33)$$

One can see that matrix R contains most of parameters of the z-domain transfer function of the controlled plant, and matrix Q id defined as

$$Q = \begin{bmatrix} b_{11} & c_{11} \\ b_{22} & c_{22} \end{bmatrix}$$

Assume that matrix $\Phi(i)$ and matrix $\Theta(i)$ are obtained from R and Q correspondingly by replacing appropriate system parameters by their RLSM estimates. Then the predicted system outputs can be expressed as

$$Y^{PRED}(i+1)=\Phi(i)V(i)+\Theta(i)U(i)$$

and the predicted system error as

$$E^{PRED}(i+1)=Y_M(i+1)-Y^{PRED}(i+1)=Y_M(i+1)-\Phi(i)V(i)-\Theta(i)U(i)$$

Following the proposed control law, the control effort is defined to assure zero value of

the predicted error, i.e.

$$U(i)=\Theta(i)^{-1}[Y_M(i+1)-\Phi(i)V(i)] \qquad (2.34)$$

Now let us assess the "posterior" error, i.e. the system error which takes place when control effort (2.34) has been applied at the i-th step of the control algorithm:

$$E(i+1)=Y_M(i+1)-Y(i+1)=Y_M(i+1)-RV(i)-QU(i), \text{ or}$$

$$E(i+1)=Y_M(i+1)-RV(i)-Q\Theta(i)^{-1}[Y_M(i+1)-\Phi(i)V(i)], \text{ or}$$

$$E(i+1)=Y_M(i+1)-Q\Theta(i)^{-1}Y_M(i+1)-RV(i)+Q\Theta(i)^{-1}\Phi(i)V(i), \text{ or}$$

$$E(i+1)=[I-Q\Theta(i)^{-1}]Y_M(i+1)-[R-Q\Theta(i)^{-1}\Phi(i)]V(i) \qquad (2.34)$$

Assume that

$$\Phi(i)=R+\Delta(i) \text{ and } \Theta(i)=Q+\delta(i)$$

where

$\Delta(i)$ and $\delta(i)$ are random matrices of estimation errors and, due to successful performance of the RLSM procedure, their norms, $\|\Delta(i)\|$ and $\|\delta(i)\|$, are effectively small. Then

$$Q\Theta(i)^{-1}=Q[Q+\delta(i)]^{-1} \approx I \text{ and } I-Q\Theta(i)^{-1} \approx 0$$

Similarly,

$$R-Q\Theta(i)^{-1}\Phi(i) \approx R-\Phi(i) = R-R-\Delta(i) =-\Delta(i)$$

This analysis indicates that accurate estimation/tracking of parameters of the controlled plant guarantees the feasibility of accurate model-following.

3. IMPLEMENTATION AND TESTING OF MR CONTROL OF OPTICAL MIRRORS

Implementation of the developed MR control systems in the laboratory conditions is crucial for the evaluation of the feasibility of the developed technology. It allows to obtain convincing information on the advantages and disadvantages of particular MR schemes in comparison with the existing control methods. The following claims based upon simulation studies are to be proved (or disproved) by laboratory tests described in this section,

MR approach allows for extending bandwidth of particular control channels of beam steeres

- MR approach allows for the elimination of "bending modes" from transient response of control channels of a beam steerer
- MR reference approach results in the elimination of cross-coupling between control channels of a beam steerer
- MR approach results in the reduction of jitter effects on the beam positioning accuracy
- MR approach results in the increased robustness of a beam positioning system
- MR approach can be implemented at relatively low cost.

Developed control techniques were implemented using the laser communication pointing-acquisition-tracking (PAT) testbed of Rome Laboratory equipped with 500 Hz and 5KHz optical mirrors and PC-based control systems and interfaces. A PC equipped with data monitoring software package was utilized for generating test signals and acquisition of system responses along with standard data probes. Various MR schemes were implemented using analog and digital circuitry, and subjected to three basic experiments. The first experiment was designed to test the system's ability to modify dynamic response of a single control channel. The second experiment tested the decoupling effects. The third experiment was aimed at the evaluation of the jitter reduction effect.

3.1 High Bandwidth Steering Mirror

The PAT testbed [2] provides the test environment for the high bandwidth mirror. The hardware of the PAT system includes a Hewlett Packard model-330 computer, an electronics rack housing the support electronics for the electro-optic and electro-mechanical components, and a pair of optical isolation tables upon which the components of the primary and remote stations are mounted.

The primary station optic and electro-optic systems can be categorized into six groups: lasers, detectors, beam conditioners, ray optics, filters and beam directors. The primary station is equipped with two semiconductor lasers having optical output powers of 10 mW and 100 mW, and center wavelengths of 830 nm and 800 nm respectively. There are three types of optical detectors in the primary station, two types for tracking purposes and one for communications. The tracking detector is a quadrant silicon avalanche photodiode, the acquisition detectors are improved tetra-lateral position sensitive devices (PSD) and the communication detector is a silicon avalanche photodiode. The beam conditioners and ray optics assure the required characteristics of the communication and beacon laser beams for detection and transmission. The optical filters are used to separate these beams so that each can be processed individually. The beam directors, coarse steering mirrors (CSM1 and CSM2) and the fast steering mirror (FSM), are used to direct the transmitted beam and to position the received beam.

The primary station electric and electro-mechanic systems include: the computer, the computer interface, the fine steering subsystem, the coarse steering subsystem, and the wide field of view (WFOV) subsystem. The computer interface consists of a HP general purpose input/output (GPIO) board and interface electronics. Both the fast steering subsystem and the coarse steering subsystem are analog closed-loop control circuits. The WFOV camera is synchronized, monitored and controlled by the computer." [1]

The configuration of the remote station is similar to that of the primary station without the acquisition and tracking functions. Two remote station reside on a single 4x8' optical table. Remote station 1 is fixed while remote 2 is mounted on a rail and can be driven over a 4 foot distance. The beacon and communication lasers have output powers of 10 mW and 50 mW, and center wavelengths of 780 nm and 810 nm respectively.

Optically, the tracking laser from remote terminal 2 propagates across the laboratory (15 m) impinging on the #2 coarse steering mirror. The beam is relayed through a 40x beam expander to the fine steering mirror. This expansion takes place to accurately simulate a link distance between a low Earth satellite and a geostationary one (roughly 30,000 km). From the fine steering mirror the beam is relayed via dichroic mirrors through the communication beam pick off and a 10 nm optical filter and 400 mm lens to the quadrant detector. Only the tracking laser was used for these measurements.

The control system for the coarse steering mirror (CSM) system is operated in a manual mode adjusting the beam so that it is placed in the field of view of the quadrant detector. The CSM is further adjusted to provide a beam intensity at the quad cell sufficient to exceed the threshold required for the operation of the fine track control loop. Once the CSM position is set, the quad cell is adjusted such that the beam is centered on it. Figure 3-1 and Figure 3-2 below feature voltage vs. position characteristics of the quadrant detector employed as the beam position sensor. Note that zero angle occurs with the spot at the edge of the detector for the axis being measured and centered for the other axis. Figure 3-2 shows an expanded view of the linear region (measurement span). This shows that a measurement accuracy of 0.25 μ radians is possible. It is desired to operate the system such that the beam remains below ±400 mV so that it remains in a linear operating region.

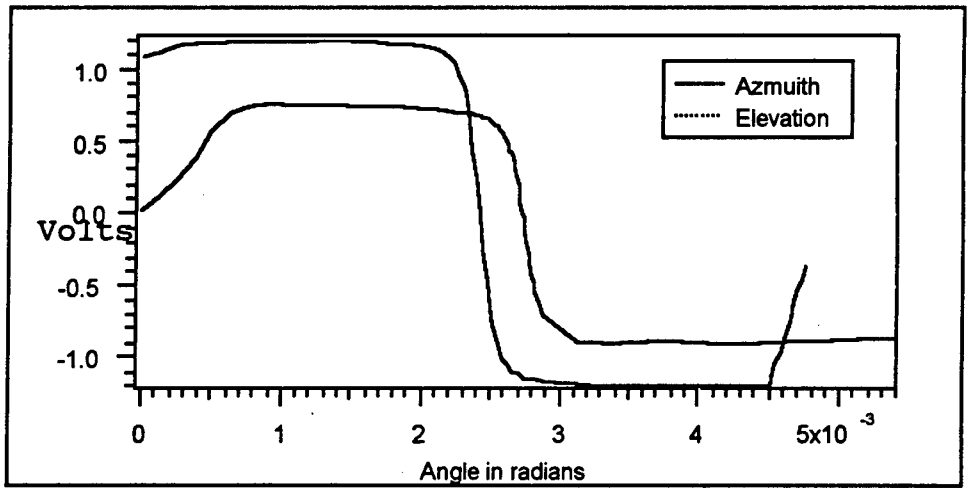

Figure 3-1 Voltage versus angle for PAT quad cell.

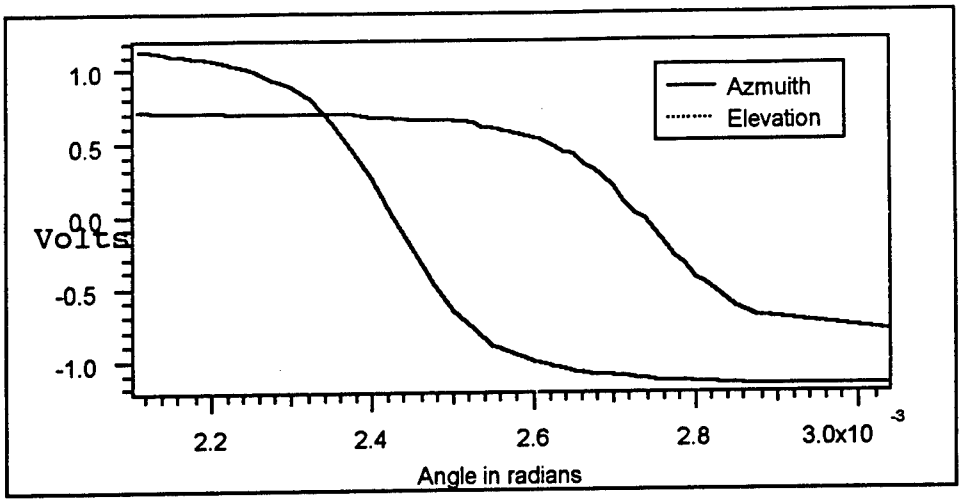

Figure 3-2. Expanded view of measurement span.

Implementation of the Reference Model and Compensator. The reference model and compensator were implemented in analog circuitry according to the transfer functions derived in the previous chapter. For the inverting operational amplifier configuration, shown in Figure 3-3, the transfer function is given by (using the infinite gain approximation):

$$\frac{V_o}{V_i} = \frac{1/R_1C_1}{S + 1/R_2C_1}$$

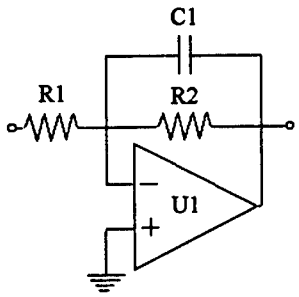

Figure 3-3. Reference model.

The component values were chosen from standard parts available in the lab producing a model with the following transfer function:

$$m_{11}(s) = m_{22}(s) = \frac{3030}{s+3030}$$

Similarly, the transfer function for the lead elements of the compensator, shown in Figure 3-4, is given by:

$$\frac{V_o}{V_i} = \frac{R_5(R_4C_3S+1)}{R_4(R_5C_4S+1)}$$

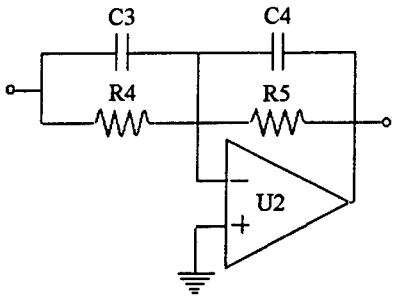

Figure 3-4. Lead network

Again, component values were chosen from standard parts producing a lead network with the following transfer function:

$$\frac{6.2E-5S+1}{6.2E-6S+1}$$

These values will yield a lead network with a gain value of 10 dB at a frequency of 8.117 kHz.

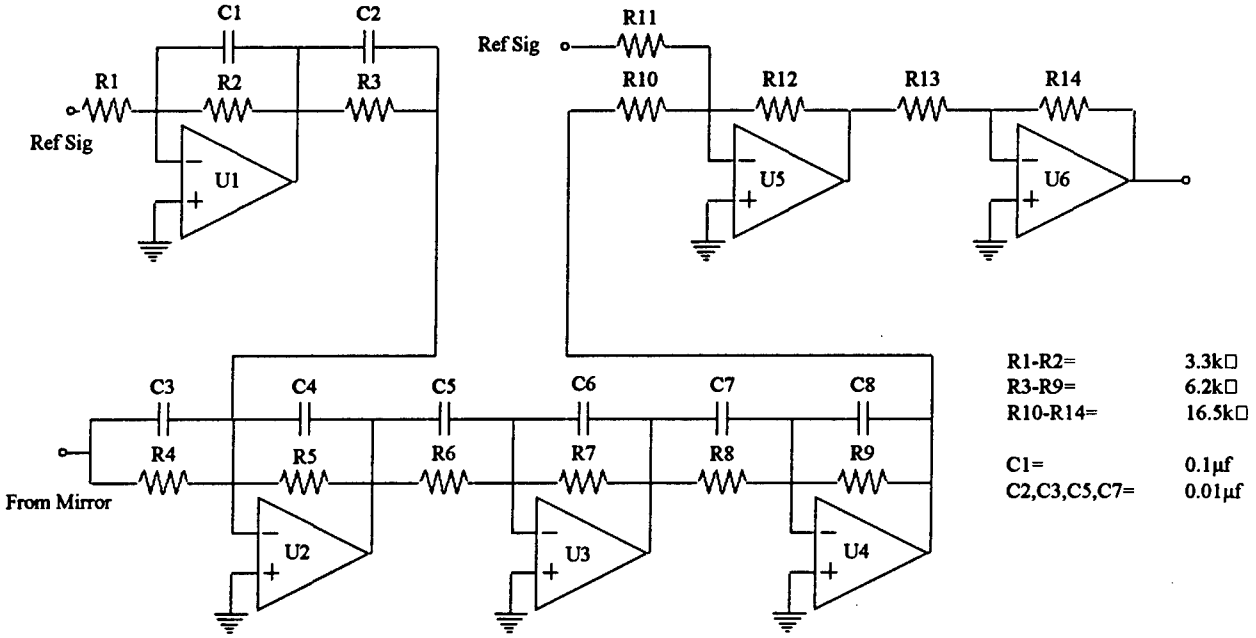

Figure 3-5. Circuit Diagram of single channel of reference model and compensator.

In the circuit shown in Figure 3-5, U1, R1, R2, and C1 make up the reference model. The output of the reference model is inverted with respect to its input and is added to the position signal from the mirror via C2 and R3. The resulting error signal is applied to U2, U3, and U4, which represent the three lead elements of the compensator. The output of the compensator is then added to the reference signal and applied to the mirror drive. The compensator and model for both elevation and azimuth were built on proto-boards.

A square wave input from a HP 8116 function generator with an amplitude of ±200 mV was applied first to the input of the azimuth channel and then to the elevation channel and the outputs were measured using a Phillips digital oscilloscope. Figure 3-6 and Figure 3-7 show the response of the system with the conventional control. It should be noted that while the conventional controller deals exclusively with the "main dynamics" of the controlled plant, the model reference controller improves the "main dynamics" and, in this case, reduces the cross-coupling and the effects of jitter.

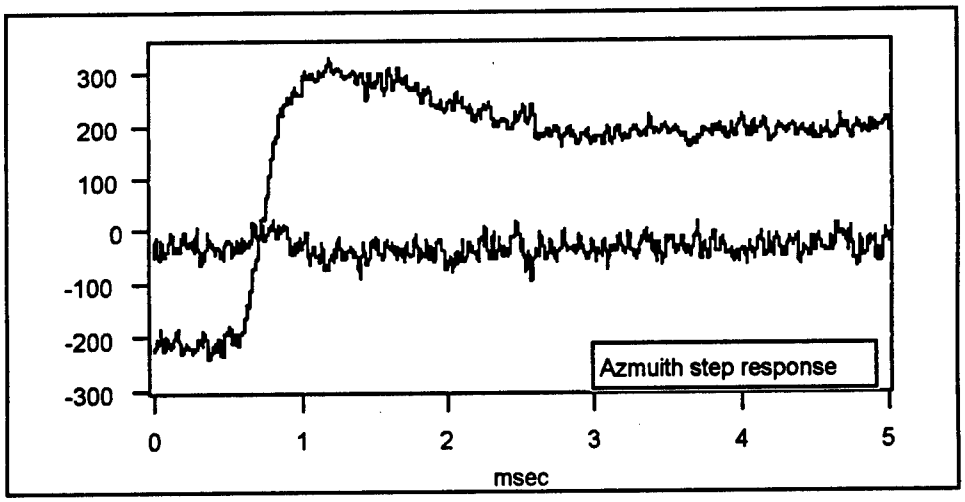

Figure 3-6. Step response of conventional control with azimuth channel excited.

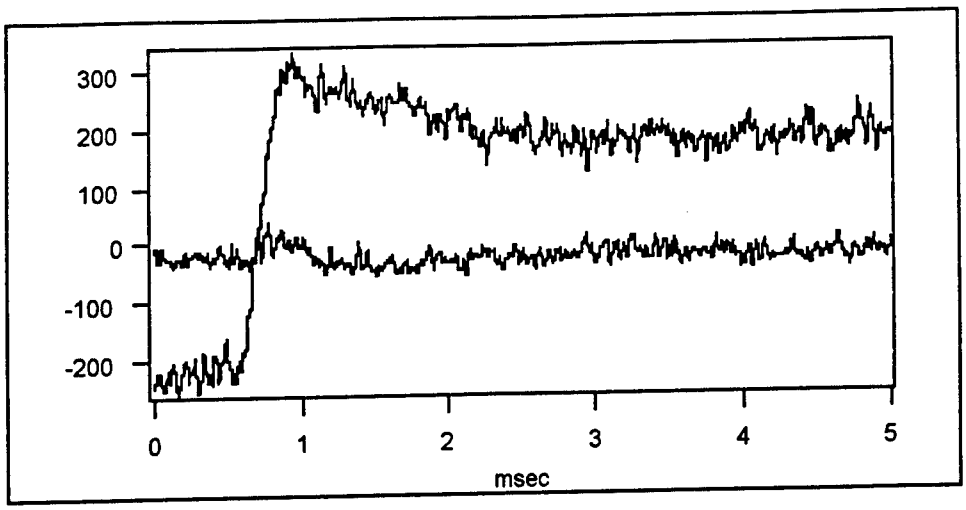

Figure 3-7. Step response of conventional control with elevation channel excited.

Figure 3-8 and Figure 3-9 represent the step response of the azimuth and elevation channels using a reference model. Note that while perfect model following is not exhibited, clearly the dynamic characteristics are the same or better than the original system. The overshoot has been significantly reduced along with a reduction in the cross-channel coupling.

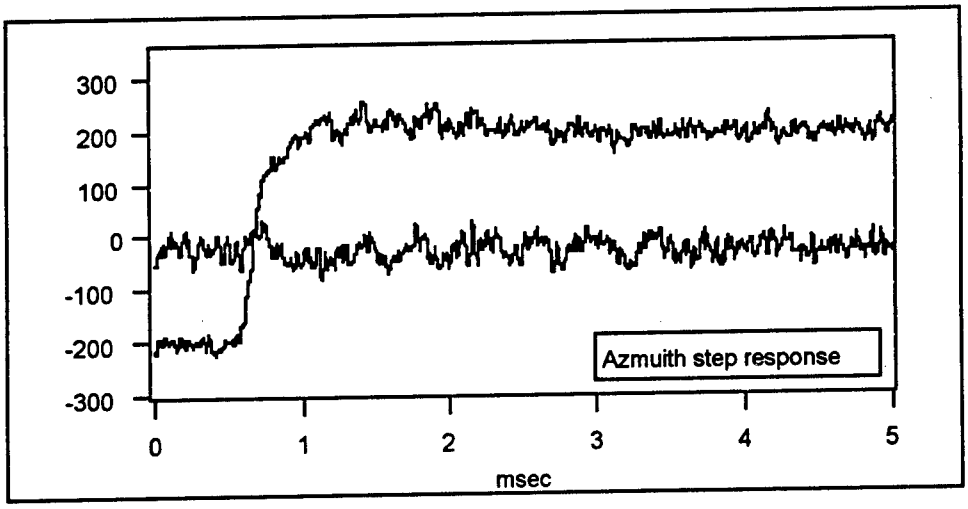

Figure 3-8. Step response of model reference control, azimuth channel excited.

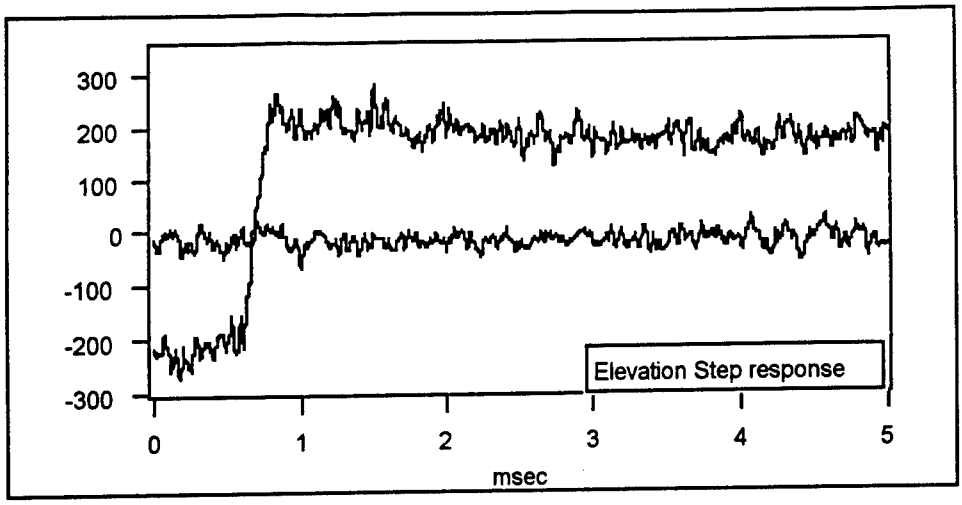

Figure 3-9. Step response of model reference control, elevation channel excited.

The system's response to jitter was measured through the introduction of acoustic vibration. The vibration was produced by applying a 400 mV sinusoid with sweeping frequencies from 10 to 1000 Hz to a audio amplifier and speaker. The acoustic vibration is additive to the jitter due to atmospheric transmission. Figure 3-10 depicts the jitter spectrum of the elevation axis due to the atmosphere alone. The atmospheric jitter in this axis was much worse than that of the azimuth axis and is the result of the air flow patterns in the laboratory. For terrestrial applications of free space laser communication, this jitter represents the fine steering problem and seems to have the same power spectral density as that of satellite jitter [2]. The spectra shown are the average of 20 traces. It can be seen that the conventional controller offers a reduction in jitter at frequencies below 300 Hz. The model reference control adds little additional improvement below 300 HZ but effectively adds an additional 7 dB improvement at higher frequencies. The addition of the acoustic jitter excites various mechanical modes in the table as demonstrated by the peaks in Figure 0-14. Again, when fine tracking is implemented a large reduction in jitter is seen at frequencies below 300 Hz along with an equalization of the modes above 400 Hz. Once model reference control is added, a 5 dB improvement can be seen. The presence of modes at 60, 120, and 180 Hz is due to electrical noise pick-up in the protoboard used to implement the compensator circuit.

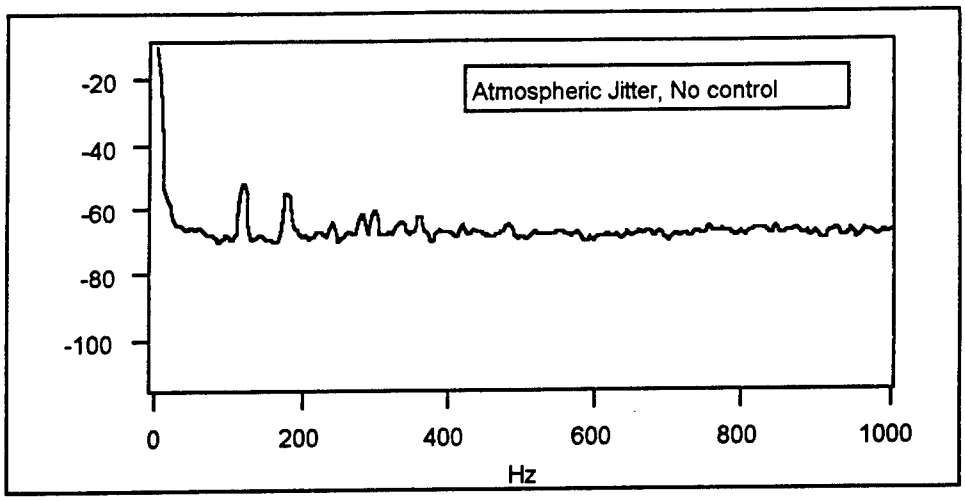

Figure 3-10. Atmospheric jitter spectrum no control effort applied

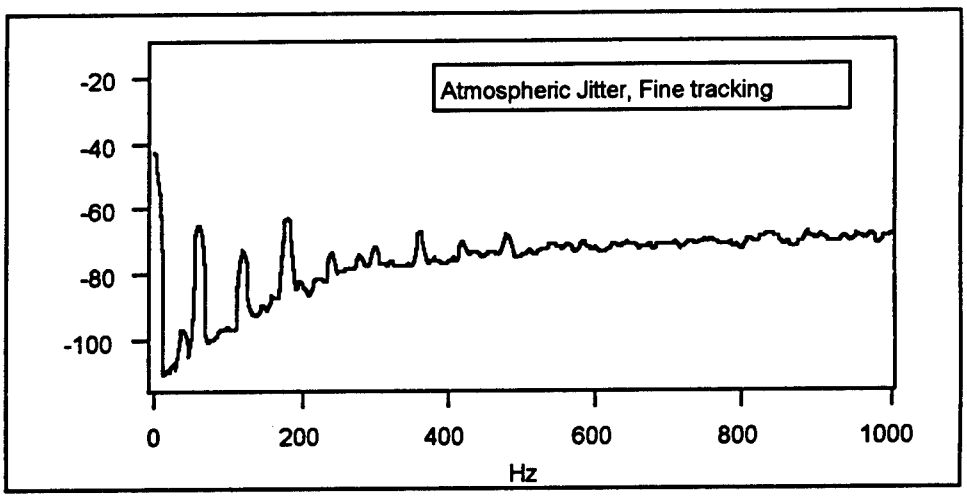

Figure 3-11. Atmospheric jitter spectrum using standard feedback control.

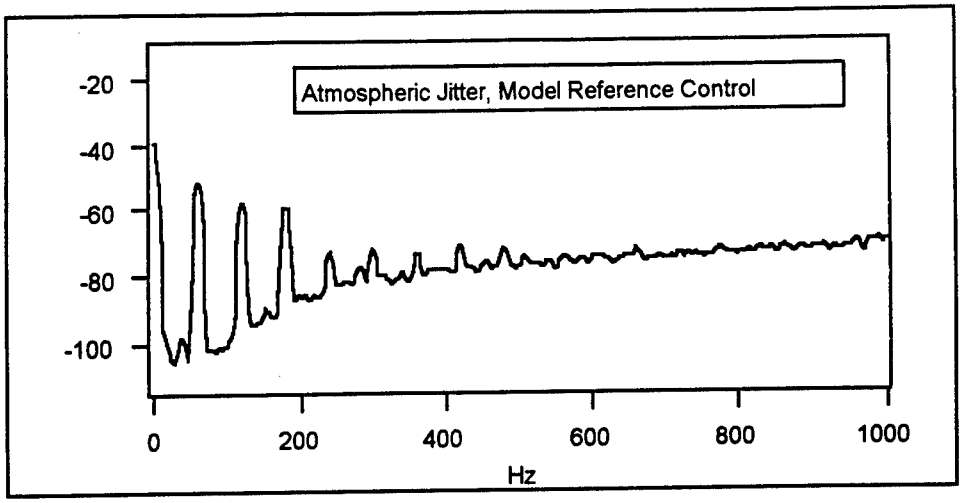

Figure 3-12. Atmospheric jitter spectrum using model reference control.

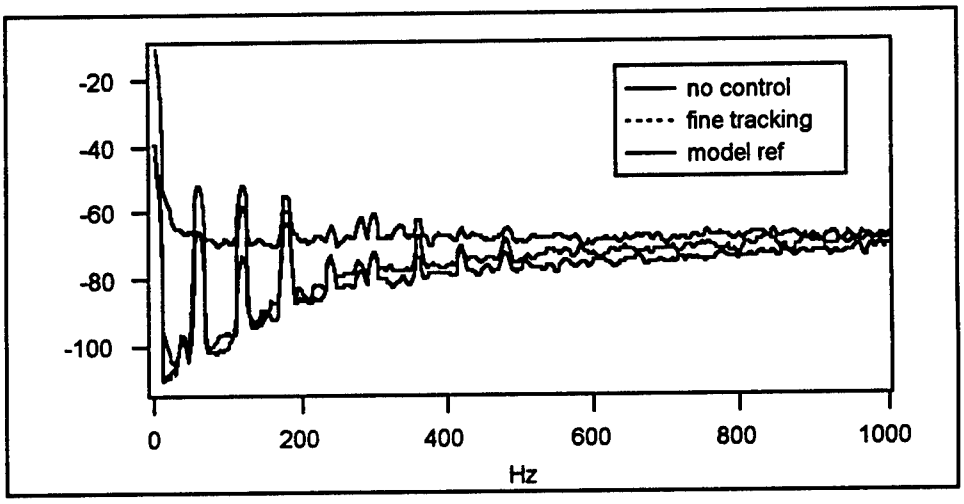

Figure 3-13. Composite atmospheric jitter spectrum.

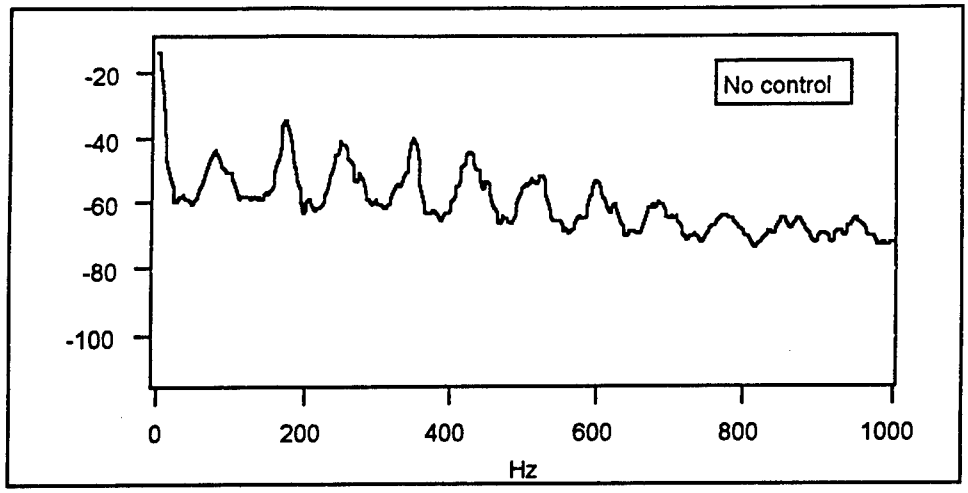

Figure 3-14. Acoustic jitter induced spectrum no control effort applied.

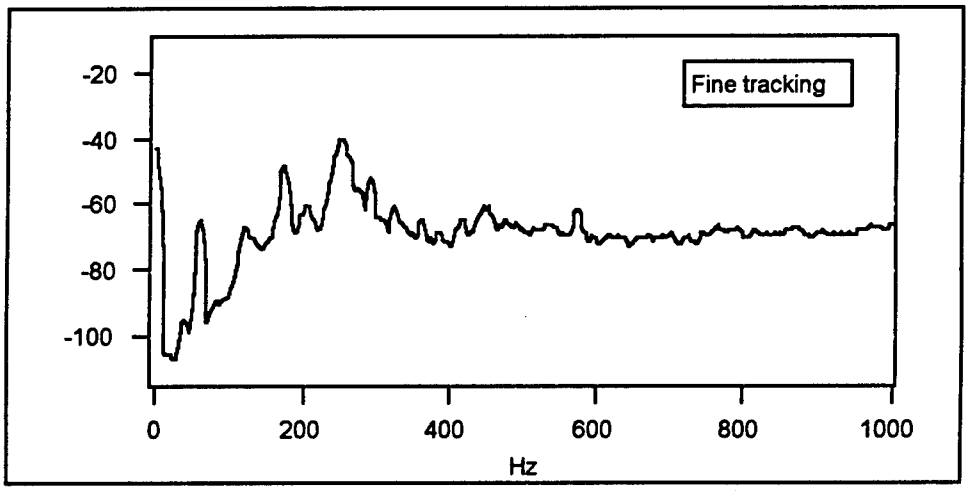

Figure 3-15. Acoustic jitter induced spectrum with standard feedback control.

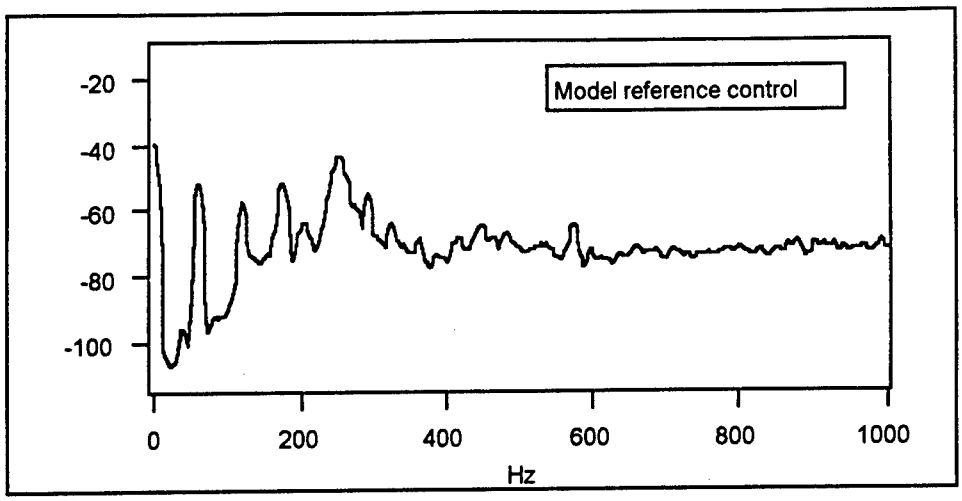

Figure 3-16. Acoustic jitter induced spectrum with model reference control.

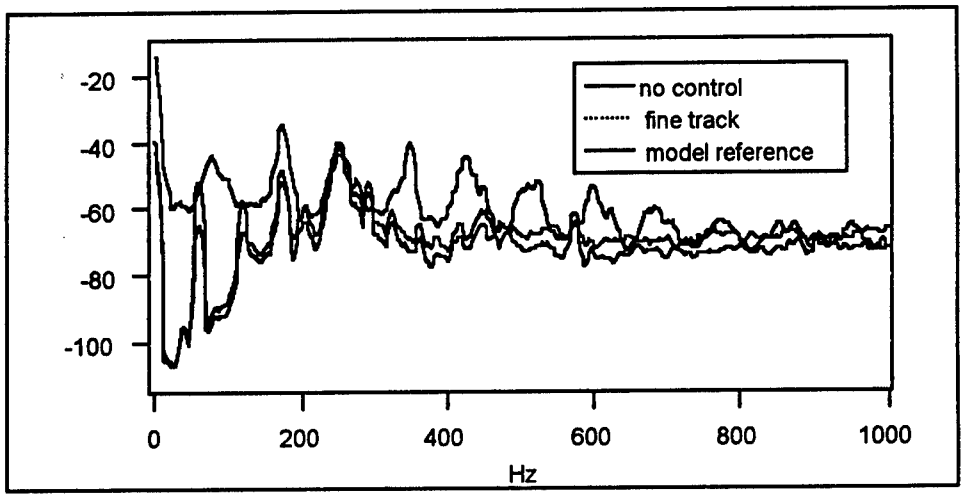

Figure 3-17. Acoustic jitter induced spectrum with model reference control.

3.2 Low Bandwidth Mirror:

The model reference control technique was also applied to a Physik Instrument model S-320.2 three axis tilting platform that provides an overall steering angle of ±1 mr.

The experimental setup used a collimated HeNe laser passed through a variable aperture to provide a collimated beam with a diameter smaller than that of the mirror. This beam was then directed to the steering mirror and then through a 1500 mm lens to a RCA 30927E quadrant detector . Figure 3- below shows the quad cell output voltage V_{AZ}

and V_{EL} as a function of angle. Unlike the PAT system, the laser was not modulated nor were electrical or optical bandpass filters used on the output of the quad cell. In order to reduce the effect of ambient light induced noise in the system, the laser power was kept high and the room lights were turned down.

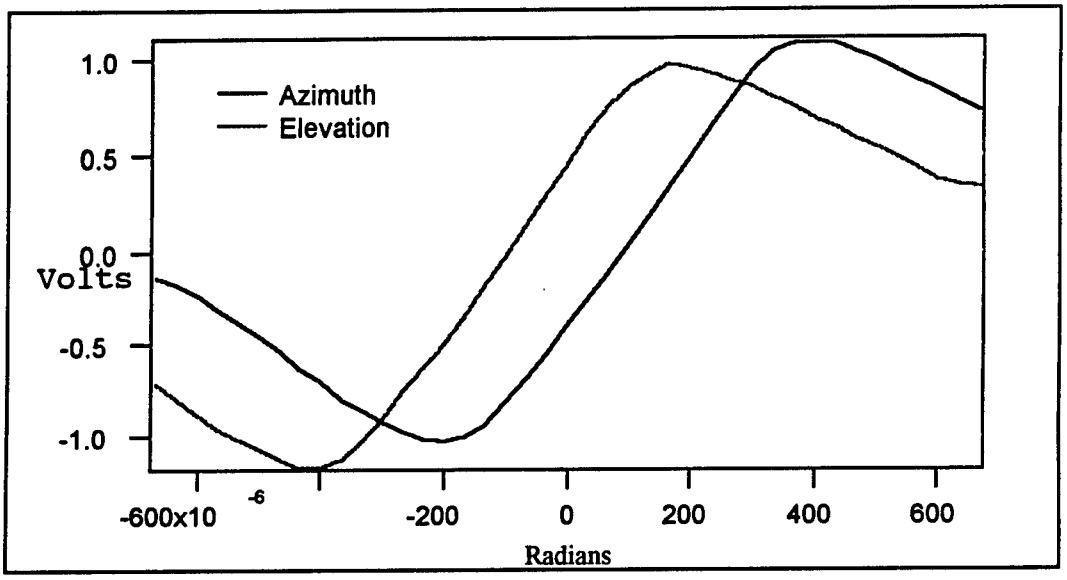

Figure 3-18. Quad cell response.

The control for this system was implemented digitally using a Macintosh Quadra 650 computer. The control system is shown in Figure 3-19. The shadowed boxes represent functions which take place in the DSP card. As before, M(s) is the reference model and is given by:

$$M(s) = \begin{bmatrix} m_{11}(s) & 0 & 0 \\ 0 & m_{22}(s) & 0 \end{bmatrix}$$

One can see that the reference model does not exhibit cross-coupling and cannot be affected by environmental jitter. The particular choice of transfer function

$$m_{11}(s)=m_{22}(s)=\frac{4000}{s+4000}$$

This model is a little faster than the model used for the high bandwidth mirror since one of the goals of this research is to demonstrate improved performance from commercially available devices. The controller provided by Physik Instrument has a bandwidth of 500 Hz and does not provide for any decoupling between axis. As previously discussed, the

mirrors step response was poorly damped and highly coupled. It was necessary therefore to introduce several sections of lag in the forward path and an explicit decoupler. They are represented by H(s). C(s) is an additional lowpass filter introduced to insure that frequencies above the Nyquist rate were eliminated before conversion.

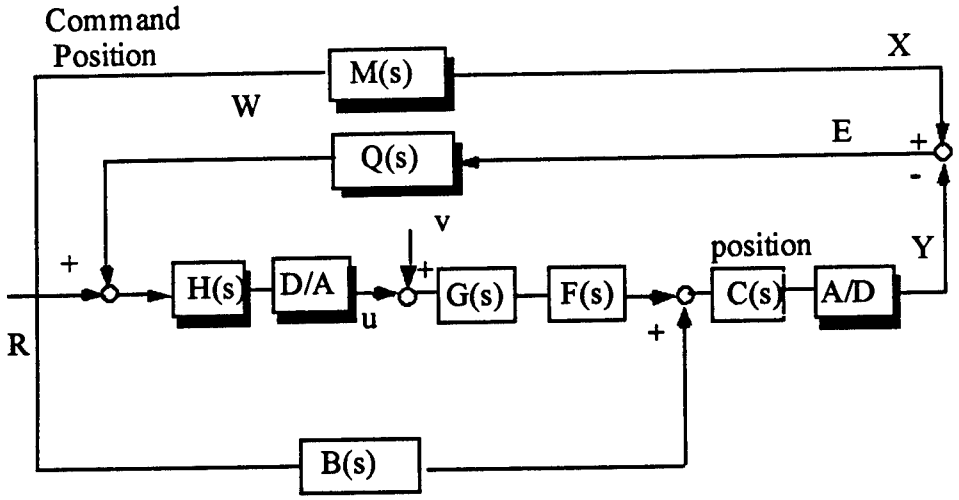

Figure 3-19. Piezo mirror control system

Once again Q(s) is a 3 stage lead network providing gain of 64 dB. Both Q(s) and M(s) were implemented as single stage IIR filters. The reference signal was synthesized in the dsp and represents a ±200 mv square wave with a period of 21 Hz. Position signals were measured at the output of the quad cell prior to filtering by the Kronhite analog filter (C(s)).

Figure 3-20 below shows the open loop response of the system when only the lag filter and decoupler are in place in response to excitation of the azimuth channel. The system exhibits a first order response with a settling time of about 5 ms. There is very little evidence of coupling.

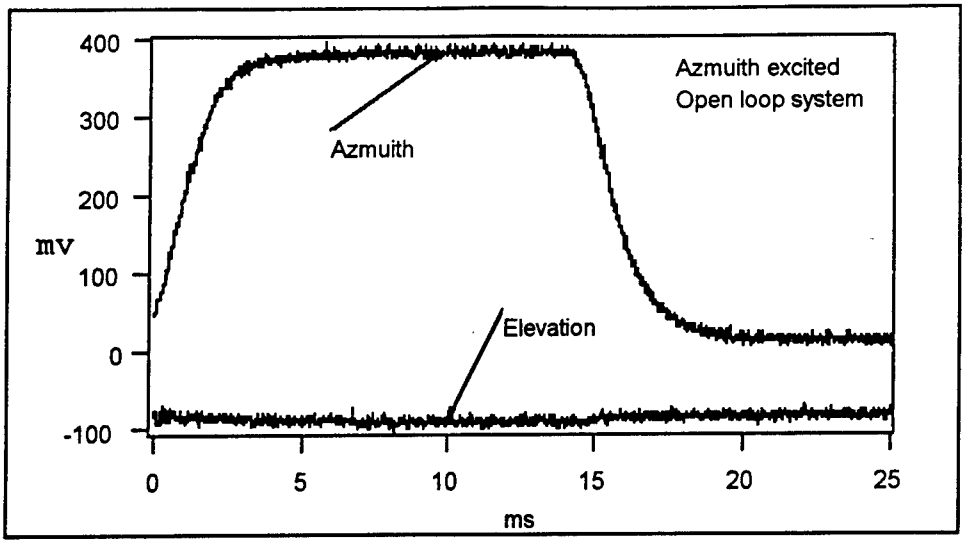

Figure 3-20. Open loop response to a step applied to the azimuth axis.

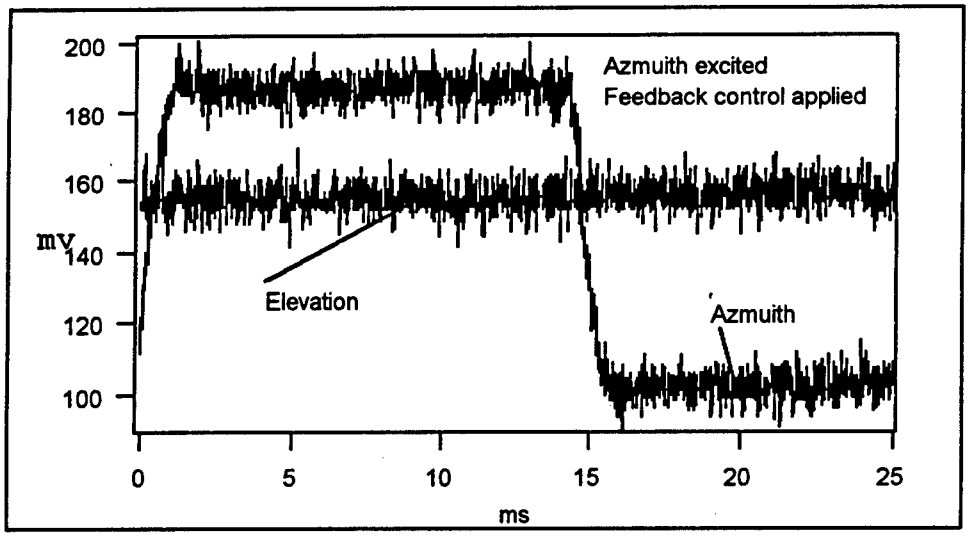

Figure 3-21. Azimuth step response when feedback alone is applied.

For the case where only feedback is applied (Figure 3-21), we note an improvement in performance but fail to achieve good model following.

With model reference control (Figure 3-22) good model following is achieved.

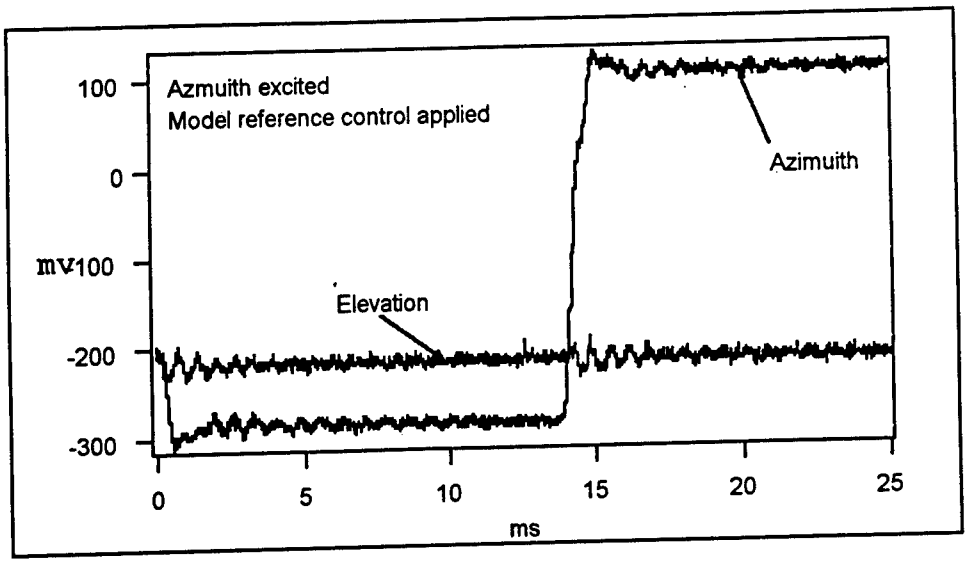

Figure 3-22. Azimuth step response with model reference control applied.

Acoustic jitter was introduced to the table by sweeping frequencies from 10 to 1000 Hz via an audio amplifier and speaker system. Measurements of the beam position spectra were made using a HP3561A dynamic signal analyzer for both the azimuth and elevation channels. Since the data were similar we will only present the results of the azimuth channel. Figure 3-23 demonstrates the response of the system when only the commercial controller is in place. There are prominent modes in the table at 90 and 340 Hz.

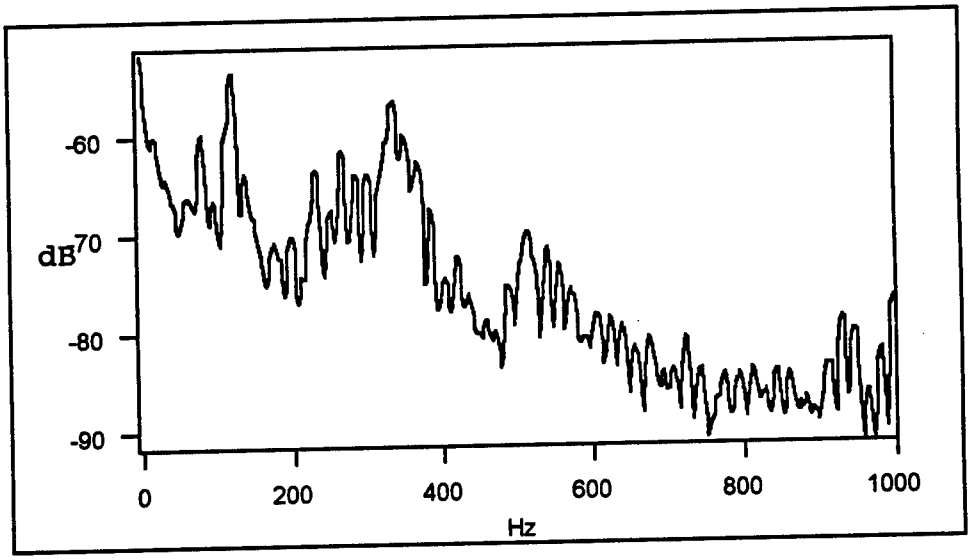

Figure 3-23. Acoustic induced jitter control is provided by the commercial controller.

Figure 3-24 illustrates the improvement in jitter rejection when model reference control is applied. It can be seen that there is a significant improvement over the conventional controller.

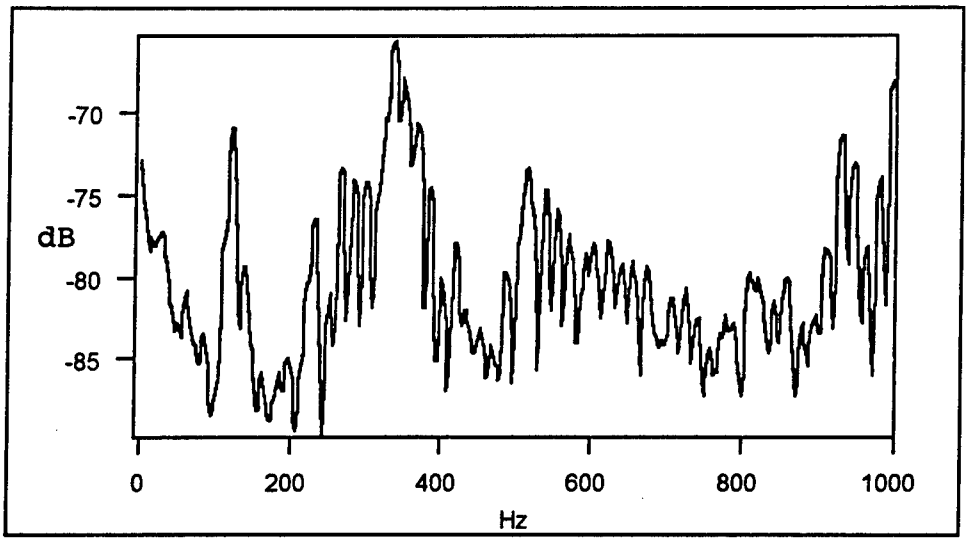

Figure 3-24. Acoustic induced jitter model reference control.

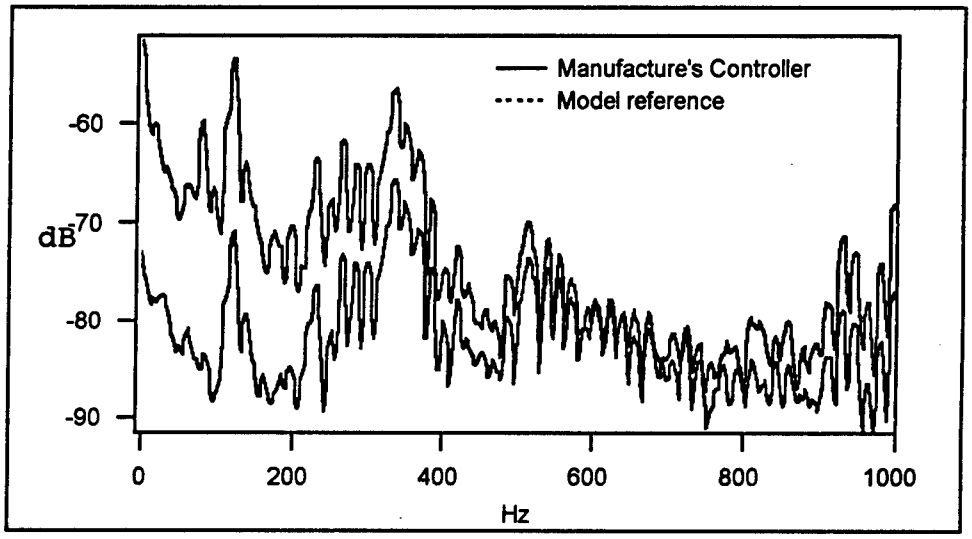

Figure 3-25 Comparison of commercial versus model reference control.

3.3 Summary

A simplified model following control was demonstrated on both a high bandwidth fine steering mirror and a commercially available piezo-driven mirror. Both analog and digital implementations were demonstrated . The performance of both systems showed an improved step

response consistent with previously obtained simulation results. The most dramatic improvements were seen in the piezo mirror. Its performance was enhanced to the level of that of the very expensive high bandwidth mirror. This conclusively demonstrates that improvements in the control system will allow the use of piezo mirrors for beam stabilization in lasercom systems.

The ability to "enforce" dynamics of a time-invariant reference model on a beam steering mirror indicates that the developed approach results in the enhanced robustness of the resultant control system.

While reference models are completely protected from any environmental effects, such as jitter, the jitter performance of the system should be improved by application of MR controllers. This improvement was successfully demonstrated with a 7 dB decrease in the error spectrum. This is particularly impressive at frequencies above 200 Hz since previous methods required physical modifications to the mirror.

It was shown that implementation of MR control, in addition to conventional feedback controllers, results in the increased efficiency of beam steerers without the penalty of increased costs and payloads.

---

4. POWER CONTROL

Modification of the laser beam steering control results in the improved positioning accuracy. This allows to assure, with some degree of confidence, that laser beam power is concentrated within a much smaller angle thus improving the signal-to-noise ratio at the receiver cite. Therefore, the minimum received power requirement, corresponding to the acceptable rate of communication errors, can be satisfied with a smaller overall transmitted laser power. Once the laser communication system is designed, and placed on orbit, variations of the laser beam positioning accuracy can be utilized for incremental changes to the transmitted power. Operation of the laser source at lower than nominal power level results in improved reliability of electronics and reduced cycling of electric batteries. It has been proposed to optimize the transmitted laser power on the basis of the amount of the residual jitter [13,15].

4.1 General Considerations

Assume that the laser source of a transmitting satellite and the light sensitive device of a receiving satellite are ideally aligned. Any change in the orientation of the transmitter with respect to receiver can be represented using two orthogonal position errors, e_x and e_y, defined as angular deviations from the original position. It could be seen that

$$-\pi/2 \le e_x \le \pi/2 \quad \text{and} \quad -\pi/2 \le e_y \le \pi/2 \tag{4.1}$$

and the laser power can be characterized by a symmetric, distribution $\Psi(e_x,e_y)$ with a maximum at $e_x=e_y=0$. The full power of the laser source can then be defined as

$$W_o = \int_{-\frac{\pi}{2}}^{\frac{\pi}{2}} \int \Psi(e_x, e_y) de_x de_y \tag{4.2}$$

Introduce a generalized angular position error, assuming radial symmetry,

$$e=(e_x^2+e_y^2)^{1/2} \tag{4.3}$$

Represent the power distribution as

$$\Psi(e_x,e_y)=W_o\Psi(e), \tag{4.4}$$

where

$$\int_{-\frac{\pi}{2}}^{\frac{\pi}{2}} \Psi(e)de = 1$$

Assume that at a particular distance between the transmitting and the receiving satellites (which is irrelevant at this point) some threshold value of intensity, δ, can be defined, such that any intensity below δ is not sufficient for reliable operation of the communication system. Define the maximum position error corresponding to this threshold, e_{MAX} by solving the following equation:

$$W_O \Psi(e_{MAX}) = \delta, \text{ or } \Psi(e_{MAX}) = \delta / W_O \tag{4.5}$$

Since $\Psi(e)$ is a bell-shaped distribution, it can be seen that a decrease of the δ/W_O value results in the increase of the solution e_{MAX}. This is not surprising: increased power of the laser source always results in the increased tolerance of any laser communication system to position errors.

Now consider the probability density of the position error which can be described by a normal distribution with mean μ and variance σ^2:

$$P(e) = \Phi(e, \sigma)$$

The probability of a failure in the communication system caused by position errors can be defined now as

$$P_F = 2 \int_{e_{max}}^{\infty} \Phi(e, \sigma)de \tag{4.6}$$

One can realize that due to the shape of the normal distribution, a decrease of the standard deviation σ results in the decrease of the failure probability P_F.

Summarizing the above discussion, probability P_F can be expressed as some function of the power of the laser source and the standard deviation of the position error:

$$P_F = f(W_O, \sigma)$$

It could be seen that derivatives of the probability of failure

$$\frac{\partial f(W_o, \sigma)}{\partial W_o} < 0 \quad \text{and} \quad \frac{\partial f(W_o, \sigma)}{\partial \sigma} < 0 \tag{4.7}$$

Consider the following equation, presenting the "balance" between the power of the laser source and the standard deviation of the communication error:

$$\frac{\partial f(W_o,\sigma)}{\partial W_o}\Delta W_o + \frac{\partial f(W_o,\sigma)}{\partial \sigma}\Delta\sigma = 0 \qquad (4.8)$$

where

ΔW_O and $\Delta\sigma$ are increments of the power of the laser source and the standard deviation of position error.

Equation (4.8) holds for small increments ΔW_O and $\Delta\sigma$ and has the potential of laser power control on the basis of on-line estimation of changes $\Delta\sigma(t)$ caused by satellite jitter. The derivatives utilized in (4.8) can be precalculated and used as coefficients of a linear control law.

The following equation, is not limited to the magnitude of increments and, therefore, is more convenient for engineering calculations:

$$f(W_O+\Delta W_O,\sigma)+f(W_O,\sigma+\Delta\sigma)=0 \qquad (4.9)$$

Although an analytical solution of (4.9) is possible, it constitutes a formidable analytical task. A numerical solution of (4.9) can be obtained by specification of the particular standard deviation of the position error, $\sigma^*=\sigma+\Delta\sigma$, and application of a direct search procedure for the minimization of the norm $|f(W_O+\Delta W_O,\sigma)+f(W_O,\sigma^*)|$ with respect to ΔW_O.

The block diagram of Figure 4-1 below illustrates the suggested numerical solution procedure.

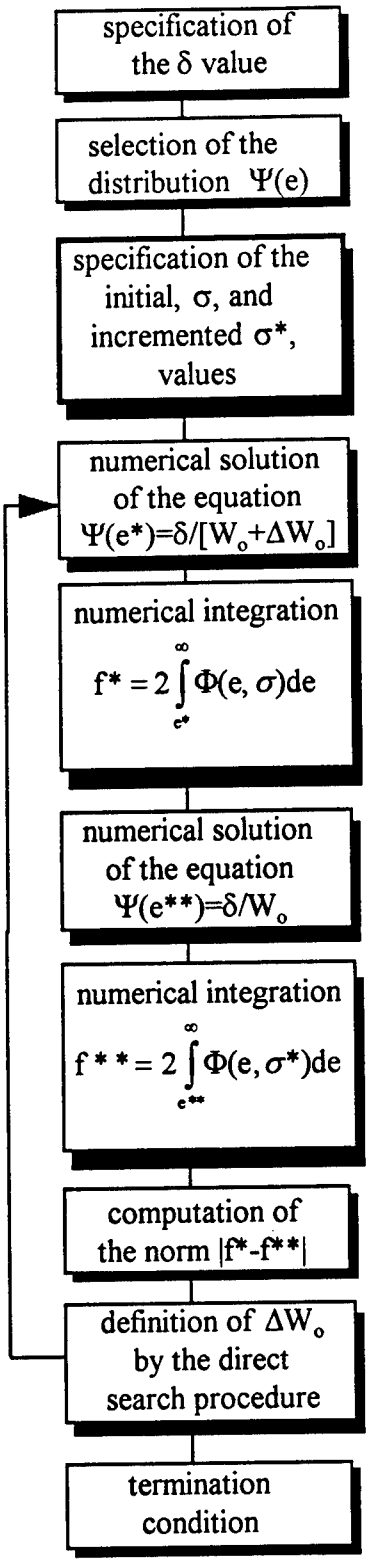

Figure 4-1 Block diagram of the power control procedure

4.2 Description of a Direct Detection PPM System

The expression for the number of received signal photons for a M-ary pulse position modulation (PPM) scheme can be written as [21] :

$$K_S(P_T, G_T, \theta_T) = \eta_T G_T \left(\frac{\lambda}{4\pi z}\right)^2 \eta_R G_R L_T(G_T, \theta_T) M\left(\frac{\eta}{h\nu}\right) P_T T_S \qquad (4.10)$$

where

η_T, η_R are efficiencies of the transmitter and receiver optics G_T, G_R, are the transmitter and receiver antenna gains,

$L_T(G_T,\theta_T)$ is the pointing loss factor associated with the pointing error θ_T,

η is the quantum efficiency of the detector,

$h\nu$ is the photon energy,

P_T is the average power,

T_s is the time slot period, and

it is assumed that the peak power is M times the average power.

This equation can be recognized as very similar to the link equation introduced in chapter 1 for a range of z and a wavelength λ. For this discussion, consider the receiver gain based on an unobscured circular aperture with a wide enough field of view that the receiver pointing error has a negligible effect on the received signal power. Given these assumptions the receiver gain is determined by

$$G_R = \left(\frac{2\pi r_R}{\lambda}\right)^2 \qquad (4.11)$$

where r_R is the radius of the aperture.

Similarly for a transmitter illuminated by a Gaussian beam with rms width W and an unobscured aperture; G_T and L_T are given by:

$$G_T = \left(\frac{2\pi W}{\lambda}\right)^2 \qquad (4.12)$$

$$L_T(G_T,\theta_T)=\exp(-G_T\theta^2_T). \qquad (4.13)$$

Figure 4-2 shows the number of photons received as a function of mispoint angle for two power levels. The minimum signal requirement is dictated by the desired probability of bit error. The intersection of the minimum signal line with the number of photons vs. angle curve defines

the maximum angle before a burst error occurs. It is not surprising that the higher the power the larger the allowed angle.

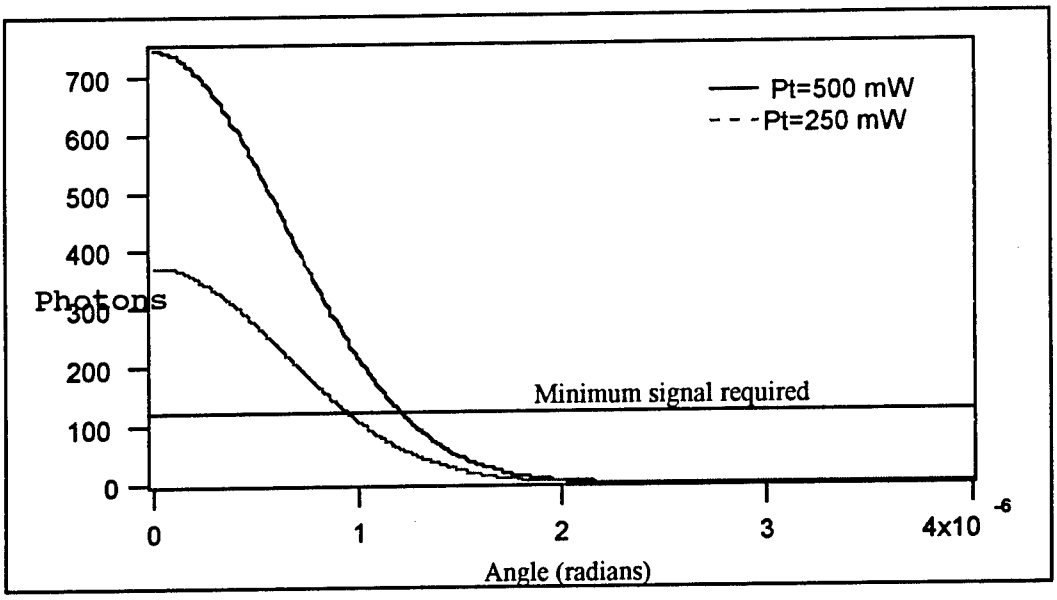

Figure 4-2. Number of photons received vs. angle.

The two axis pointing and control system is assumed to have a coarse outer loop which will respond to slow changes and a inner fine steering loop that will be responsible for fast changes. It is the responsibility of the coarse loop to cancel any bias in the system. This allows us to assume that the single axis probability for mispoint is a Gaussian function with single-axis pointing errors θ_x and θ_y. The Gaussian function has standard deviation σ_x and σ_y. We assume radial symmetry, so that $\sigma_\theta = \sigma_x = \sigma_y$ and $\theta = \sqrt{\theta_x^2 + \theta_x^2}$. The radial distribution in normalized from can be recognized as the Rayleigh distribution.

$$P(\theta) = \frac{\theta}{\sigma^2} \exp\left(\frac{-\theta^2}{2\sigma^2}\right) \tag{4.14}$$

Recall that by definition a burst error occurs when the signal irradiance falls below the level required to maintain the average probability of bit error. The probability of burst error is given by:

$$P_E^* = \int_{\theta^*}^{\infty} \frac{\theta}{\sigma^2} \exp\left(\frac{-\theta^2}{2\sigma^2}\right) d\theta \tag{4.15}$$

where

$\theta = \theta^*$ represents the mispoint angle that produces the minimum number of photons necessary to close the link for a given probability of bit error. The solution of equation (4.15) yields the reference angle in terms of the probability of burst error and the standard deviation of the Gaussian probability distribution for the single -axis pointing error

$$\theta^* = \sigma\sqrt{2(-\ln P_E^*)} \tag{4.16}$$

The probability of error for an M-ary PPM scheme using avalanche photodiodes as the detector is given by [21, 22, 23] :

$$P_E = \frac{M}{2(M-1)}\left\{1-\left[\int_{-\infty}^{\infty}\frac{1}{\sigma_1\sqrt{2\pi}}\exp-\left(\frac{(x-\mu_1)^2}{2\sigma_1^2}\right)\cdot\left[\int_{-\infty}^{x}\frac{1}{\sigma_0\sqrt{2\pi}}\exp-\left(\frac{(y-\mu_0)^2}{2\sigma_0^2}\right)dy\right]^{M-1}dx\right]\right\} \tag{4.17}$$

where:

$$\sigma_0^2 = G^2F\left(K_B + \frac{I_bT_S}{e}\right) + \frac{I_sT_S}{e} + \frac{2k_BT_{eq}T_S}{R_Le^2} \tag{4.18}$$

$$\sigma_1^2 = G^2F\left(K_S + K_B + \frac{I_bT_S}{e}\right) + \frac{I_sT_S}{e} + \frac{2k_BT_{eq}T_S}{R_Le^2} \tag{4.19}$$

$$\mu_0 = G\left(K_B + \frac{I_bT_S}{e}\right) + \frac{I_sT_S}{e} \tag{4.20}$$

$$\mu_1 = G\left(K_S + K_B + \frac{I_bT_S}{e}\right) + \frac{I_sT_S}{e} \tag{4.21}$$

The parameters G, and F are the gain and the excess noise factor of the APD, I_b, and I_s are the gain dependent and gain independent APD dark current, e is the electron charge, k_B is the Boltzmann's constant, T_{eq}, R_L are the detector noise equivalent temperature and load resistance respectively, and K_B is the background photon count.

The solution of (4.17) for a desired average probability of bit error and given background signal yields the minimum number of photons necessary to close the link, Ks_{MIN}. This value can then be substituted in (4.17) which can then be solved for the corresponding maximum mispoint angle θ^*. It is given by :

$$\theta^* = \sqrt{\frac{1}{G_T}\left(-\ln\frac{Ks_{MIN}}{\alpha_o G_T P_T}\right)} \tag{4.22}$$

where

$\alpha_o = \eta_T \left(\frac{\lambda}{4\pi z}\right)^2 \eta_R G_R M \left(\frac{\eta}{h\nu}\right) T_S$ is a constant that is independent of the transmitted power and transmitted antenna gain.

Equating (4.16) and (4.22) results in the following expression

$$P_T = \frac{Ks_{MIN}}{\alpha_o G_T} \exp\left[2G_T\sigma^2(-\ln P_E^*)\right] \tag{4.23}$$

This relationship forms the basis for the adjustment of the transmitted power based on the measured values of the variance of the pointing error.

In this case, we have an explicit relationship between the variance of the jitter and the necessary transmitted power. Therefore, the partial derivatives are unnecessary and the transmitted power can be calculated on line as a function of the variance of the jitter.

REFERENCES

1. *Eric A. Swanson and James K. Roberge,* "Design Considerations and Experimental Results for Direct-Detection Spatial Tracking Systems", Optical Engineering, Vol. 28 No. 6. June 1989.

2. *R. Dumas and B. Laurent,* "System Testbed for Demonstration of the Optical Space Communications Feasibility", SPIE Vol. 1218, Free-Space Laser Communication Technologies II, 1990.

3. "An Experimental Spatial Acquisition and Tracking System for Optical Intersatellite Crosslinks", Technical Report prepared for the Department of the Air Force under contract F19628-90-C-0002, December 1991.

4. "The Flexural Behavior of PACSAT in Orbit", Technical Report prepared for the Defense Advanced Research Projects Agency by Rand Corporation, February 1983.

5. *Held, K.J. and J.D. Barry,* "Precision Optical Pointing and Tracking from Spacecraft With Vibrational Noise". SPIE Vol 616 Optical Technologies for Communication Satellite Applications, 1986.

6. *Witting, M. L. Van Holtz, D.E.L. Tunbridge and H.C. Vermeulen,* "In-Orbit Measurements of Microaccelerations of ESA's Communication Satellite OLYMPUS". SPIE Vol 1218 Free-Space Laser Communication Technologies II, 1990 pages 205-214.

7. *Elliot, S.J., Boucher, C.C., and Nelson, P.A.,* "The Behavior of a Multiple Channel Active Control System", IEEE Transactions on Signal Processing, Vol 40, No.5, May 1990

8. *J.D. Barry, and G.S. Mecherle,* "Beam Pointing Error as a Significant Design Parameter for Satellite-Borne, Free Space Optical Communication Systems", Optical Engineering, Vol.24(6), 1049-1054, 1985

9. *Skormin, V.A., Tascillo, M.A., Herman, C.R., and Nicholson, D.J.*, "Mathematical Modeling and Simulation Analysis of a Pointing, Acquisition and Tracking System for Laser-Based Intersatellite communication", Optical Engineering, November 93. Also in the Milestone Series volume "Selected Papers on Precision Stabilization and Tracking Systems for Acquisition, Pointing, and Control Applications"

10. *Skormin, V.A., Tascillo, M.A., and Nicholson, D.J.*, "A Jitter Rejection Technique in a Satellite-Based Laser Communication Systems", Optical Engineering, November 93.

11. *Skormin, V.A., Busch, T.E., and Tascillo, M.A.*, "An Adaptive Jitter Rejection Technique Applicable to Airborne Laser Communication System", Optical Engineering, 1995. **Also in the** Milestone Series volume "Selected Papers on Precision Stabilization and Tracking Systems for Acquisition, Pointing, and Control Applications"

12. *Skormin V.A., T.E. Busch, and M.A. Givens,* "Model Reference Approach for Compensation of Bending Modes in Fine Steering Mirrors", SPIE Free-Space Laser Communications 1995.

13. *Skormin, V.A., Busch, T.E., Givens M.A.,* "Model Reference Control of a Fast Steering Mirror of a Pointing, Acquisition and Tracking System for Laser Communication", Proceedings of the National Aerospace Electronics Conference NAECON'95, Dayton OH, May 95.

14. *Skormin, V.A.*, "Mathematical Modeling, Simulation, Analysis and Control of a Satellite-Based Laser Communication System", Report to SRI International (Subcontract No. C-b0189/ SRI Project ECU-4007), Binghamton, NY, July 1993

15. *Skormin, V.A.*, "Optical Crosslink Control System Modeling", Final Report to CALSPAN-UB Research Center, Berkshire, NY, January 1995

16. *T.E. Busch and Skormin V.A.,* "Model Reference Approach for Compensation of Bending Modes in Fine Steering Mirrors", SPIE Free-Space Laser Communications 1995.

17. *Skormin, V.A., Busch, T.E., and Tascillo, M.A.,* "Demonstration of Jitter Rejection Technique for Free Space Laser Communication", IEEE Transactions on Aerospace and Electronic Systems, April 1997.

18. *Skormin, V.A., Busch, T.E., and Nicholson, D.J.*, "Adaptive Feedforward Compensation of Structural Vibrations in Satellite-Based Laser Communication Systems", Proceedings of the International Conference on Informatics and Control (sponsored by US Air Force) in St. Petersburg, Russia, June, 97

19. *Skormin, V.A. and Busch, T.E*, "Model-Following Decoupling Control for 2-Axis Beam Steering Mirrors for Satellite-Based Laser Communication Systems", Proceedings of the International Conference on Informatics and Control (sponsored by US Air Force) in St. Petersburg, Russia, June, 97

20. *Skormin, V.A. and Busch, T.E*, "Numerical Model Reference Control of a Gantry Positioning System", will be presented at the 26-th Annual Symposium on Incremental Motion Control Systems and Devices, San-Jose CA, July 1997

21. *Busch, T.E.,* "Beam Steering Techniques for Free Space Laser Communications", Ph.D. Dissertation, Binghamton University, Binghamton NY, May 1997

22. *C.C. Chen and C.S. Gardner,* "Impact of Random Pointing and tracking Errors on the Design of Coherent and Incoherent Optical Intersatellite Communication Links", IEEE Transactions on Communications, Vol. 37, No. 3, pp. 252-260, 1989

23. *J.B. Abshire,* "Performance of OOK and Low-Order PPM Modulations in Optical Communications when using APD-Based Receivers", IEEE Transactions on Communications, Vol. COM-32, No. 10, pp. 1140-1143, 1984

☆U.S. GOVERNMENT PRINTING OFFICE: 1997-610-130-61077

MISSION

OF

ROME LABORATORY

Mission. The mission of Rome Laboratory is to advance the science and technologies of command, control, communications and intelligence and to transition them into systems to meet customer needs. To achieve this, Rome Lab:

a. Conducts vigorous research, development and test programs in all applicable technologies;

b. Transitions technology to current and future systems to improve operational capability, readiness, and supportability;

c. Provides a full range of technical support to Air Force Materiel Command product centers and other Air Force organizations;

d. Promotes transfer of technology to the private sector;

e. Maintains leading edge technological expertise in the areas of surveillance, communications, command and control, intelligence, reliability science, electro-magnetic technology, photonics, signal processing, and computational science.

The thrust areas of technical competence include: Surveillance, Communications, Command and Control, Intelligence, Signal Processing, Computer Science and Technology, Electromagnetic Technology, Photonics and Reliability Sciences.